

## Basic Notations

$a$	= length of crack or crack band
$a_0$	= initial (pre-existing) notch or crack length
$a_e$	= elastically equivalent (effective) crack length
$b$	= thickness of two-dimensional specimen
$c$	= elastically equivalent crack extension
$d$	= characteristic dimension (or size) of structure (or specimen)
$f_t$	= tensile strength
$s$	= crack spacing
$u$	= displacement
$w_c$	= width of crack band
$E$	= Young's modulus of elasticity
$E'$	= $E$ for plane stress, $E' = E(1 - \nu^2)$ for plane strain
$G$	= energy release rate
$G_{Ic}$	= critical energy release rate for Mode I
$G_f$	= fracture energy
$G_f^R$	= fracture energy obtained by the RILEM Method
$K_I, K_{II}, K_{III}$	= stress-intensity factors for Modes I, II, III, respectively
$K_{Ic}$	= critical stress-intensity factor for Mode I, fracture toughness
$P$	= load
$P_u$	= maximum (ultimate load)
$\alpha$	= relative crack length, $a/d$
$\beta$	= brittleness number
$\delta_c$	= crack-opening displacement
$\delta_{CTOD}$	= critical effective crack-tip opening displacement
$\delta_{CMOD}$	= crack-mouth opening displacement
$\delta_{LPD}$	= load-point displacement
$\epsilon$	= strain
$\sigma$	= stress
$\sigma_N$	= nominal stress at ultimate load
$\nu$	= Poisson's ratio
$\Delta a$	= extension of crack or crack band
$\Pi$	= potential energy

# Fracture Mechanics of Concrete: Concepts, Models and Determination of Material Properties

Report by ACI Committee 446, Fracture Mechanics\*

Zdeněk P. Bažant<sup>1,2</sup>  
(Chairman)

Vellore S. Gopalaratnam<sup>1,3</sup>  
(Secretary)

## Members

Oral Buyukozturk <sup>1</sup>	Victor C. Li <sup>1</sup>	Gilles Pijaudier-Cabot <sup>3</sup>
Luigi Cedolin <sup>1</sup>	Feng-Bao Lin <sup>1</sup>	Victor Saouma <sup>1,3</sup>
David Darwin <sup>3</sup>	Steven L. McCabe	Surendra P. Shah <sup>1,3</sup>
Manuel Elices <sup>1,3</sup>	Sheng-Taur Mau <sup>3</sup>	Robert L. Sierakowski
Shu-Jin Fang	Jacky Mazars <sup>3</sup>	Wimal Suaris <sup>1</sup>
Walter Gerstle	Sidney Mindess	Stuart E. Swartz <sup>1,2</sup>
Neil M. Hawkins	Antoine E. Naaman <sup>1</sup>	Tatsuya Tsubaki
Hideyuki Horii <sup>1</sup>	C. Dean Norman	C. Vipulanandan <sup>1</sup>
Jeremy Isenberg	Phillip A. Pfeiffer	Methi Wecharatana <sup>1</sup>

The committee wishes to recognize the contributions of the following non-voting members:

Farhad Ansari <sup>1</sup>	Arne Hillerborg <sup>1</sup>	Pere C. Prat <sup>1</sup>
Ravindra Gettu <sup>3</sup>	B. L. Karihaloo <sup>1</sup>	Hans W. Reinhardt <sup>1</sup>

<sup>1</sup>Members of Subcommittee I (chaired by Bažant) which prepared the report

<sup>2</sup>Principal Authors

<sup>3</sup>Contributing Authors

\*This report was approved by a vote of the full ACI Committee 446 in December 1989. It does not reflect research after that date.

## SYNOPSIS

In the first of its series of four state-of-the-art reports under preparation, the Committee describes the basic concepts of fracture mechanics of concrete, the existing theoretical models, and the methods for determining the material fracture parameters. Chapter 1 offers five reasons for introducing fracture mechanics into certain aspects of design of concrete structures, including some code provisions: (1) a theoretical energy argument; (2) the need to achieve objectivity of finite element solutions, i.e., eliminate spurious mesh sensitivity; (3) the progressive (propagating) nature of failure, implied whenever the load-deflection diagram lacks a yield plateau; (4) the need to rationally predict ductility and energy absorption capability; and most importantly, (5) the effect of structure size on the nominal strength (i.e., nominal stress at maximum or ultimate load) as well as on ductility and energy absorption capability. The size effect is due to stored energy release into the fracture front, and is not governed by Weibull-type statistical theory. Experimental evidence on the existence of the size effect, hitherto ignored in design practice and code provisions, is documented.

Chapter 2 gives a brief review of the necessary basic results of linear elastic fracture mechanics (LEFM). In concrete, departures from this classical theory are caused by the existence of distributed cracking (or damage) in a progressively softening fracture process zone which surrounds the tip of a continuous crack. In Chapter 3 nonlinear fracture models characterizing the softening stress-displacement or stress-strain relations (such as those of Hillerborg's fictitious crack model, crack band model, nonlocal strain-softening models, etc.) are described and random particle simulation of aggregate microstructure is discussed. The principles of implementation of these models in finite element programs are also outlined. Chapter 4 presents simpler nonlinear fracture models which represent adaptations of linear elastic fracture mechanics, such as Jenq and Shah's model and the R-curve, along with determination of geometry-dependent R-curves from the size effect law proposed by Bažant. This law, describing the approximate dependence of the nominal stress at maximum load on structure size, is discussed in Chapter 5, and structural response is characterized by the brittleness number.

Chapter 6 presents in considerable detail the current methods for experimental and analytical determination of material fracture parameters, including the quasi-LEFM methods, RILEM (work-of-fracture) method, the Jenq-Shah and Karihaloo-Nallathambi methods, and the size-effect method. Experimental determination of the characteristic length for nonlocal continuum models and the strain-softening properties is then examined, and material parameters for modes II and III, shear fractures and mixed mode fracture are also discussed. Chapter 7 then proceeds to describe various influencing factors, such as the loading rate, humidity and temperature, as well as the effect of cyclic loading. Chapter 8 is devoted to the effect of reinforcing bars and their bond slip on fracture propagation, and to fracture of fiber-reinforced concrete. Chapter 9 deals with more theoretical problems of modeling systems of interacting cracks. Attention is focused on systems of parallel growing cracks. Their stability decides the spacing and width of the cracks from the mechanics viewpoint.

It is concluded that, after a decade of rapid progress in research, the time appears ripe for introducing fracture mechanics into design practice. This should not only bring about more uniform safety margins, thus improving safety and economy of design, but also pave the way for safer and more efficient use of high-performance concretes and permit design extrapolations beyond the range of previous experiments and design.

**KEYWORDS:** Brittleness, concrete, concrete structures, crack spacing and width, cracking, damage mechanics, design codes, ductility, failure, fiber-reinforced concrete, nonlocal continuum models, reinforced concrete, size effect, strain softening, structural design, testing methods, ultimate loads.

## Introduction

Concrete structures are full of cracks. Failure of concrete structures typically involves stable growth of large cracking zones and the formation of large fractures before the maximum load is reached. Yet design is not based on fracture mechanics, even though the basic fracture mechanics theory has been available since the middle of this century. So why has not fracture mechanics been introduced into concrete design? Have concrete engineers been guilty of ignorance? Not at all. The forms of fracture mechanics which were available until recently were applicable only to homogeneous brittle materials such as glass, or to homogeneous brittle-ductile metals. The question of applicability of these classical theories to concrete was explored long ago – the idea of using the stress intensity factor appeared already in the early 1950's (e.g., Bresler and Wollack, 1952) and serious investigations started in the 1960's (e.g., Kaplan, 1961, and others). But the answer was, at that time, negative (e.g., Kesler, Naus and Lott, 1971). As is now understood, the reason was that in concrete structures one must take into account strain-softening due to distributed cracking, localization of cracking into larger fractures prior to failure, and bridging stresses at the fracture front. A form of fracture mechanics that can be applied to such structures has been developed only during the last decade.

Concrete design has already seen two revolutions. The first, which made the technology of concrete structures possible, was the development of the elastic no-tension analysis during 1900-1930. The second revolution, based on a theory conceived chiefly during the 1930's, was the introduction of plastic limit analysis, which occurred during 1940-1970. There are good reasons to believe that the introduction of fracture mechanics into the design of concrete structures, both reinforced and unreinforced, might be the third major revolution. The theory, formulated mostly during the last dozen years, finally appears to be ripe.

Fracture researchers have at the present no doubt that the introduction of fracture mechanics into the design criteria for all brittle failures of reinforced concrete structures (such as diagonal shear, punching shear, torsion or pull out, or for concrete dams), can bring about significant benefits. It will make it possible to achieve more uniform safety margins, especially for structures of different sizes. This, in turn, will improve economy as well as structural reliability. It will make it possible to introduce new designs and utilize new concrete materials. Fracture mechanics will be particularly important for high strength concrete structures, fiber-reinforced concrete structures, concrete structures of unusually large sizes, and for prestressed structures. The application of fracture mechanics is most urgent for structures such as concrete dams and nuclear reactor vessels or containments, for which the safety concerns are particularly high and the consequences of a potential disaster enormous.

Surveys of concrete fracture mechanics have recently been prepared by various committees (Wittmann, 1983, and Elfgren, 1989). However, due to the rapidly advancing research, the contents of the present state-of-the-art report are quite different. A unified, systematic presentation, rather than a compilation of all the contributions by various authors, is attempted in the present state-of-the-art report. The report is aimed primarily at researchers, not necessarily specialists in fracture mechanics. However, it should also be of interest to design

engineers because it describes a theory that is likely to profoundly influence the design practice in the near future. Subsequent reports dealing with applications in design, finite element analysis of fracture, and dynamic fracture analysis, are in preparation by ACI Committee 446.

## Chapter 1. WHY FRACTURE MECHANICS?

Fracture mechanics, in a broad sense, is a failure theory which (1) uses energy criteria, possibly in conjunction with strength criteria, and (2) which takes into account failure propagation through the structure.

### 1.1 Five Reasons for Fracture Mechanics Approach

Since concrete structures have been designed and successfully built according to codes which totally ignore fracture mechanics theory, it might seem unnecessary to change the current practice. Nevertheless, there are five compelling reasons for doing so.

#### Reason 1: Energy Required for Crack Formation

From the strictly physical viewpoint, it must be recognized that while crack initiation may depend on stress, the actual formation of cracks requires a certain energy – the fracture energy – which represents the surface energy of a solid. Hence, energy criteria should be used. This argument might suffice to a physicist but not a designer. But there are other reasons.

#### Reason 2: Objectivity of Calculations

Any physical theory must be objective in the sense that the result of calculations made with it must not depend on subjective aspects such as the choice of coordinates, the choice of mesh, etc. If a theory is found to be unobjective, it must be rejected. There is no need to even compare it to experiments. Objectivity comes ahead of experimental verification.

A powerful approach to finite element analysis of concrete cracking is the concept of smeared cracking, introduced by Rashid (1968). According to this approach, the stress in a finite element is limited by the tensile strength of the material,  $f'_t$ , and after reaching this strength limit, the stress in the finite element must decrease. As initially practiced, the stress was assumed to decrease suddenly to zero, in a vertical drop; but soon it was realized that better and more realistic results are usually obtained if the stress is reduced gradually, i.e., the material is assumed to exhibit strain-softening (Scanlon, 1971; Lin and Scordelis, 1975); see Fig. 1.1a. The concept of strain-softening, though, proved to be a mixed blessing. After strain-softening had been implemented in large finite element programs and widely applied, it was discovered that the convergence properties are incorrect and the calculation results are not objective with regard to the analyst's choice of the mesh, i.e., the results significantly change if the mesh is refined (Bažant, 1976, 1982; Bažant and Cedolin, 1979, 1980, 1983; Bažant and Oh, 1983a; Darwin, 1985; Rots, Nauta, Kusters and Blaauwendraad, 1985). Similar problems are encountered when cracking is modeled as discrete interelement cracks,

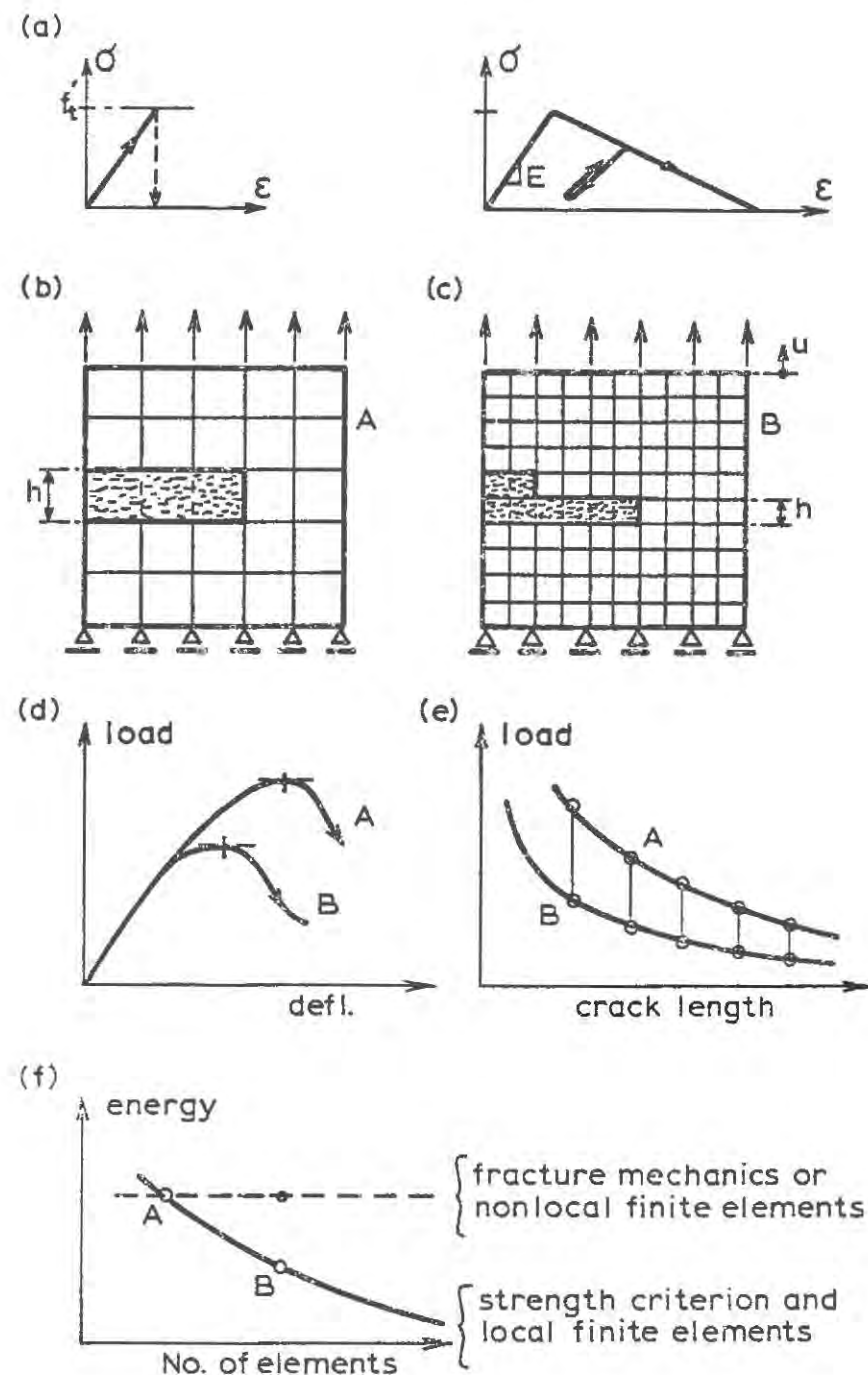


Fig.1.1 Spurious Mesh Sensitivity

based on the strength concept (this approach was introduced into finite element analysis by Clough, 1962, and by Ngo and Scordelis, 1967).

The problem of spurious mesh sensitivity can be illustrated, for example, by the rectangular panel in Fig. 1.1b and c, which is subjected to a uniform vertical displacement at the top boundary. A small region near the center of the left side is assumed to have a slightly smaller strength than the rest of the panel, and consequently a smeared crack band starts growing from left to right. The solution is obtained by incremental loading with two finite element meshes of very different mesh sizes as shown. By stability checks it is found that the cracking must always localize into a band of single element width at the cracking front (Fig. 1.1b,c). The typical numerical results for this, as well as various other problems are illustrated in Fig. 1.1d,e,f. In the load-deflection diagram (Fig. 1.1d), it is seen that the peak load as well as the post-peak softening is strongly dependent on the mesh size, being roughly proportional to  $h^{-1/2}$  where  $h$  is the element size. Plotting the load (reaction) versus the length of the crack band, large differences are again found (Fig. 1.1e).

The energy which is dissipated due to cracking decreases with the refinement of the finite element mesh (Fig. 1.1f) and converges to 0 as  $h \rightarrow 0$ .

The foregoing unobjectivity is physically unacceptable. The only way to avoid it is some form of fracture mechanics. By specifying the energy dissipated by cracking per unit length of the crack or the crack band, the overall energy dissipation is forced to be independent of the element subdivision (the horizontal dashed line in Fig. 1.1f), and so is the maximum load.

### Reason 3: Lack of Yield Plateau

Based on load-deflection diagrams, one may distinguish two basic types of structural failure: plastic and brittle. The typical characteristic of plastic failure is that the structure develops a single-degree-of-freedom mechanism such that failure in various parts of the structure proceeds simultaneously, in proportion to a single parameter. Such failures are manifested by the existence of a long yield plateau on the load-deflection diagram (Fig. 1.2a). If the load-deflection diagram does not have such a plateau, the failure is not plastic but brittle (or brittle-ductile) (Fig. 1.2b). If there are no significant geometric effects such as the  $P-\Delta$  effect in buckling, the absence of a plateau implies the existence of softening in the material due to fracture, cracking or other damage; it implies that the failure process cannot develop a single degree-of-freedom mechanism but consists of propagation of the failure zone throughout the structure. So the failure is non-simultaneous and propagating.

To illustrate this behavior, consider the punching shear failure of a slab (Fig. 1.3). The typical (approximate) distributions of tensile stress  $\sigma$  along the failure surface are drawn in the figure. If the material is plastic, the cross section gradually plasticizes until all its points are at the yield limit. However, if the material exhibits softening, then the stress peak moves across the failure zone, leaving a reduced stress (softening) in its wake. The stress reduction is mild only if the structure is small, in which case the plastic limit analysis is not so far off. If the structure is large, however, the stress profile develops a steep stress drop behind the peak-stress point, and therefore the limit analysis solutions grossly over-estimate the failure

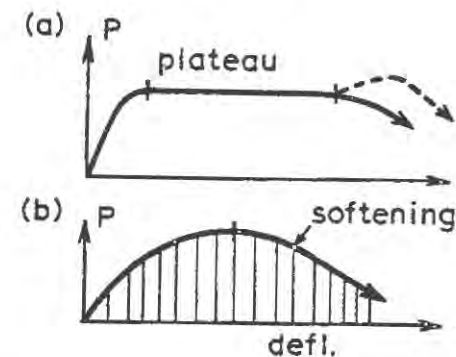


Fig.1.2 Load Deflection Diagram of Ductile and Brittle Structures

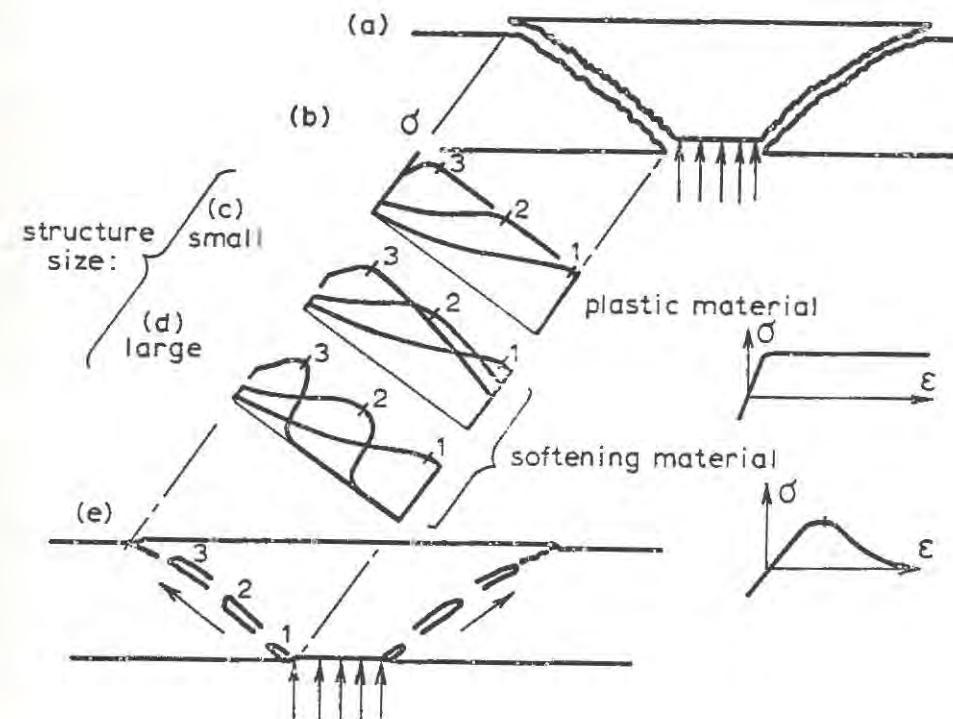


Fig.1.3 Progressive Nature of Failure Illustrated for Punching Shear of a Slab

load.

**Reason 4: Energy Absorption Capability and Ductility**

The area under the entire load deflection diagram represents the energy which the structure will absorb during failure and must therefore be supplied by the loads. Consideration of this energy is important especially for dynamic loading, and determines the ductility of the structure. Plastic limit analysis can give no information on the post-peak decline of the load and the energy dissipated in this process. Some form of fracture mechanics is necessary.

**Reason 5: Size Effect**

The size effect is, for design engineers, probably the most compelling reason for using fracture mechanics, and so a thorough discussion is in order.

The size effect is defined through a comparison of geometrically similar structures of different sizes, and is conveniently characterized in terms of the nominal stress  $\sigma_N$  at maximum (ultimate) load,  $P_u$ . When the  $\sigma_N$ -values for geometrically similar structures of different sizes are the same, we say that there is no size effect. A dependence of  $\sigma_N$  on the structure size (dimension) is called the size effect.

The nominal stress need not represent any actual stress in the structure but may be defined simply as  $\sigma_N = P_u/bd$  when the similarity is two-dimensional, or as  $P_u/d^2$  when the similarity is three-dimensional;  $b$  - thickness of the two-dimensional structure, and  $d$  characteristic dimension of the structure, which may be chosen as any dimension, e.g., the depth of the beam, or its span, since only the relative values of  $\sigma_N$  matter.

According to the classical theories, such as elastic analysis with allowable stress, plastic limit analysis, as well as any other theories which use some type of strength limit or failure criterion in terms of stresses (e.g., viscoelasticity, viscoplasticity),  $\sigma_N$  is constant, that is, independent of the structure size. This may be illustrated, e.g., by considering the elastic and plastic formulas for the strength of beams in bending, shear and torsion (regarding the definition  $\sigma_N = P_u/bd$  for torsion, note that one may set  $P_u = T_u/r$  where  $T_u$  = ultimate torque,  $P_u$  = force acting on an arm,  $r$ , such that  $r/H$  or  $r/a$  is constant for similar structures of different sizes;  $H$  = cross section depth,  $a$  = crack length). It is seen that these formulas are of the same form except for a factor. Thus, if we plot  $\log \sigma_N$  vs.  $\log d$ , the failure states according to a strength or yield criterion are always given by a horizontal line (dashed line in Fig. 1.4). So failures according to strength or yield criteria exhibit no size effect.

By contrast, failures governed by linear elastic fracture mechanics exhibit a rather strong size effect which in Fig. 1.4 is described by the inclined dashed line of slope  $-1/2$ . The reality for concrete structures is a transitional behavior illustrated by the solid curve in Fig. 1.4. This curve approaches the horizontal line for the strength criterion if the structure is very small, and the inclined straight line for linear elastic fracture mechanics if the structure is very large (the precise meaning of "very small" and "very large" will be clarified by Eq. 5.11). This size effect, which is generally ignored by current codes (with a few exceptions), is obviously important in design.

Another size effect which calls for the use of fracture mechanics is effect of size on ductility.

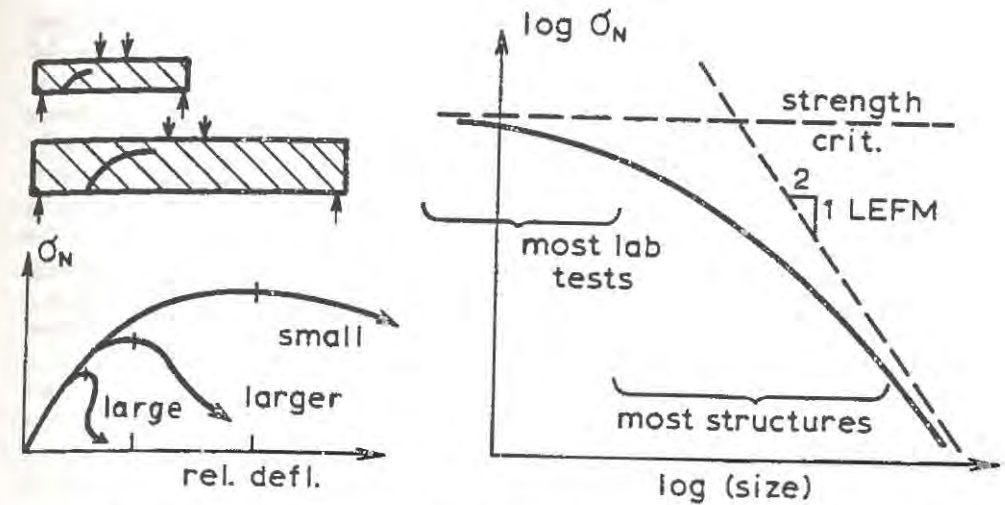


Fig.1.4 Fracture Mechanics Size Effect for Geometrically Similar Structures of Different Sizes

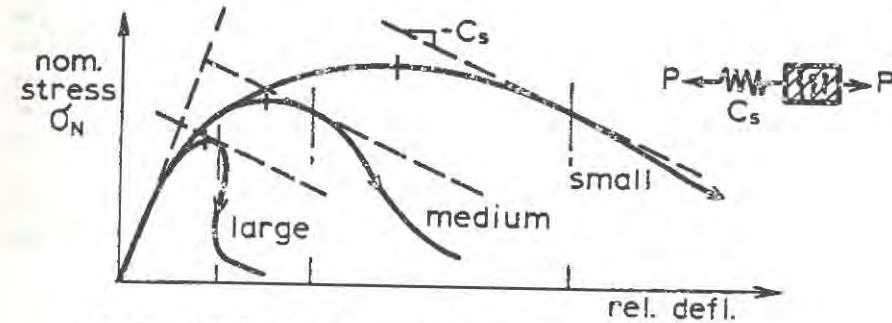


Fig.1.5 Load-Deflection Diagrams of Geometrically Similar Structures of Different Sizes

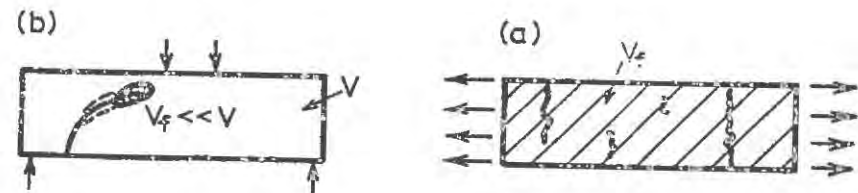


Fig.1.6 Possible Final Fracture Locations Caused by Randomness of Strength

Ductility of a structure may be characterized by the deformation at which the structure fails under a given type of loading. For loading in which the load is controlled, structures fail (become unstable) at their maximum load, while structural elements that are loaded under displacement control (i.e. imposed displacement) or through displacement-controlled elastic devices fail in their post-peak, strain-softening range. In a plot of  $\sigma_N$  versus deflection, the failure point is characterized by a tangent (dashed line in Fig. 1.5) of a certain constant slope  $-C_s$ , where  $C_s$  is the stiffness of the loading device (e.g. Bažant and Cedolin, 1990, Sec. 13.2). Geometrically similar structures of different sizes typically yield curves of the type shown in Fig. 1.5. As illustrated, failure occurs closer to the peak as size increases. This effect is again generally predicted by fracture mechanics, due to the fact that in a larger structure more strain energy is available to drive the propagation of the failure zone. A decrease of ductility of a structure represents an increase in its brittleness.

The well-known effect of structure size or member size on crack spacing and crack width is also explicable by fracture mechanics. The spurious effect of mesh size (Reason 2) can be regarded as a consequence of the structural size effect (this can be shown by considering structures of different size but with the same mesh size, and then scaling all structures to the same size along with the meshes).

## 1.2 Is Weibull's Statistical Theory of Size Effect Applicable?

Traditionally, the size effect has been explained statistically, by randomness of the strength value. The failure load of a chain is determined by the minimum value of the strength of the links in the chain, and the statistical size effect is due to the fact that the longer the chain, the smaller is the strength value that is likely to be encountered in the chain. This explanation, which is certainly correct for the size effect observed in the failure of a long uniformly stressed concrete bar in tension (Fig. 1a), is described by Weibull's weakest link statistics. However, applications of this theory to concrete structures have been overdone and are questionable for the following reason.

According to Weibull-type theory of failure (Weibull, 1939; Zaitsev and Wittmann, 1973; Mihashi and Zaitsev, 1981; and Carpinteri, 1986), the probability of failure of a structure under load  $P$  and the mean nominal stress at failure are:

$$\text{Prob}(P) = 1 - \exp \left\{ - \int_V \left[ \frac{\sigma(P, \mathbf{x})}{\sigma_0} \right]^m \frac{dV(\mathbf{x})}{V_r} \right\} \quad (1.1)$$

$$\bar{\sigma}_N = \frac{\bar{P}}{bd} = \frac{1}{bd} \int_0^\infty [1 - \text{Prob}(P)] dP \quad (1.2)$$

where  $\bar{P}$  = mean load,  $\mathbf{x}$  = coordinate vectors,  $V$  = volume of structure,  $V_r$  = representative volume of material (the smallest volume for which a material with discrete microstructure can be treated as a continuum),  $m$  = Weibull modulus of the material,  $\sigma_0$  = scale parameter.

The key to applications of the Weibull theory is function  $\sigma(P, \mathbf{x})$ , representing the stress caused by load  $P$  at point  $\mathbf{x}$  (for three-dimensional stresses,  $\sigma$  may be regarded as the maximum principal stress). For some structures, such as aircraft wings and metal structures

in general, failure occurs right at the initiation of the macroscopic crack growth. For those structures, function  $\sigma(P, \mathbf{x})$  is known;  $\sigma(P, \mathbf{x}) = Ps_e(\xi)$  where  $\xi = \mathbf{x}/d$  = relative coordinate vectors,  $d$  = characteristic dimension of the structure, and  $s_e(\xi)$  is the elastic stress distribution due to unit load ( $P = 1$ ). The same assumptions have often been implied in various Weibull-type studies of concrete structures.

Concrete structures, however, behave differently. Due to reinforcement as well as the existence of strain-softening in a large zone of microcracking ahead of the tip of a continuous crack, concrete structures do not fail at crack initiation. In fact, design codes require the failure load to be significantly higher than the crack initiation load; for bending, at least 1.25 times higher for unprestressed beams and 1.2 times higher for prestressed beams (according to ACI 318), but in practice this ratio is usually much higher. Consequently, a concrete structure undergoes pronounced inelastic deformation and macroscopic crack growth prior to reaching the failure load. This causes stress redistributions, such that the stress distribution  $\sigma(P, \mathbf{x})$  at failure is very different from the elastic stress distribution  $s_e(\xi)$ .

This distribution is difficult to determine, but the near-tip asymptotic elastic stress field,  $Ps_e(\xi)$ , may be used as an approximation at distances not too far from and not too close to the tip of the macrocrack at the moment of failure. Now, due to singularity of this field, the stress values farther away from the tip of the macrocrack are relatively small and make a negligible contribution to  $\bar{\sigma}_N$  (Eq. 1.2) compared to the stresses in the volume  $V_f$  of the fracture process zone around the tip. This of course reflects the fact that the volume in which the macrocrack tip at failure might be located (as dictated by the laws of mechanics) is very small (e.g. the diagonal shear crack in Fig. 1.6b cannot grow toward the lower midspan region or toward the upper left corner of the beam, regardless of the strength values there).

Consequently, the statistical size effect must be smaller than in a uniformly stressed tensile bar, where failure is precipitated by a macrocrack anywhere within the volume of the bar. Thus, as pointed out by Bažant (1986, 1987a), if one calibrates Weibull parameters  $m$  and  $\sigma_0$  on the basis of uniaxial strength tests and then uses the same parameters to predict  $P_f$  and  $\bar{\sigma}_N$  for diagonal shear failure, one must find the statistical size effect to be rather small. Thus, even though limited test results for diagonal shear failures have been successfully fitted by formulas based on the Weibull distribution, the size effect data for both the diagonal shear failures and the uniaxial failures cannot be successfully fitted using the same material parameters (unless an incorrect elastic stress field  $Ps_e(\xi)$  is used).

Thus, the principal fault of the Weibull-type statistical explanations of the size effect in concrete structures is that they ignore the size effect caused by the redistribution of stress  $\sigma(P, \mathbf{x})$  prior to failure. This size effect, which is of the fracture mechanics type, is associated with the energy release into the front of a large crack and would exist even if the material behavior were deterministic.

Therefore, the proper approach is to fit the size effect data for a concrete structure first by a fracture mechanics theory, and only if some part of the observed size effect remains unaccounted for it may be attributed to Weibull-type statistical phenomena (Bažant, 1986, 1987a).

Weibull theory then describes a size effect of the volume of the structure, expressing the

fact that the larger the volume, the greater is the chance of encountering a critical microscopic flaw that triggers failure. Thus, as far as the load at initiation of cracking (or damage) is concerned, Weibull-type theory is, of course, applicable. Saouridis (1989) demonstrated that by analysis of L'Hermite's tests of size effect in unnotched beams. Indeed, as long as there are no stress redistributions, i.e., all stresses are fixed in their proportion to the load, the interaction of the elements of the structure is mathematically equivalent to a series coupling of elements, the same as in a uniaxially stressed bar of variable cross section. When there are stress redistributions, however, the structure behaves as a combination of series and parallel couplings. But Weibull's theory is valid only for series coupling, as in a chain of elements (hence the term "weakest-link statistics").

### 1.3 Simple Energy Explanation of Size Effect

The fracture mechanics type size effect, which is due to energy release, can be simply explained by considering the uniformly stressed panel with a crack or crack band of initial length  $a = a_0$ , shown in Fig. 1.7. It may be imagined that the formation of a crack band of thickness  $h$  reduces the strain energy density  $\sigma_N^2/2E$  in the cross-hatched area to zero ( $E =$  elastic modulus of concrete). When the crack band extends by  $a$ , the additional strain energy that is released comes from the densely cross-hatched strip of horizontal dimension  $\Delta a$  (Fig. 1.7a). If the failure modes are geometrically similar, as is usually the case, then the larger the panel, the longer is the crack band at failure. Consequently, the area of the densely cross-hatched strip is also larger, being given by  $h\Delta a + 2ka\Delta a$  where  $k =$  empirical constant depending on the shape of the structure. This illustrates that, in a larger structure, more energy is released by the same extension of the crack band. The energy released from the strip is  $-\delta\Pi/\delta a = G_f b$ , i.e.,

$$\frac{1}{\Delta a} (h\Delta a + 2ka\Delta a) \frac{\sigma_N^2}{2E} = G_f b \tag{1.3}$$

where  $\Pi =$  potential energy stored in the structure,  $b =$  thickness and  $G_f =$  fracture energy (dimension  $J/m^2$ ) = energy needed to create a fracture or crack band of unit length and (in the third direction) unit width. The value of  $G_f$  is approximately constant and represents a material property. Solving from Eq. 1.2 for the nominal stress, one obtains the size effect law proposed by Bažant (1984a):

$$\sigma_N = B f_i' (1 + \beta)^{-1/2}, \quad \beta = d/d_0 \tag{1.4}$$

where  $B = (2G_f E b/h)^{1/2} / f_i'$ ,  $d_0 = (h/2k)(d/a)$  = reference size which depends on the shape of the structure but is independent of structure size if the structures are geometrically similar (because  $d/a =$  constant);  $f_i' =$  tensile strength, introduced for convenience; and  $h =$  width of the crack band front, which may be treated approximately as constant, independent of structure size. Empirically,  $d_0 \approx n d_a$  where  $d_a =$  maximum aggregate size and  $n$  is approximately constant when  $d$  or  $d_a$  is varied, but depends on structure geometry. Eq. 1.4 will be discussed more in Chapter 5 and derived in Appendix I.

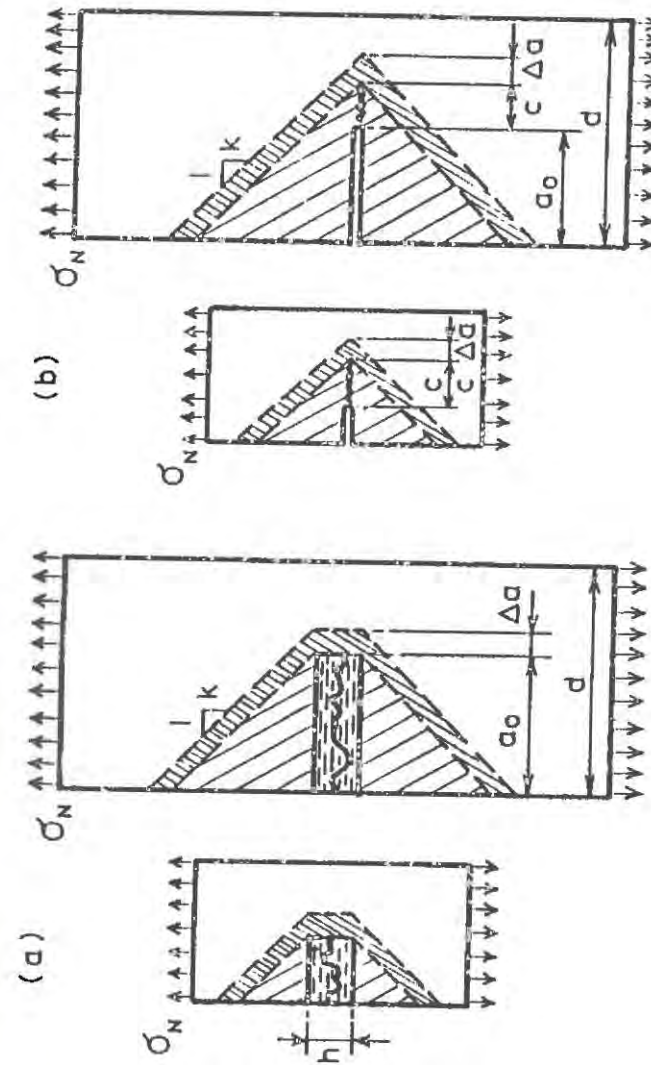


Fig.1.7 Areas of Energy Release in Similar Small and Large Specimens

Lest one might get the impression that this explanation of the size effect works only for a crack band but not for a sharp line crack, consider the same panel with a line crack of length  $a_0$  shown in Fig. 1.7b for similar panels of different sizes. In concrete, there is always a sizeable fracture process zone ahead of the tip of a continuous crack, of some finite length which may, in the crudest approximation, be considered constant. Over the length of this zone, the transverse normal stress gradually drops from  $f'_t$  to 0. Because of this zone, the elastically equivalent crack length which causes the release of strain energy from the adjacent material is longer than the continuous crack length,  $a$ , by a distance  $c$  which is approximately a material constant. (Strictly speaking,  $c$  varies, but much less than in proportion to the size. Anyway, a more involved derivation in which  $c$  is variable yields the same result, and will be indicated just before Eq. 5.5.)

When the crack extends by length  $\Delta a$ , the fracture process zone travels with the crack-tip, and the area from which additional strain energy is released consists of the strips of horizontal dimension  $\Delta a$  which are densely cross-hatched in Fig. 1.7b. Their area is  $k(a_0 + c)\Delta a$  where  $k$  is approximately a constant. The energy released per unit crack advance,  $-\delta\Pi/\delta a$ , must equal to  $G_f b$  where  $G_f$  = the fracture energy of the material, and so

$$\frac{1}{\Delta a} 2k(a_0 + c)\Delta a \frac{\sigma_N^2}{2E} = G_f b \quad (1.5)$$

Solving this equation for  $\sigma_N$ , one again obtains the size effect law in Eq. 1.4 in which now  $B = (EG_f b/kc)^{1/2}/f'_t$ ,  $d_0 = c(d/a) = \text{constant}$ .

Eq. 1.4, which describes the transitional size effect given by the solid curve in Fig. 1.4, is also obtained for various other structural geometries. For large sizes, the curve of Eq. 1.4 in Fig. 1.4 approaches a straight line of slope  $-1/2$ , which represents the size effect of linear elastic fracture mechanics (see Sec. 1.2).

Eq. 1.4 can also be derived, in a completely general way, by dimensional analysis and similitude arguments (Bažant, 1984a). This general derivation rests on two basic hypotheses: (1) the propagation of a fracture or crack band requires an approximately constant energy supply (the fracture energy,  $G_f$ ) per unit area of fracture plane, and (2) the potential energy released by the structure due to the propagation of the fracture or crack band is a function of both the fracture length and the size of the fracture process zone at the fracture front.

It must be kept in mind that Eq. 1.4 is approximate, valid only within a size range of about 1:20 (i.e., the largest structure for which Eq. 1.4 can be applied is about 20 times larger than the smallest structure). For a broader size range, a more complicated formula would be required. Nevertheless, the aforementioned size range is sufficient for most practical purposes.

The main problem with the Weibull-type statistical theory for the size effect is that the existing works ignore stress redistributions and the consequent energy release from the structure (as illustrated in Fig. 1.7 and manifested by the size effect law). The statistical size effect should properly appear only as an addition to the fracture mechanics type size effect (which is deterministic), and would have to describe only that part of the size effect which is not explained by the fracture mechanics size effect. So far, such comparisons have

not indicated any large systematic deviations which would require some other explanation, such as statistical.

Applications of Eq. 1.4 to brittle failures of concrete structures rest on two additional hypotheses: (3) the failure modes of geometrically similar structures of different sizes are also geometrically similar (e.g., a diagonal shear crack has at failure about the same slope and the same relative length), and (4) the structure does not fail at crack initiation (which is a requirement of good design). These hypotheses are usually applicable, but not always over the entire size range of interest. A sufficiently large change of size may alter the failure mode and thus render Eq. 1.4 inapplicable beyond that size. (This apparently is the case for the brazilian split cylinder tests.)

## 1.4 Experimental Evidence for Size Effect in Structures

Extensive tests have been carried out to verify Eq. 1.4 for various types of failure of concrete structures (using microconcrete specimens). Good agreement of Eq. 1.4 with test results has been demonstrated for:

1. Diagonal shear failure of beams (Bažant and Cao, 1986b; Bažant and Kazemi, 1989a).
2. Punching shear failure of slabs (Bažant and Cao, 1987).
3. Torsional failure of beams (Bažant, Sener and Prat, 1987).
4. Pullout failure of reinforcing bars (Bažant and Sener, 1988).
5. Double-punch tests of cylinders (Marti, 1989).

Typical experimental results, which can be regarded as a verification of the applicability of fracture mechanics to the brittle failures of concrete structures, are shown in Fig. 1.8-1.11 (tests made at Northwestern University on microconcrete specimens with aggregate of maximum diameter 3/8 in. or 1/4 in.). As further evidence of applicability of fracture mechanics, Fig. 1.12 shows, for the punching shear failure, that the post-peak load drop becomes steeper and larger as the size increases. This is because in a larger specimen there is (for the same  $\sigma_N$ ) more energy to be released into a unit crack extension, but since the fracture extension dissipates the same amount of energy, the value of  $\delta_N$  (and thus the load) must be reduced as the structure size increases.

Note also that the shape of the measured size effect curves (Fig. 1.8-1.11) does not really agree with the Weibull-type statistical model, for which the slope of the curve would have to diminish rather than increase with increasing size and approach a horizontal asymptote.

The existing test data on concrete specimens with regular-size aggregate reported in the literature also offer evidence of size effect, and the need of a fracture mechanics based explanation has been pointed out by various researchers, e.g., Reinhardt (1981a, 1981b) or Bažant and Kim (1984). The data from the literature are generally found to agree with Fig. 1.4, but this evidence is not very strong because the data exhibit very large statistical

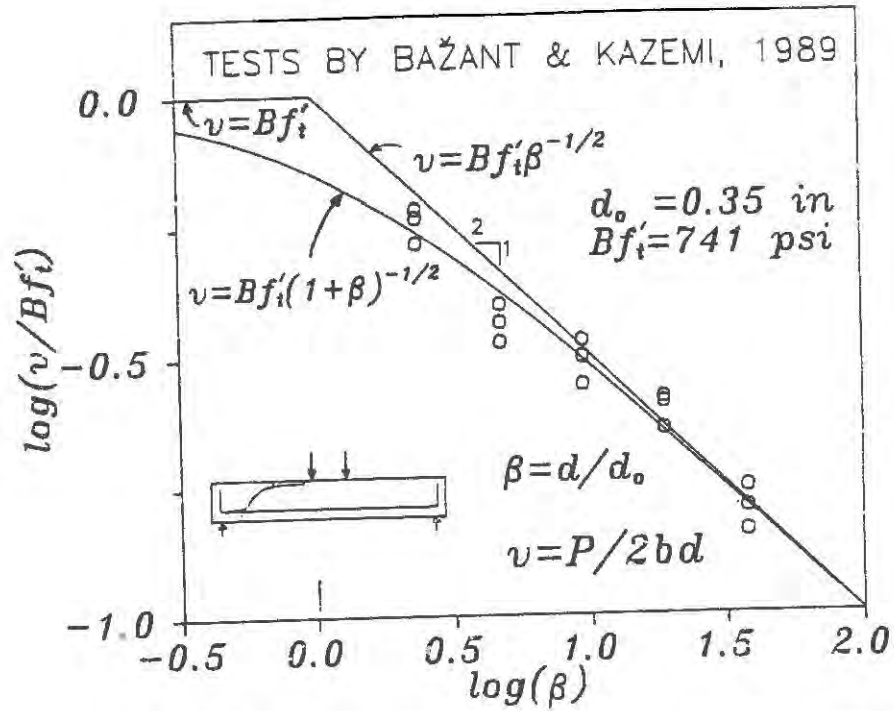


Fig.1.8 Test Results (Bažant and Kazemi, 1989a) on Size Effect in Diagonal Shear Failure;  $v$  is the nominal shear strength

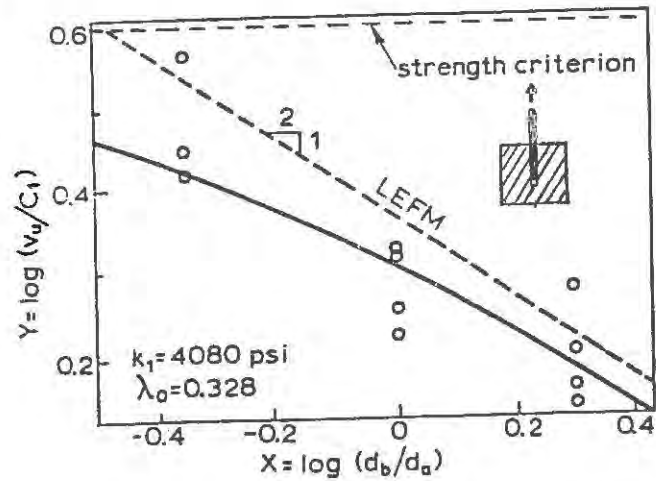


Fig.1.9 Test Results (Bažant and Sener, 1988) on Size Effect in Pull-out Failure of Bars ( $d_b$  = bar diameter,  $v_u$  = nominal pullout strength,  $C_i$ ,  $K_i$  and  $\lambda_0$  = empirical constants)

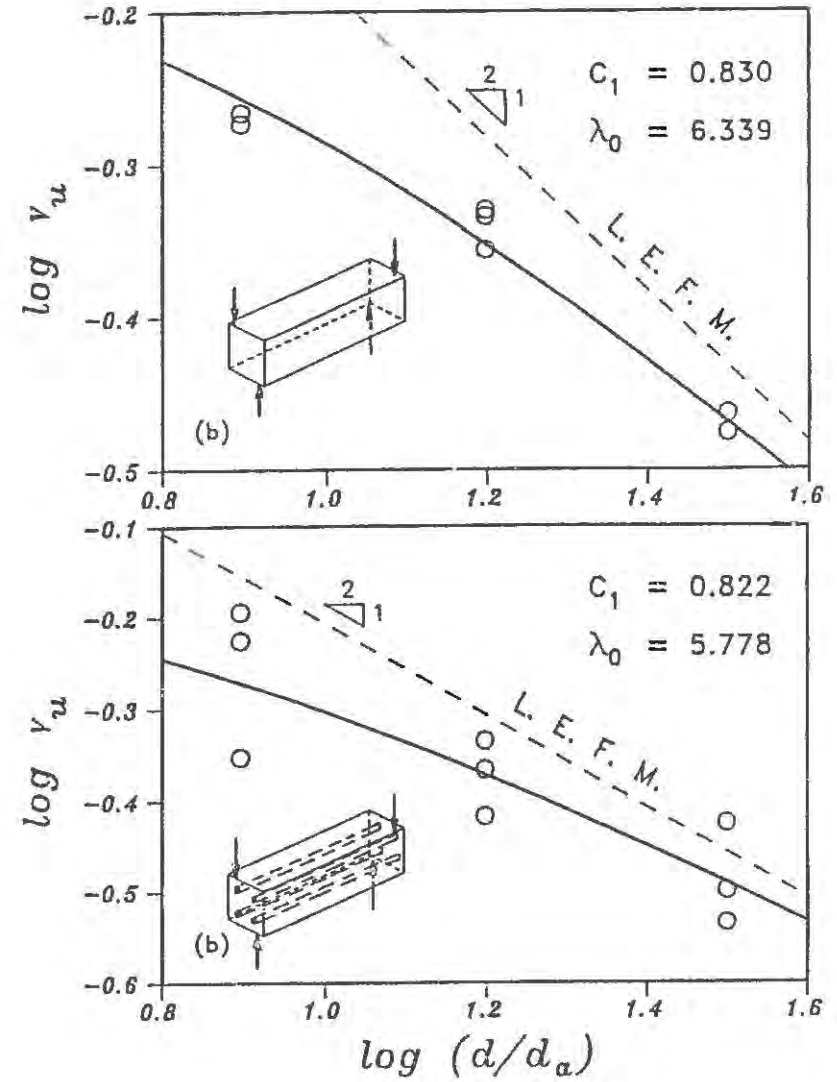


Fig.1.10 Test Results (Bažant, Sener and Prat, 1989) on Size Effect in Torsional Failure of Plain and Reinforced Beams ( $d$  = depth of beam,  $v_u$  = nominal torsional strength,  $c_i$ ,  $\lambda_0$  = empirical constants)

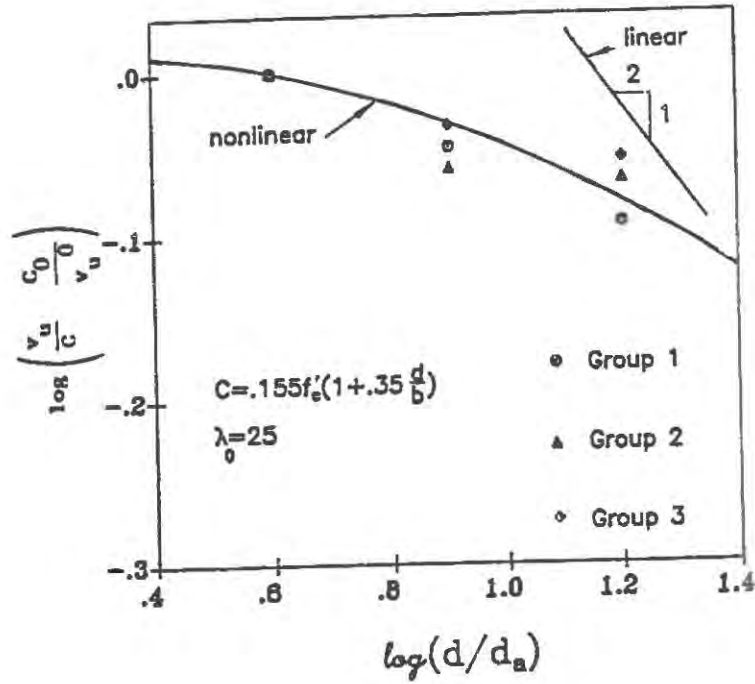


Fig.1.11 Test Results (Bažant and Cao, 1987) on Size Effect in Diagonal Shear Failure in Slabs ( $v_u$  = nominal shear strength,  $d$  = slab thickness,  $b$  = punch diameter,  $v_u^0$  and  $c_0 = v_u$  and  $C$  for smallest slab,  $\lambda_0$  = empirical constants)

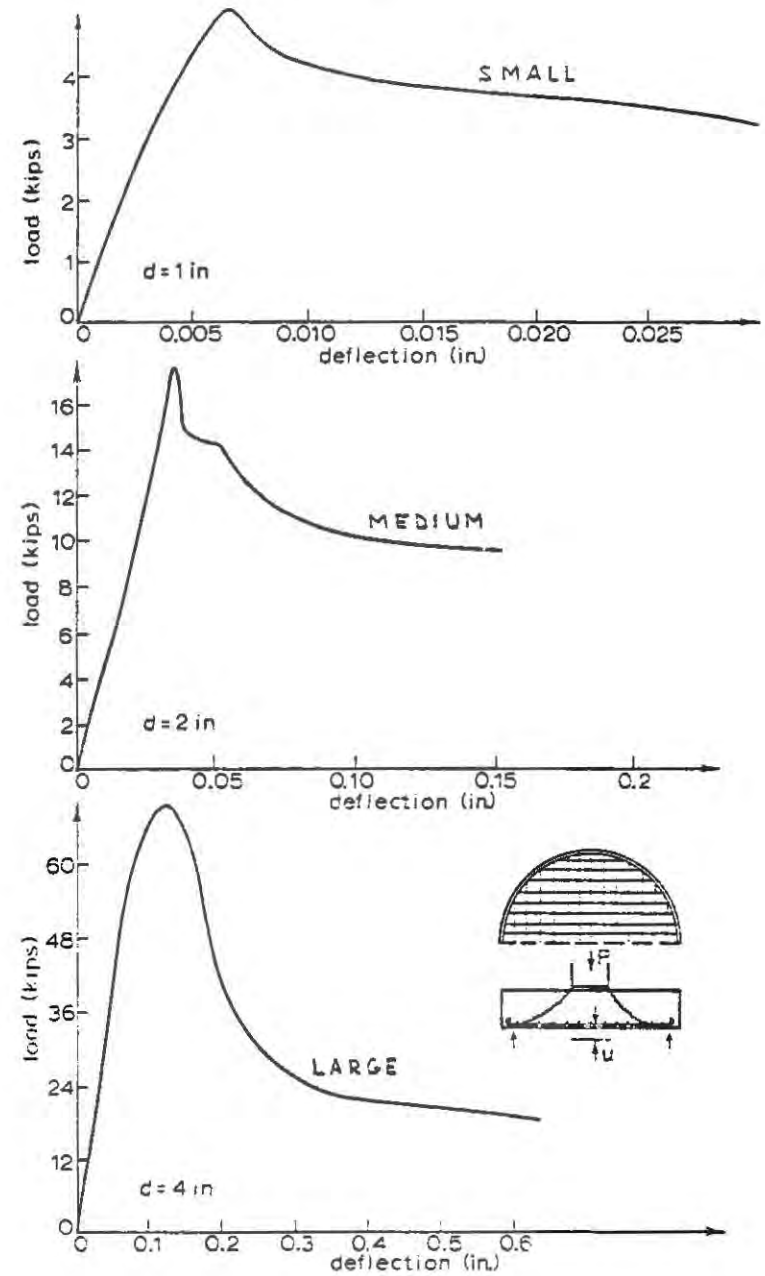


Fig.1.12 Measured Load-Deflection Diagrams of Small, Medium and Large Slabs (Bažant and Cao, 1987)

scatter. Due to scatter, about equally good fits can be obtained with other theories of size effect, e.g., Weibull's statistical theory. Although part of the scatter is inevitable and random, most of the huge scatter observed in brittle failures such as diagonal shear probably stems from the fact that the test specimens of various sizes were not geometrically similar, and so theoretical adjustments must be made for the factors of shape before a comparison with Eq. 1.4 can be made. Since the exact theory is not known, such adjustments introduce additional errors. In addition to the structures listed above, available comparisons with test data also include the beam and ring failures of unreinforced pipes (Gustafson and Hillerborg, 1984; Bažant and Cao, 1986a). Comparisons with the bulk of test data available in the literature were made for diagonal shear failures of both unprestressed and prestressed beams, and beams without and with stirrups (Bažant and Kim, 1984; Bažant and Sun, 1987; Bažant and Cao, 1986b), as well as torsional failures (Bažant and Sener 1987). Statistical analysis was included in these studies.

### 1.5 Explanation of Size Effect on Ductility

Structural action is normally a combination of series and parallel couplings of the cracking zones and the uncracked (elastic) zones. The size effect on ductility is explained by the series coupling aspect. Consider a cracking element coupled with an elastic element as shown in Fig. 1.13. The load-displacement diagrams of these elements are also shown. Since the force in both elements is the same and the deformations are superimposed, the response of both elements combined is obtained by passing a horizontal line at each level  $P$  and summing the corresponding deformations  $a$  and  $b$ , as shown in Fig. 1.13. If the elastic element is sufficiently soft, this can obviously produce a load-displacement diagram which exhibits the so-called snapback, in which the displacement diagram turns back at a positive slope. The snapback behavior is unstable even under displacement control, and the structure fails at the maximum displacement, labeled as  $u_{cr}$ . This displacement represents a ductility limit for the system. Since the addition of an elastic element is equivalent to increasing the size of the structure, it is clear that an increase of size tends to decrease ductility. Ductility is not a material property but a structure property which is governed by fracture mechanics and depends on structure size (as well as the type of concrete). It is worth noting that Hawkins (1984) identified twenty-nine provisions in the ACI Code which seem to be empirical but could probably be explained by fracture mechanics. They include various ductility limitations, conditions for minimum reinforcement, crack spacing and crack width, etc.

To sum up, the experimentally observed structural size effect, as well as the related spurious effect of the mesh size, presents the most potent argument for the application of fracture mechanics to concrete structures.

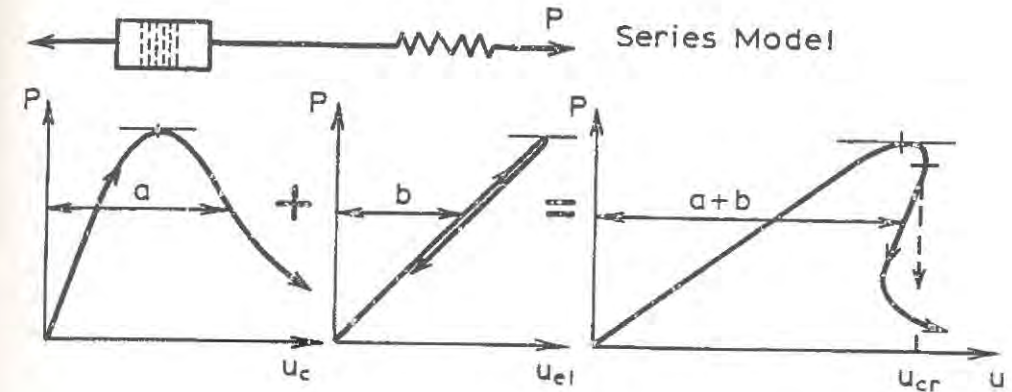


Fig.1.13 Change in Post-Peak Load-Deflection Diagram Due to Series Coupling with Elastic Element

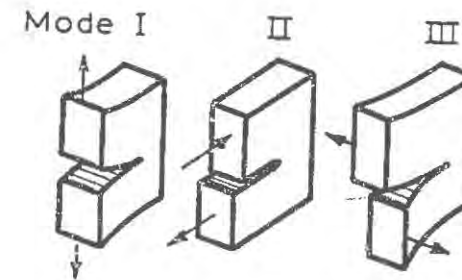


Fig.2.1 Modes I, II and III (Opening, Plane Shear, Anti-Plane Shear Fractures)

## Chapter 2. ESSENTIAL RESULTS FROM LINEAR ELASTIC FRACTURE MECHANICS

In linear elastic fracture mechanics (LEFM) it is assumed that all of the fracture process happens at the crack tip and that the entire volume of the body remains elastic. Under this assumption, the questions of crack propagation and structural failure can be solved by methods of linear elasticity.

It is convenient to distinguish three elementary fracture modes, Modes I, II and III, also called the opening mode, the planar shear mode and the antiplane shear mode; see Fig. 2.1. Modes I and II are planar symmetric and antisymmetric, while Mode III is three-dimensional. General fracture is a linear combination of these three modes.

### 2.1 Stress Singularity

Introduction of a crack into a linear elastic body produces stress concentrations near the crack tips. This may be illustrated by the perturbation of the trajectories of the maximum principal stress shown in Fig. 2.2. The stress field is singular at the crack tip, with all the nonzero stress components approaching infinity as the radial distance  $r$  from the crack tip tends to zero (Fig. 2.3). In a sufficiently close neighborhood of the sharp crack tip, the stress components  $\sigma_{ij}$  are the same regardless of the shape of the body and the manner of loading, and may be expressed as:

$$\sigma_{ij}^I = K_I f_{ij}^I(\theta)(2\pi r)^{-1/2}, \sigma_{ij}^{II} = K_{II} f_{ij}^{II}(\theta)(2\pi r)^{-1/2}, \sigma_{ij}^{III} = K_{III} f_{ij}^{III}(\theta)(2\pi r)^{-1/2} \quad (2.1)$$

Here the subscripts and superscripts I, II and III refer to the elementary modes,  $\theta$  is the polar angle,  $K_I$ ,  $K_{II}$  and  $K_{III}$  are parameters called the stress intensity factors, and functions  $f_{ij}^I$  are the same regardless of the body geometry and the manner of loading. For example,  $f_{11}^I(\theta) = \cos \alpha(1 - \sin \alpha \sin 3\alpha)$ ,  $f_{22}^I(\theta) = \cos \alpha(1 + \sin \alpha \sin 3\alpha)$ ,  $f_{12}^I(\theta) = \cos \alpha \sin 2\alpha \cos 3\alpha$ , where  $\alpha = \theta/2$ ; see e.g., Knott (1973), Broek (1974), Owen and Fawkes (1983), Hellan (1984), and Kanninen and Popelar (1985).

### 2.2 Energy Criterion

The fact that, according to the theory of elasticity, the stress near the crack tip approaches infinity, no matter how small the load, was noted by Griffith (1921, 1924) on the basis of the previous solution for elliptical holes by Inglis (1913). He concluded that, if linear elasticity is used, one cannot introduce a strength criterion as a condition of failure, but must instead decide failure on the basis of an energy criterion. As the crack tip propagates, energy flows into the crack tip where it is dissipated by the fracture process. The energy flow is characterized by the energy release rate which is expressed as:

$$G_b = -\frac{\partial \Pi(a)}{\partial a} \approx -\frac{1}{\Delta a} \left[ \Pi\left(a + \frac{\Delta a}{2}\right) - \Pi\left(a - \frac{\Delta a}{2}\right) \right] \quad (2.2)$$

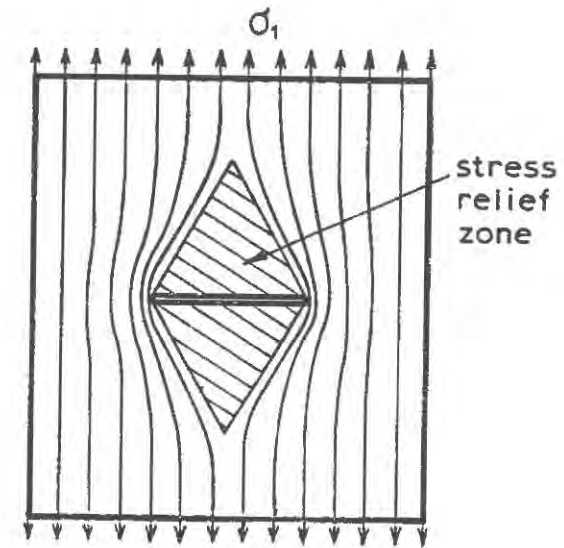


Fig.2.2 Principal Stress Trajectories in a Cracked Specimen

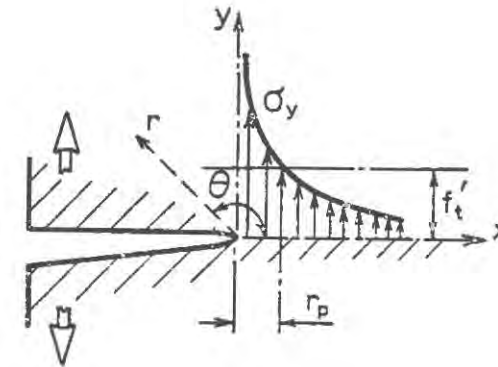


Fig.2.3 Stress Distribution Near Crack Tip

in which  $\Pi = U - W =$  potential energy of the structure,  $W =$  work of loads, and  $U =$  strain energy of the structure as a function of the crack length  $a$ . Eq. 2.2 also gives a finite difference approximation which may be used to calculate  $G$  by the finite element method. For that purpose one may model the crack as a line gap between adjacent elements and calculate the strain energy stored in the mesh for the crack tip displaced by either  $-\Delta a/2$  or  $\Delta a/2$ . Instead of using an interelement line crack, one may, for the sake of convenience, model the crack by considering a band of elements to have zero stiffness (if one uses a mesh of square elements whose size is not more than about 0.1 of the cross section dimension, the error of considering a crack band instead of a line crack is usually less than 1%; see Bažant and Cedolin, 1979).

According to Griffith, the condition of crack propagation (critical state) is

$$G = G_f \quad (2.3)$$

$G$  is the fracture energy, which has the dimension of  $J/m^2$  (or  $N/m$ ) and represents a basic material property. For  $G < G_f$ , the crack cannot propagate, and for the case  $G > G_f$  equilibrium is impossible. If  $G = G_f$  and  $\partial G/\partial a > 0$ , which is normally the case, the crack is unstable under load control (i.e., the structure fails). There exist, however, some cases in which  $G = G_f$  and  $\partial G/\partial a < 0$ , and then the crack can grow under load control in a stable manner.

The energy release rate for modes I, II and III may be expressed on the basis of the stress intensity factors as follows:

$$G_I = K_I^2/E', \quad G_{II} = K_{II}^2/E', \quad G_{III} = K_{III}^2/\mu \quad (2.4)$$

in which  $\mu =$  elastic shear modulus, for the case of plane stress  $E' = E =$  Young's elastic modulus, for the case of plane strain  $E' = E/(1 - \nu^2)$ , and  $\nu =$  Poisson's ratio. For general loading, the total energy release rate is:

$$G = G_I + G_{II} + G_{III} \quad (2.5)$$

The stress intensity factors are proportional to the applied load, and may generally be expressed in the form:

$$K_I = \frac{P}{bd} \sqrt{\pi a} f(\alpha) = \frac{P}{bd} \sqrt{d} \varphi(\alpha), \quad \alpha = a/d \quad (2.6)$$

in which  $f$  is a certain nondimensional function of the relative crack length  $\alpha$  ( $d =$  characteristic structure dimension), and  $\varphi(\alpha) = f(\alpha)\sqrt{\pi a} =$  another non-dimensional function. For various simple geometries of notched fracture specimens, accurate expressions for function  $f$  are available in textbooks and handbooks (e.g., Tada et al., 1985, and Murakami, 1987). For other geometries, the function  $f$  can always be calculated by linear elastic analysis; e.g., through a finite element program. For the special case of a single line crack of length  $a$  in an infinite solid subjected at infinity to nominal stress  $\sigma_N$  in the direction normal to the crack plane, one has  $f(\alpha) = 1$ . Eq. 2.6 shows that, for geometrically similar structures of different

sizes, the stress intensity factor is proportional to the square root of the size, and the energy release rate is proportional to the size of the structure.

Instead of Eq. 2.3, the condition of mode I crack propagation (critical state) can be expressed in terms of the stress intensity factor as:

$$K_I = K_{Ic} \quad (2.7)$$

in which  $K_{Ic} =$  critical value of  $K_I$ , which is also called fracture toughness and represents a material property;  $K_{Ic} = G_f E'$ . If Eq. 2.7 is substituted into Eq. 2.6, the nominal stress at failure (crack propagation) is obtained as:

$$\sigma_N = \frac{K_{Ic}}{\sqrt{\pi a} f(\alpha)} = \frac{K_{Ic}}{\sqrt{d} \varphi(\alpha)} \quad (2.8)$$

It may be noted that, according to Eq. 2.8,

$$\log \sigma_N = -\frac{1}{2} \log d + \text{const.} \quad (2.9)$$

This relation shows that the size effect plot according to linear elastic fracture mechanics is an inclined straight line of slope  $-1/2$  (Fig. 1.4).

## 2.3 Limits of Applicability

In reality, the fracture process cannot take place at a point. The fracture process zone must have some finite size. According to Irwin (1958), a crude estimate of the length  $r_f$  of the fracture process zone may be obtained by setting the transverse normal stress in Eq. 2.1 to be equal to the tensile strength  $f_t'$ . This yields

$$r_f = \frac{1}{2\pi} \frac{K_{Ic}^2}{f_t'^2} = \frac{\ell_0}{2\pi}, \quad \ell_0 = \frac{K_{Ic}^2}{f_t'^2} = \frac{E' G_f}{f_t'^2} \quad (2.10)$$

Note that this length is expressed only in terms of material properties, and therefore is a material property, too. An alternative estimate of the size of the fracture process zone of concrete can be based on the maximum aggregate size  $d_a$ . Bažant and Oh (1983a) concluded that the length and effective width of the fracture process zone of concrete in three-point bend specimens are roughly  $12d_a$  and  $3d_a$ , respectively.

Linear elastic fracture mechanics is applicable when  $r_f$  is much smaller than the cross section dimension of the structure. This condition is not satisfied for most concrete structures, with the possible exception of some very large structures such as concrete dams. However, a more precise criterion for the applicability of linear elastic fracture mechanics, which also takes into account the structure shape and the manner of loading, can be given in terms of the so-called brittleness number,  $\beta$ , which will be explained in Sec. 5.2.

The inapplicability of linear elastic fracture mechanics to brittle failures of typical concrete structures is clearly apparent from the test results shown in Fig. 1.8-1.11. The data points indicate a milder size effect than the straight line of slope  $-1/2$ .

## Chapter 3. NONLINEAR FRACTURE MODELS WITH SOFTENING ZONE

The reason for deviations of concrete behavior from linear elastic fracture mechanics is the development of a relatively large fracture process zone which undergoes progressive softening damage due to microcracking. The effect of this microcracking is: (1) to reduce the flux of energy that can be released into the crack tip; and (2) at the same time to increase the combined surface area of cracking, and thus enhance the energy absorption capability of the fracture process zone.

Therefore, a relation describing the softening damage needs to be included in the fracture model. This can be done basically in two ways: (1) in the form of a stress-displacement relation for the frontal zone of a line crack, or (2) a stress-strain relation for the strain-softening (microcracking) region in front of the main crack. We will first describe these approaches and then discuss their relative merits (For further discussions, see e.g. Planas and Elices, 1988a; Rots, 1988).

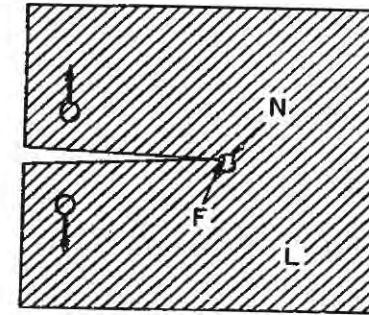
In general, one may distinguish two types of nonlinear fracture mechanics: (1) ductile (metals), and (2) nonductile (concrete, as well as ceramics); see Fig. 3.1. In contrast to linear elastic fracture mechanics, the nonlinear zone is large for both types of nonlinear fracture mechanics. For ductile fracture mechanics, most of the nonlinear zone undergoes plastic hardening or perfect plasticity, and the fracture process zone is still a very small part of the nonlinear zone. By contrast, for nonductile fracture mechanics, which is the case for concrete, the fracture process zone is large and occupies nearly the entire nonlinear zone. Thus, although many results of the fracture theory of metals which evolved earlier are useful, most of them cannot be directly transplanted.

Remarks: The fracture process zone is defined as the zone in which the material undergoes strain-softening, i.e., the stress normal to the crack-plane decreases with increasing strain. The stress can be understood as the macrostress or average stress  $\sigma_{ij}$  that is calculated as  $(1/\Omega_1)$ -times the force resultant transmitted across area  $\Omega_1$  on which the heterogeneous material with aggregates and microcracks can be approximated as a continuum (on the macroscale). Alternatively, (and customarily),  $\sigma_{ij} = \int_{V_r} \sigma_{ij}^m dV/V_r$  where  $\sigma_{ij}^m$  are the microstresses (actual stresses in the aggregates, matrix and interfaces, which show high random local scatter), and  $V_r$  is for the representative volume of the material, defined below Eq. 1.2 (its size is the characteristic length  $\ell$ ). These concepts are developed more precisely in the statistical theory of heterogeneous materials (e.g. Kröner, 1967; Krumhansl, 1968).

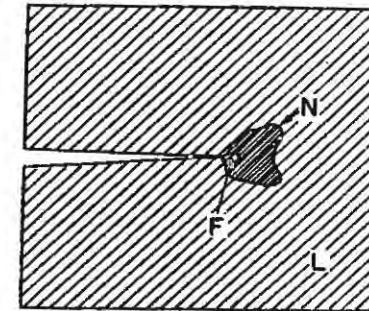
### 3.1 Softening Stress-Displacement Relations

This approach developed as a modification of a similar approach previously formulated for metals. Dugdale (1960) and Barenblatt (1959, 1962) proposed that a plastic (yielding cohesive) zone of a certain finite length must exist at the front of a crack (Fig. 3.2a). The length of this zone must be such that the stresses from the fracture process zone cancel the stress singularity caused at the tip of the equivalent elastic crack by the applied load

(a) Linear Fracture



(b) Metals



(c) Concrete

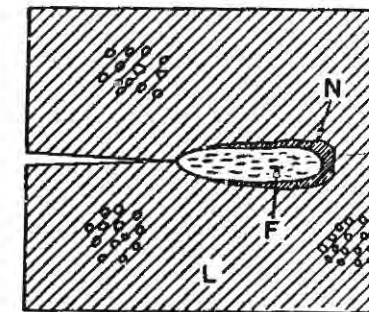


Fig.3.1 Linear Zone (L), Non-Linear Zone (N) and Fracture Process Zone (S) in Fracture of Different Materials

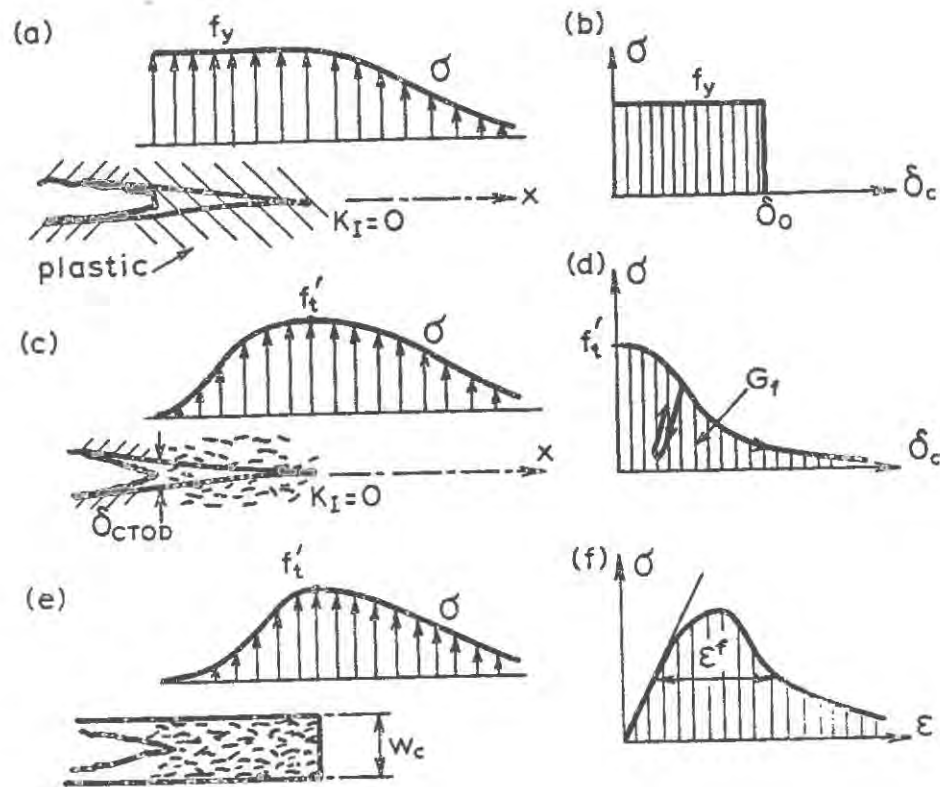


Fig.3.2 Stress Distributions In and Near the Fracture Process Zone in Different Models

(i.e.,  $K_I = 0$ ). The crack opening at the beginning of the plastic zone, where the stress suddenly drops to zero, may be regarded as a material property which controls propagation (Fig. 3.2b).

For some metals and other materials it was later noted that the cohesive zone should exhibit a gradual rather than sudden stress drop, characterized by a softening relation of the normal stress  $\sigma$  across the crack vs. the crack-opening displacement  $\delta_c$  (Fig. 3.2d); see e.g. Knauss (1974), Kfoury and Miller (1974), and Wnuk (1974). For concrete, this type of model was proposed by Hillerborg, Modeer and Petersson (1976) under the name of fictitious crack model; see also Petersson (1980a, 1981), Hillerborg (1983, 1985a, 1985b). (The term "fictitious" refers to the fact that the portion of a crack which transmits tensile stress cannot be a continuous crack with full separation of the surfaces; the real crack ends at the point where the stress is reduced to zero; Fig. 3.2d.) In this model, which has been widely applied in finite element analysis of concrete fracture, the material fracture properties are defined by the softening stress- displacement relation:

$$\sigma_y = f(\delta_c) \quad (3.1)$$

(see Fig. 3.2d), where  $\sigma_y$  is the stress in the direction normal to the crack. The area under the curve represents the fracture energy of the material, i.e.:

$$G_f = \int_0^{\infty} \sigma_y d\delta_c \quad (3.2)$$

The crack begins to open when the stress at the tip reaches the tensile strength limit  $f'_t$ . If the shape of the softening curve is fixed, then the fracture properties are completely characterized by two parameters:  $f'_t$  and  $G_f$ . The precise shape of the softening stress-displacement diagram has a considerable influence on the calculation results. In various works this shape is considered triangular or bilinear, in which case the stress is reduced to zero at a finite displacement  $\delta_0$ . An exponential shape has also been used. When the softening zone is unloaded and reloaded (Fig. 3.2d), the behavior is as sketched in Fig. 3.2d.

Hillerborg's fictitious crack model was verified and calibrated by various comparisons with test data. However, it seems that an exhaustive comparison with all the important concrete fracture data from the literature has not yet been presented. But due to equivalence with the crack band model, the extensive comparisons of the latter with test data (Bažant and Oh, 1983a) indirectly validate the fictitious crack model.

The shape of the stress-displacement curve was studied on the basis of micromechanics of microcracks by Horii (1988), Horii et al. (1987, 1988), and Bažant (1987b), and on ceramics with similar behavior by Ortiz (1988). From these models it transpired that the microcrack coalescence generally tends to produce snapback instability of the stress-displacement curve. However, the existing measurements, albeit limited in scope, do not show any snapback. It may well be that some other mechanism, such as frictional pullout of aggregate and fragments

from the crack faces, eliminates the snapback.

### 3.2 Softening Stress-Strain Relations

Since the cracks in concrete are not straight but tortuous, and the microcracking zone in front of the continuous fracture is not likely to develop along a straight line, the behavior of the fracture process zone can equally well be described by stress-strain relations with strain-softening, i.e., declining stress at increasing strain. This approach is quite convenient for computer programming since no separation of the nodes of two adjacent elements needs to be introduced and fracture is handled by adjustments of the incremental stiffness of finite elements, basically in the same way as any inelastic behavior.

Strain-softening in the form of a sudden vertical drop was introduced in finite element analysis by Rashid (1968). The need to consider progressive strain-softening in tension was recognized by Scanlan (1971), who introduced a sequence of small stress drops. The fact that concrete exhibits strain-softening in tension was experimentally observed by L'Hermite (1959), Rusch and Hilsdorf (1963), Hughes and Chapman (1966), and Evans and Marathe (1968). Extensive and carefully controlled measurements were recently reported by Petersson (1981), Reinhardt and Cornellsen (1984), Gopalratnam and Shah (1985), and others.

From the continuum mechanics viewpoint, the concept of strain-softening involves certain severe mathematical difficulties, such as imaginary wave speed (or change of type of the partial differential equation of motion from hyperbolic to elliptic) and ill-posedness of the boundary value problem, which were pointed out and analyzed by Hadamard (1903), Thomas (1961), Bažant (1976), Sandler (1984), Read and Hegemier (1984), Wu and Freund (1984), Bažant, Belytschko and Chang (1984), and others. The chief problem is that the zone of energy dissipation tends to localize to a zone of zero volume (a surface) so that the total energy dissipation at failure is incorrectly indicated to be zero (cf. review by Bažant, 1986). These difficulties are circumvented if strain-softening in finite element models is introduced through fracture concepts in one of two forms: (1) the crack band model and (2) the nonlocal model. The latter requires a finer mesh but allows better resolution of localized strain fields.

#### 3.2.1 Crack Band Model

The basic idea of the crack band model, which was proposed by Bažant (1976), is:

- (1) to characterize the material behavior in the fracture process zone in a smeared manner through a strain-softening constitutive relation, and
- (2) to impose a fixed width  $w_c$  of the front of the strain-softening zone (crack band), representing a material property.

The imposition of constant  $w_c$  is required in order to avoid spurious mesh sensitivity and achieve objectivity, assuring that the energy dissipation due to fracture per unit length (and unit width) is a constant, equal to the fracture energy of the material,  $G_f$ . In keeping with the classical approach to smeared cracking, the detailed formulation of the crack band model (Bažant and Cedolin, 1979, 1980, 1983) first employed a sudden stress drop instead

of a gradual softening. Later comparisons with numerous test results, however, indicated that the reduction of stress to zero must be gradual, thus creating a relatively long fracture process zone ahead of the front of the fracture (Fig. 3.2e). This formulation, which was given in detail by Bažant (1982), and Bažant and Oh (1983a) has been shown to agree with essentially all the basic fracture test data available in the literature, particularly those on the effect of specimen size on the maximum load, the R-curve (see Chapter 4), and the differences between various specimen geometries. At the same time it was shown that the crack band model and Hillerborg's fictitious crack model give essentially the same results, except when closely spaced parallel cracks occur. (Thus, the extensive experimental justification of the crack band model also indirectly provided justification for the fictitious crack model.)

Softening is caused by fracturing strain,  $\epsilon^f$ , which is superimposed on the elastic strain. Assuming all the cracks to be parallel and smeared (continuously distributed), and choosing axis  $x_2$  to be normal to the cracks, we have in two dimensions ( $x_1 - x_2$  plane):

$$\begin{Bmatrix} \epsilon_{11} \\ \epsilon_{22} \\ \gamma_{12} \end{Bmatrix} = \begin{bmatrix} C_{1111} & C_{1122} & 0 \\ C_{2211} & C_{2222} & 0 \\ 0 & 0 & C_{1212}/\beta \end{bmatrix} \begin{Bmatrix} \sigma_{11} \\ \sigma_{22} \\ \sigma_{12} \end{Bmatrix} + \begin{Bmatrix} 0 \\ \epsilon^f \\ 0 \end{Bmatrix} \quad (3.3)$$

The column matrices on the left hand and right hand sides consist of the strain and stress components ( $\gamma = 2\epsilon_{12}$  = shear angle),  $C_{1111}, C_{1122} = C_{2211}, C_{2222}$  and  $C_{1212}$  are the elastic compliances, and  $\beta$  is an empirical factor, ( $0 < \beta \leq 1$ ), called the shear retention factor (introduced by Suidan and Schnobrich, 1972, and Yuzugullu and Schnobrich, 1973, Phillips, 1973, and Phillips and Zienkiewicz, 1976). If the material is isotropic,  $C_{1111} = C_{2222} = 1/E'$ ,  $C_{1122} = C_{2211} = \nu'/E'$ ,  $C_{1212} = 2^{(1+\nu)}/E$ , in which  $E' = E$ ,  $\nu' = \nu$  for plane stress, and  $E' = E/(1 - \nu)$ ,  $\nu' = \nu/(1 - \nu)$  for plane strain. The fracturing strain can be incorporated into the compliance, in which the expression  $\epsilon = [\omega C_{2222}/(1 - \omega)]\sigma_{22}$  has been introduced:  $\omega$  can be regarded as damage and can be considered to be a function of the strain normal to the crack,  $\epsilon_{22}$ , or the maximum principal strain;  $\omega/(1 - \omega) = \phi(\epsilon_{22})$ . Initially we have  $\omega = 0$  (no damage), and complete damage (continuous fracture) occurs for  $\omega = 1$ . Always  $0 \leq \omega \leq 1$ . The fracture energy is obtained as

$$G_f = w_c \int_0^\infty \sigma_{22} d\epsilon^f \quad (3.4)$$

The fully cracked state is obtained for  $\omega \rightarrow 1$ . It was shown (Bažant and Oh, 1983a) that if Eq. 3.4 is inverted and the limit of the ensuing stiffness matrix for  $\omega \rightarrow 0$  is calculated, the result coincides with the well-known stiffness matrix for a material that is cracked unidirectionally and continuously, as introduced by Rashid (1968).

Eq. 3.4 reflects only a very special form of damage. In general, damage needs to be introduced through the formulation of the internal variable theory (for concrete, see e.g. Pijaudier-Cabot and Mazars, 1989, and Pijaudier-Cabot and Bažant, 1988).

The uniaxial softening stress-strain relation underlying the crack band model is characterized by function  $\phi(\epsilon_{22})$ , which defines damage  $\omega$ . The results are as sensitive to the shape of the softening stress-strain relation as are those for the fictitious crack model. It appears

that the simple formula  $\phi(\epsilon) = (E/f'_t) \exp a(\epsilon - \epsilon_p)$ , with empirical constants  $a$  and  $\epsilon_p$ , is generally adequate. A straight line softening, i.e., a triangular stress-strain diagram, has also been used successfully.

There are two simple variants to the crack band model. The original one (Bažant and Oh, 1983a) presumes that the smeared parallel cracks start to form in the direction normal to the maximum principal stress but subsequently the crack orientation is fixed in the material even if the principal stress direction rotates. More recent research (e.g., Gupta and Akbar, 1984; Cope, 1984) seems to indicate that it is better to assume that the crack orientation rotates with the direction of the maximum principal stress, which means that shear stresses on the crack plane can never arise. For this variant, the general triaxial stress-strain relation for the microcracked material can be written in the form (Bažant and Lin, 1988b):

$$\epsilon_{ij} = \left( C_{ijkl} + \frac{\omega}{(1-\omega)E'} n_i n_j n_k n_l \right) \sigma_{km} \quad (3.5)$$

in which  $n_i$  = direction cosines of the current maximum principal stress direction (repeated tensorial subscripts imply summation) and  $C_{ijkl}$  is the elastic (undamaged) compliance tensor.

When the principal stress directions rotate significantly, the nonrotating crack method must be generalized to allow for the formation of secondary and tertiary cracking of different orientations. Such multidirectional smeared cracking models were especially perfected by de Borst (1984).

In reality, the microcracks prior to the final continuous fracture are distributed over all orientations, with different frequencies for various orientations. This feature is captured by the microplane model (Bažant and Oh, 1985) which seems to be physically the most realistic as well as conceptually simplest model of damage due to cracking but is very demanding for computer time. In this model (which will be considered further in Section 3.2.5), the hypothesis that the cracking strain tensor is additive to the elastic strain tensor is abandoned and cracking is modelled as strain-softening separately on planes of all orientations (called microplanes), subject to the hypothesis that the strain components on each microplane are the resolved components of the (macroscopic) strain. The stresses after cracking on the planes of various orientations are not exactly in equilibrium, but overall equilibrium is enforced by using the principle of virtual work.

It may be pointed out that linear elastic stability analysis in which the microcracks are assumed to grow in a homogeneous elastic continuum indicates that the softening stress-displacement or stress-strain relation should exhibit a maximum displacement or strain (snapback), after which the stress suddenly drops to zero (Bažant, 1987b). But it is not yet known whether the prediction of snapback also results from models taking into account inhomogeneities, inelastic behavior, and friction.

The width of the crack band front can be assumed to be approximately  $w_c \simeq 3d_a$  ( $d_a$  = maximum aggregate size). This conclusion was drawn on the basis of optimum fitting of numerous test data (Bažant and Oh, 1983a). However, the optimum was not sharp;  $w_c$  values ranging from  $d_a$  to  $6d_a$  gave almost equally good results, provided, of course, the

post-peak function  $\phi(\epsilon_{22})$  was adjusted for each different value of  $w_c$ .

Once the shape of the softening stress-strain relation is fixed, the crack band model is fully characterized by three material parameters:  $f'_t$ ,  $G$  and  $w_c$  (although the influence of the  $w_c$  - value is rather weak for situations with isolated cracks). By contrast, the fictitious crack model has only two basic parameters,  $f'_t$  and  $G_f$ . Why the extra parameter in the crack band model? The extra parameter,  $w_c$ , is important only in situations when there are parallel cracks (e.g., in the presence of tension reinforcement); then  $w_c$  basically determines the minimum possible crack spacing, as a material property. It should be pointed out that the fictitious crack model, because of its lack of the extra parameter  $w_c$ , can give results that are not objective in situations with parallel closely spaced cracks. (A certain length has also been defined as an additional material parameter in the fictitious crack model; however, in contrast to  $w_c$ , it is not an independent parameter.)

The finite element size  $h = w_c$ , required by the crack band model, may be too small in the case of very large structures. In that case, it is possible to enlarge the element size (i.e. use  $h > w_c$ ) provided that the softening stress-strain relation is adjusted so as to assure the same energy dissipation,  $G_f$ . This is illustrated in Fig. 3.3. In view of the series coupling model, already discussed in connection with Fig. 1.8, the given stress-strain diagram OPA for the strain-softening crack band needs to be replaced, at increasing element size  $h$ , by diagrams OPB, OPC, OPD, etc., such that when the areas under any of these diagrams is multiplied by  $h$  the same fracture energy value  $G_f$  is obtained (Fig. 3.3c). In terms of the stress-displacement diagrams for length  $h$  of finite element, a change in  $h$  requires that the actual stress-displacement diagram 012 in Fig. 3.3b be replaced by diagrams 032, 042, 052, etc. These stress-displacement diagrams have the property that the area under them is constant, thus assuring constant fracture energy  $G_f$ .

One can, of course, also use elements with  $h < w_c$  (say  $0.1w_c$ ), provided the post-peak slope is decreased as shown by the  $\sigma - \epsilon$  diagram OPF in Fig. 3.3c so that the  $\sigma - \delta$  diagram 082 (Fig. 3.3b) would again have the same area as 012. In this case, the row of cracked elements can be narrower than the adjacent elements and the mesh may look as shown in Fig. 3.4a but with  $w_c$  replaced by  $h$ . Obviously, when  $h \rightarrow 0$ , the crack band model in the limit becomes identical to Hillerborg's model (which in this sense is a special case of the crack band model).

As the element size is increased, the softening slope gets steeper, until for a certain element size  $h_0$  a vertical stress drop OPC or 42 is obtained. For a still larger element size, the diagram OPD or 052 would exhibit snapback, which would cause numerical difficulties. In that case, one may replace the snapback segment 52 of the element stress-displacement diagram by a vertical stress drop, 67 in Fig. 3.3b. The point of vertical drop is determined again from the condition that the area under the diagram 067 must be the same as the area under the diagram 012 or 042. This consideration indicates that the equivalent tensile strength  $f_{eq}$  of the large finite element of size  $h > w_c$  is given by

$$f_{eq} = f'_t \sqrt{\frac{h_0}{h}}, \quad h_0 = \frac{2EG_f}{f'^2} = \frac{K_{fc}^2}{f'^2} \quad (\text{for } h \geq h_0) \quad (3.6)$$

(e.g., Bažant and Cedolin, 1979, 1980) in which  $h_0$  is the element size for which a vertical stress drop (diagram 042) is obtained. Note that the expression for  $h_0$  is similar to Irwin's Eq. 2.10 for the size of the yielding zone.

The foregoing adjustments are ideally defined for square finite elements subjected to tension or shear (normal or parallel to the sides). However, extensions to non-square elements are possible. In this case, if the dimension of the element in each direction is about the same, one may again use Eq. 3.7 in which  $h = \sqrt{A}$ , where  $A$  = element area (in 2D).

Eq. 3.7 follows from the relation  $h f_{eq}^2/2E = h_0 f_t^2/2E = G_f$  where  $h$  represents either the actual width of the cracking element in the direction normal to the cracks, provided the element is square or rectangular, or the effective width of the element defined as  $h = w_c A_{el}/A_b$  where  $A_{el}, A_b$  are the areas of the element and of the crack band within the element. For element width  $h < h_0$ , for which the post-peak slope is reduced but the strength limit is kept as  $f_t'$ , the stress-strain diagram may be expressed, according to the series model (Fig. 1.8), as follows:

$$\epsilon = \frac{w_c}{h} \epsilon_{soft} + \left(1 - \frac{w_c}{h}\right) \epsilon_{unt}, \quad h = w_c \frac{A_{el}}{A_b} \quad (\text{for } h < h_0) \quad (3.7)$$

$\epsilon_{soft}, \epsilon_{unt}$  = the strains corresponding to the same stress according to the strain-softening stress-strain diagram and an unloading stress-strain diagram starting from the peak stress point.

If larger elements need to be used, another possibility is to keep the size of the elements on the line of crack band constant, equal to size  $w_c$ , and enlarge all the remaining elements as shown in Fig. 3.4a. If the crack band is much thinner than the adjacent finite elements, the model, of course, becomes practically identical to the fictitious crack model.

In the case of crack propagation in an arbitrary direction, the crack band model as well as the fictitious crack model requires remeshing so that the boundary lines of the crack band or the crack line would conform to the interelement boundaries (for the fictitious crack model, these techniques were perfected by Ingraffea (1985), Ingraffea and Gerstle (1985), and Ingraffea and Saouma (1985). If the remeshing is not done, it is still possible to approximately represent fracture running in an arbitrary direction by allowing the crack band to have a zig-zag form as shown in Fig. 3.4b. Some adjustments of the fracture energy are then necessary to take into account the average width of such a zig-zag band (Bažant, 1985a).

Even with such adjustments, however, there is a certain bias imposed by the mesh orientation. Moreover, if shear stresses parallel to the overall crack band direction arise, the zig-zag band can introduce spurious shear locking of the opposite faces. These problems can be overcome either by introducing a nonlocal version of the model, described later, or by enriching the finite element either with a strain field that is discontinuous along the boundaries of an arbitrarily oriented band, as proposed by Droz (1987) for tension, (similar to the models reported by Ortiz et al., 1987; Leroy and Ortiz, 1989, and Belytschko et al., 1988 for shear bands) or with displacement field discontinuous along a line, as proposed by Dvorkin et al. (1989).

The crack band model offers the possibility of introducing the influence of nonsingular

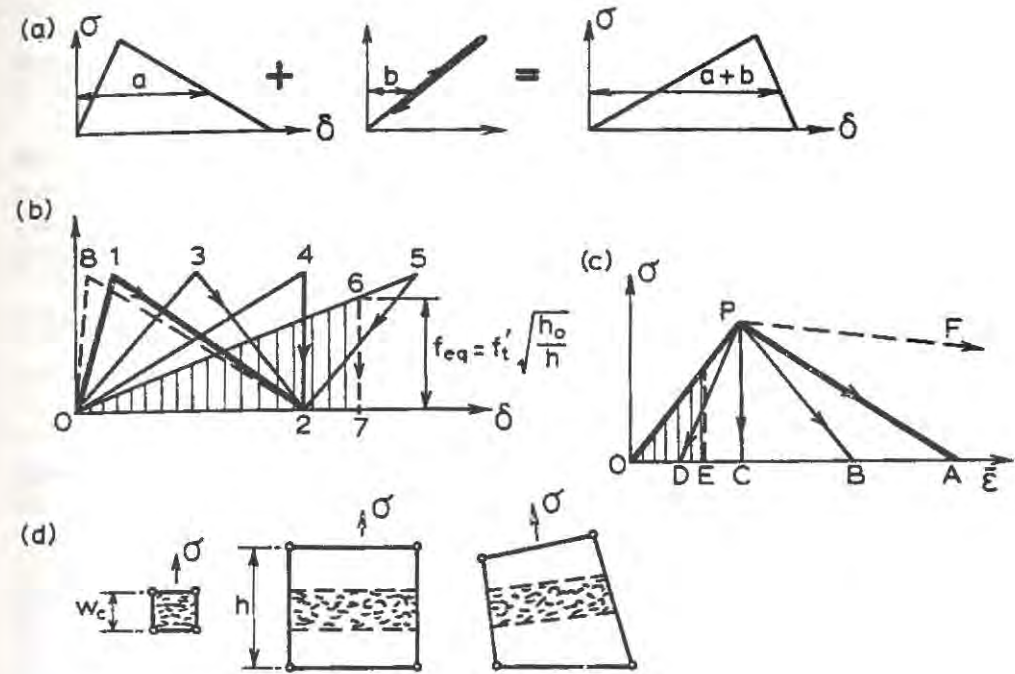


Fig.3.3 Effect of Size on the Steepness of Post-Peak Softening

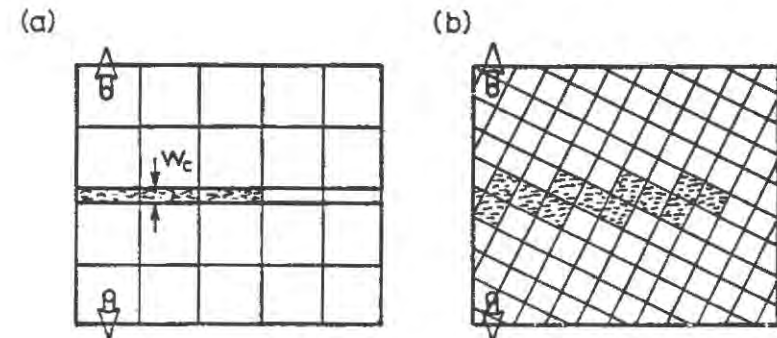


Fig.3.4 Meshes to Represent a Very Narrow Crack Band and a Zig-Zag Band

three-dimensional stresses on fracture. For example, it is known that a compressive stress  $\sigma_x$  parallel to the crack plane promotes cracking. Based on the known shape of the biaxial failure envelope of concrete, this influence (for  $\sigma_x < 0$ ) may be taken into account by replacing  $f'_i$  with

$$f'_i = f'_i{}^* (1 + \sigma_x / f'_c) \quad (3.8)$$

(Bažant, 1985a) where  $f'_c$  = compression strength. For  $\sigma = -f'_c$  (compression failure), one must have  $f'_i{}^* = 0$ , which agrees with Fig. 3.9. Note also that, in contrast,  $\sigma_x$  has no effect if linear elastic fracture mechanics is used; nor when line crack models with softening zones are used.

The crack band model has been implemented in some large general purpose finite element codes (e.g. DIANA, TEMP-STRESS, NONSAP).

### 3.2.2 Crack Layer Model

A variant of the crack band model is represented by Chudnovsky's crack layer model (Bessendorff and Chudnovsky, 1984; Chudnovsky, 1986). This model is more general than the crack band model in that the width of the crack band front is not considered to be a constant. Rather it is allowed to expand or shrink based on a material property. This property links a certain path-independent integral that characterizes the energy change due to the expansion to another path-independent integral around the crack front which characterizes the energy flow into the crack front due to crack propagation (Rice's J-integral).

This model, however, has not been developed for application in concrete and has not been compared to typical test data for concrete. The properties governing the band expansion might be unidentifiable from the experimental data at the current degree of sophistication of testing methods.

### 3.2.3 Composite Fracture Model

The composite fracture model is essentially an adaptation of the crack band model to finite elements of a larger size than the crack band width  $w_c$ , thus permitting large structures to be analyzed with a cruder mesh. The model assumes that a crack band of width  $w_c$ , which is a material property (or an equivalent line crack) is embedded within a larger finite element, approximately as illustrated in Fig. 3.3d. This idea, which is similar to Eq. 3.8, was proposed first for plastic shear bands by Pietruszczak and Mroz (1979) and later developed for tensile cracking of concrete by Willam et al. (1985, 1986). If the element size shrinks to  $w_c$ , this model becomes essentially identical to the crack band model. The crack band within the finite element is introduced by enriching the smooth distribution function with a discontinuous strain field function which characterizes cracking. The approach is similar to those by Droz (1987), Ortiz et al. (1987), Belytschko et al. (1988), Leroy and Ortiz (1989)

and Dvorkin et al. (1989) already mentioned at the end of Sec. 3.2.1.

### 3.2.4 Nonlocal Continuum with Local Strain (Nonlocal Damage)

A nonlocal continuum is a continuum in which some state variable depends not only on the stresses or strains at the same point but also on the stress or strain field in the neighborhood of the point. As shown by Kröner (1967), Krumhansl (1968), Kunin (1968), Eringen and Edelen (1972), and others (cf. Bažant, 1986), the nonlocal concept is appropriate for statistically heterogeneous materials and follows logically from statistical micromechanical considerations. Recently, the nonlocal approach has been shown to be very effective for fracture mechanics of distributed cracking.

The nonlocal concept represents a general approach which makes it possible to use stress-strain relations with strain-softening. As mentioned before, if the strain-softening concept is introduced in the local continuum, softening zones localize to a vanishing volume, causing improper convergence on mesh refinement, spurious mesh sensitivity and physically incorrect predictions such as failure with vanishing energy dissipation as the mesh size is refined to zero. To avoid such behavior, the computational model must include some mathematical device that limits the localization (Bažant, Belytschko and Chang, 1984). The simplest, albeit crudest, way to limit localization is to impose a fixed size,  $w_c$ , on the frontal finite element, as done in the crack band model (unless the post-peak stress-strain relation is artificially modified). However, this approach makes it impossible to resolve the field in the fracture process zone itself, or determine how the fracture process zone width could vary during the fracture growth (no modification of stress-strain relations could be permitted for those purposes).

A more general way to limit localization, in order to cope with such problems, is the nonlocal continuum. The concept may be introduced in various forms, such as averaging of strains or strain-related quantities over a neighborhood of a point (Bažant, 1984b; Bažant, Belytschko and Chang, 1984), or introduction of first and second spatial derivatives of strains or other quantities into the constitutive relation (e.g., Schreyer and Chen, 1986; and for the Cosserat medium formulation for rocks by Sulem and Vardoulakis, 1988). The spatial derivative formulation can be obtained by expanding the spatial averaging integral in Taylor series. Only the spatial averaging approach has so far been worked out in detail for the multidimensional analysis of fracture of materials such as concrete.

In the early formulation, spatial averaging was applied through the total strains used in the strain-softening constitutive relation. However, that approach, which resulted in a so-called imbricate continuum model (Bažant 1984b), proved to be relatively cumbersome and have some computationally inconvenient properties. Recently (Bažant and Pijaudier-Cabot, 1987, 1988a; Pijaudier-Cabot and Bažant, 1987; Bažant and Lin, 1988a, 1988b), it was found that a more effective approach is to consider the elastic strains as local (no averaging), and apply the nonlocal averaging only to the softening part of the strains which represent distributed microcracking. This new approach has the advantage that the continuum field equations of equilibrium as well as the boundary conditions remain the same as for the

classical local continuum, and that there is no possibility of zero-energy instability modes (previously shown to exist for fully nonlocal models). It has also been mathematically proven that the averaging of the fracturing part of the strains is sufficient to prevent localization of strain-softening damage into a zone of zero volume. The unloading-reloading behavior is always local in this approach.

The spatial averaging operator, denoted by an overbar, may be defined in terms of strain  $\epsilon_{11}$  as follows:

$$\bar{\epsilon}_{11}(\mathbf{x}) = \frac{1}{V_r(\mathbf{x})} \int_V \alpha(\mathbf{s} - \mathbf{x}) \langle \epsilon_{11}(\mathbf{s}) \rangle dV = \int_V \alpha'(\mathbf{x} - \mathbf{s}) \langle \epsilon_{11}(\mathbf{s}) \rangle dV \quad (3.9)$$

in which

$$V_r(\mathbf{x}) = \int_V \alpha'(\mathbf{s} - \mathbf{x}) dV, \quad \alpha(\mathbf{x} - \mathbf{s}) = \frac{\alpha(\mathbf{s} - \mathbf{x})}{V_r(\mathbf{x})} \quad (3.10)$$

$$\langle \epsilon_{11} \rangle = \epsilon_{11} \text{ if } \epsilon_{11} > 0, \quad \langle \epsilon_{11} \rangle = 0 \text{ if } \epsilon_{11} \leq 0 \quad (3.11)$$

Here  $V$  = volume of the structure,  $\mathbf{x}$  = coordinate vector,  $\mathbf{s}$  = coordinate vectors of adjacent points,  $\alpha$  = given weighting function of the distance  $|\mathbf{s} - \mathbf{x}|$ , considered to be a material property (Fig. 3.5).  $V_r$  has approximately, but not exactly, the same meaning as the representative volume in the statistical theory of heterogeneous materials.

The weighting function could be defined as uniform ( $\alpha = 1$ ) over volume  $V_r$  representing a circle in two dimensions, a bar segment in one dimension, or a sphere in three dimensions, with a zero value outside  $V_r$ . However, it has been experienced that the calculations converge better if the weighting function is smooth. One possible choice (Bažant and Pijaudier-Cabot, 1987, 1988a; Bažant and Lin, 1988b) is a Gaussian distribution function, which, however, has nonzero values over the entire structure. It seems preferable to use a polynomial bell-shaped function which is exactly zero beyond a certain distance, e.g. (Fig. 3.5)

$$\alpha(\mathbf{s} - \mathbf{x}) = \left(1 - \frac{|\mathbf{s} - \mathbf{x}|}{k\ell}\right)^2 \text{ if } |\mathbf{s} - \mathbf{x}| < k\ell, \text{ otherwise } \alpha(\mathbf{s} - \mathbf{x}) = 0 \quad (3.12)$$

Here  $k$  is a normalizing constant determined so that the integral of  $\alpha$  over a line segment, or a circle, or a sphere of size  $k\ell$  would be the same as the integral of  $\alpha = 1$  over the same region;  $k = 15/16 = 0.9375$  for 1D,  $(3/4)^{1/2} = 0.9086$  for 2D,  $k = (105/192)^{1/3} = 0.8178$  for 3D. The parameter  $\ell$  is the so-called characteristic length of the nonlocal continuum, which is a material property that defines the size of the averaging volume and is determined by the size of the inhomogeneities in the microstructure. For one quite typical concrete, measurements (Bažant and Pijaudier-Cabot, 1988b) have shown that  $\ell = 2.7d_a$  where  $d_a$  = maximum aggregate size (Sec. 6.9).

If point  $\mathbf{x}$  is too close to the surface of the body, part of the averaging zone protrudes beyond the surface. This is handled by deleting the protruding part from the integration region. This deletion causes  $V_r(\mathbf{x})$  to depend on location  $\mathbf{x}$ .

In finite element calculations, the integrals in Eq. 3.10 and 3.11a are approximately evaluated as finite sums over all the integration points of all the elements in the structure.

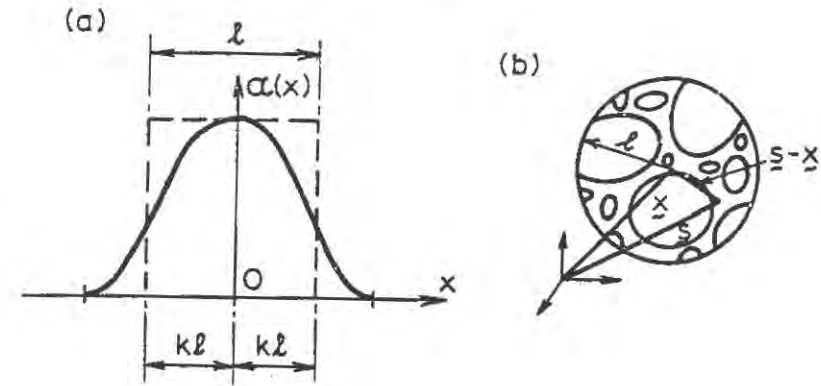


Fig.3.5 Weighting Function for Non-Local Continuum Theory and Representative Volume of the Material

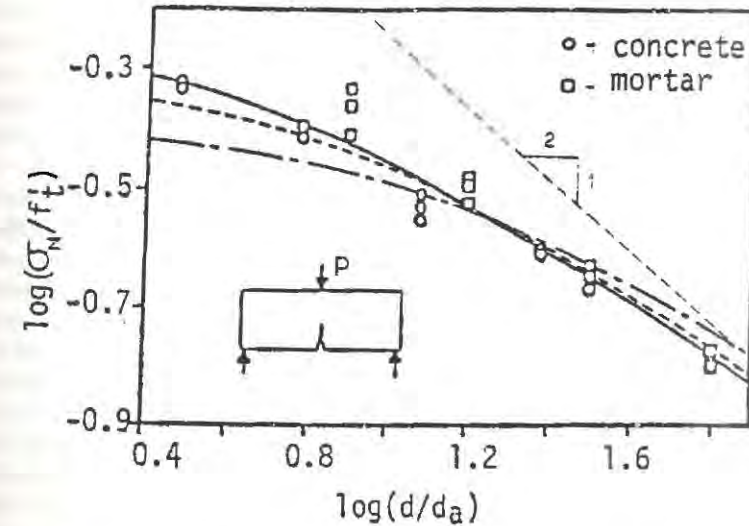


Fig.3.6 Size Effect Calculated by Non-Local Continuum Theory (Bažant and Lin, 1988b) for Exponential (dashed curve) and Linear (dash-dot curve) Tensile Strain Softening Curves, Compared with Size Effect Law of Bažant (Eq. 1.4, solid curve) and with test results of Bažant and Pfeiffer (1987) (data points)

However, the integration points whose distances from point  $\mathbf{x}$  exceed  $k\ell$  may be omitted from the sum since for them  $\alpha = 0$ .

Ideally, the form of function  $\alpha(\mathbf{s} - \mathbf{x})$  should be derivable from micromechanical modeling of the microstructure with aggregates and microcracks, same as the form of function  $\phi(\epsilon)$  in Eq. 3.4 and 3.6. However, this goal is too difficult at present, while at the same time the precise form of function  $\alpha(\mathbf{s} - \mathbf{x})$  has only little influence on computation results (this fact makes identification of function  $\alpha$  from test data problematic). What is important is the value of  $\ell$  (provided the body is not too large compared to  $\ell$ ).

The simplest nonlocal constitutive model, appropriate for unidirectional cracking, is obtained by generalizing the crack band model (Bažant and Lin, 1988b). One alternative is to assume the crack direction to be fixed at the time the cracks start to form. In this case, the nonlocal generalization is obtained by replacing  $\omega$  in Eq. 3.4 with nonlocal damage  $\bar{\omega}$ , such that

$$(1 - \bar{\omega})^{-1} = \varphi(\bar{\epsilon}_I) \quad (3.13)$$

where  $\bar{\epsilon}_I$  is the maximum nonlocal principal strain calculated from the nonlocal (averaged) strain tensor  $\bar{\epsilon}_{ij}$ .

The second alternative of the crack band model, in which the cracking direction is assumed to rotate with the maximum principal stress, is obtained by replacing  $\omega$  with  $\bar{\omega}$  in Eq. 3.6.

It has been verified (Bažant and Lin, 1988b) that this nonlocal generalization of the crack band model permits the use of finite elements of any size less than  $\ell$ , without causing spurious mesh sensitivity and improper convergence. For element sizes no smaller than  $\ell$ , the nonlocal model becomes identical to the crack band model, and the stress-strain relation for the finite element which undergoes cracking must be adjusted according to the element size, as already explained.

It has also been shown that the nonlocal smeared cracking model provides an excellent fit of various fracture test data. See e.g., Fig. 3.6, in which the test results from Bažant and Pfeiffer (1987) are compared with nonlocal finite element results of Bažant and Lin (1988b) (dashed and dash-dot curves) and with the size effect law (Eq. 1.4, solid curve) (the dashed curve corresponds to a softening tensile stress-strain relation in an exponential form, which fits the data better than the dash-dot curve which corresponds to a linear stress-strain relation; still better fits could probably be obtained with other shapes of this relation). From Fig. 3.6 it should be especially noted that a nonlocal finite element code exhibits the correct transitional size effect of nonlinear fracture mechanics, as approximately described by the size effect law proposed by Bažant. By contrast, the local finite element analysis exhibits no size effect, as observed on geometrically similar specimens of different sizes, with similar meshes.

One practical advantage of the nonlocal formulation is that if the finite element sizes are less than about 1/3 of the characteristic length  $\ell$ , then there is no directional bias of the mesh with regard to crack propagation. This has been verified (Bažant and Lin, 1988b) by analyzing the fracture of the same rectangular specimen with an aligned square mesh and a slanted square mesh. Thus, the nonlocal model can be used in general fracture situations.

An interesting, and potentially useful property of the nonlocal formulation is that the width of the cracking zone is not fixed but varies during the course of loading. The consequence is that the nonlocal fracture model does not correspond to a unique stress-displacement diagram for the line crack model (fictitious crack). This fact might explain why it has proved rather difficult to obtain unique values of the fracture energy on the basis of the fictitious crack model.

It should also be noted that a large finite element program for the nonlocal fracture model usually runs faster than the corresponding local program, despite the fact that additional computer time is needed to calculate the spatial averages. The reason apparently is that the nonlocal averaging stabilizes the response, thus causing the iterations in the loading steps to converge faster.

### 3.2.5 Multidirectional Cracking and Nontensile Fracture

For concrete structures subjected to complicated loading histories, it may be necessary to analyze fracture taking into account the existence of multidirectional cracking (Bažant 1983; de Borst, 1984, 1987a, 1987b; de Borst and Nauta, 1985; Ottosen and Dahlblom, 1986; Willam et al., 1987; Rots, 1988; Rots and Blaauwendraad, 1989; Crisfield and Wills, 1989). An effective approach to such behavior appears to be the microplane model, which was already mentioned below Eq. 3.6 in connection with the damage law. Instead of a macroscopic stress-strain relation, the material behavior in the microplane model is characterized independently on planes of various orientations, called the microplanes. In practice, only a certain number of discrete microplanes is considered, according to a numerical integration formula for spatial directions. The macroscopic response is determined as a certain average of the responses from the individual microplanes, obtained according to the principle of virtual work. This model, whose basic concept is similar to the slip theory of plasticity (Taylor, 1938; Batdorf and Budianski, 1949), was first developed in a local form (Bažant and Oh, 1985). It was also shown that this model can represent well not only the existing test data on tensile fracture but also those on crack shear, including the effects of the transverse normal stress and shear-induced expansion across the crack (Bažant and Gambarova, 1984). Recently (Bažant and Ozbolt, 1989), the microplane model has been generalized to a nonlocal form.

There are other types of fracture which need to be modeled for concrete structures. A new theory will have to be developed for Brazilian tensile splitting fracture of very large cylinders, which cannot be adequately analyzed with the existing tensile fracture models. On the other hand, shear fracture seems, at least partially, amenable to analysis by the existing tensile cracking models. In those models, the shear fracture is described as a band of inclined microcracks, governed by a softening stress-strain relation.

### 3.3 Stress-Displacement vs. Stress-Strain Softening Relations

There has been an incessant debate on the relative merits and deficiencies of the line

crack and crack band representations of fracture. There are three viewpoints to mention:

### 3.3.1 Isolated Cracks: Moot Point Computationally

First, one must realize that the line crack model (i.e. the fictitious crack model of Hillerborg) and the crack band model yield about the same results (with differences of about 1%) if the stress displacement relation in the first model and the stress-strain relation in the second model are calibrated in such a way that

$$\delta_c = w_c \epsilon^f \quad (3.14)$$

i.e., the crack opening displacement is taken as the fracture strain,  $\epsilon^f$ , accumulated over the width  $w_c$  of the crack band. This equivalence is already suggested by the fact that, in linear elastic fracture mechanics, an interelement line crack and a single-element wide crack band with a symmetry line that coincides with the line crack give essentially the same results in the calculation of the energy release rate, with differences of only about 1%, provided the element sizes near the fracture front do not exceed about 1/10 of the cross section dimension (Bažant and Cedolin, 1979). In fact, the difference between these two methods of calculation of the energy release rate for linear elastic fracture mechanics is not larger than the error of approximating the continuum by finite elements in the first place.

Therefore, the question "line crack or a crack band?" is moot from the viewpoint of approximating reality by computational modeling. The only point worthy of debate is computational effectiveness and convenience. But even in that regard, the two models appear to be equal.

Various numerical modeling aspects, however, deserve attention. Leibengood, Darwin and Dodds (1986) showed that the results for stress-displacement and stress-strain relations match closely if the cracking directions at the integration points within the finite elements are forced to be parallel to each other (and to the actual crack). If the cracking direction is not known a priori, as in the general case, it is difficult to achieve this parallelness. But then, if cracks are allowed to form at different orientations at each integration point, the response of the finite element model with smeared cracking is somewhat stiffer than that with discrete interelement cracking, even if the element sides are parallel to the true crack.

### 3.3.2 Parallel Cracks: Third Parameter

As already mentioned, if the shape of the tensile softening curve is fixed, then the line crack (fictitious crack) model is defined by two parameters,  $G_f$  and  $f_t'$ , while the crack band model is defined by three parameters  $G_f$ ,  $f_t'$  and  $w_c$ . For the fictitious crack model, too, a length parameter (called the "characteristic length") has been defined;  $\ell_0 = EG_f/f_t'^2$  (which is similar to Eq. 3.7 as well as Irwin's Eq. 2.10). However, this parameter is a derived parameter, not an independent one, while  $w_c$  is an independent parameter. Why this difference?

For isolated cracks, it turns out that the effect of  $w_c$  on the results is almost negligible,

provided that the softening part of the stress-strain diagram is adjusted so as to always yield the same fracture energy  $G_f$  for any  $w_c$ . However, the parameter  $w_c$  does make a difference in the case of densely spaced parallel cracks, since it prevents adjacent cracks to be closer than the distance  $w_c$  (otherwise the adjacent crack bands would overlap, which is inadmissible). So the physical significance of  $w_c$  is not really the width of the actual cracking zone at the fracture front, but the minimum admissible spacing of parallel cracks. Is it necessary that this spacing be a material fracture parameter?

For an answer, consider that elastic longitudinal fibers are bonded to a long, thin concrete bar subjected to tension. The cross section of the fibers is so large that the composite specimen exhibits no softening under tension, although the concrete part does. Then the state of uniform strain is always stable. According to the line crack model, cracks can form at arbitrarily close spacing in such a system, and depending on the spacing, the load-elongation diagram  $P(u)$  may follow any of the diagrams shown as 0129, 0139, 0149, or 0159 in Fig. 3.7. Thus, there is an ambiguity, or inobjectivity of response. The problem can of course be eliminated by enriching Hillerborg's line crack model with a third independent material parameter, the minimum crack spacing,  $s$  (independent of  $\ell$ ). This is, of course, equivalent to parameter  $w_c$ .

### 3.3.3 Relation to Micromechanisms of Fracture

The normal microstrains across the fracture process zone may be distributed roughly as shown in Fig. 3.8a. The line crack model simplifies this strain distribution taking it as a constant plus the Dirac delta function, Fig. 3.8b. The crack band model simplifies it, too, taking it as a constant plus another constant within the crack band (rectangular distribution), Fig. 3.8c. The nonlocal continuum model gives a smooth bell-shaped distribution across the band, as shown in Fig. 3.8d (Bažant and Pijaudier-Cabot, 1988a), and in the finite element form as Fig. 3.8e.

Measurements of the locations of acoustic emissions during the fracture process (Labuz, Shah, Dowding, 1985; Maji and Shah, 1988) indicate, despite their inevitable scatter, that the emission sources are located over a relatively wide band in the frontal region of fracture (Fig. 3.8f), as in the crack band model. On the other hand, various measurements of strains on the surface, e.g., interferometry (Cedolin, Dei Poli and Iori, 1987), and laser holography (Miller, Shah and Bjelkhagen, 1988), indicate the very high strains to occupy a very narrow zone at the front fracture, which might be better modeled by a line crack model. It may be noted that the fracture strains might be more localized at the surface of a specimen than in the interior, due to the wall effect and other effects.

As for the visible continuous fracture behind the fracture process zone, it must be noted that it is frequently highly tortuous, meandering to each side of the symmetry line by a distance of up to about the maximum aggregate size. Even if all microcracking were concentrated on a line, in view of the tortuosity of this line, the fracture is represented no better by a straight line crack than by a crack band of width of one or two aggregate sizes (however, for computational results this width really does not matter in most situations, as mentioned

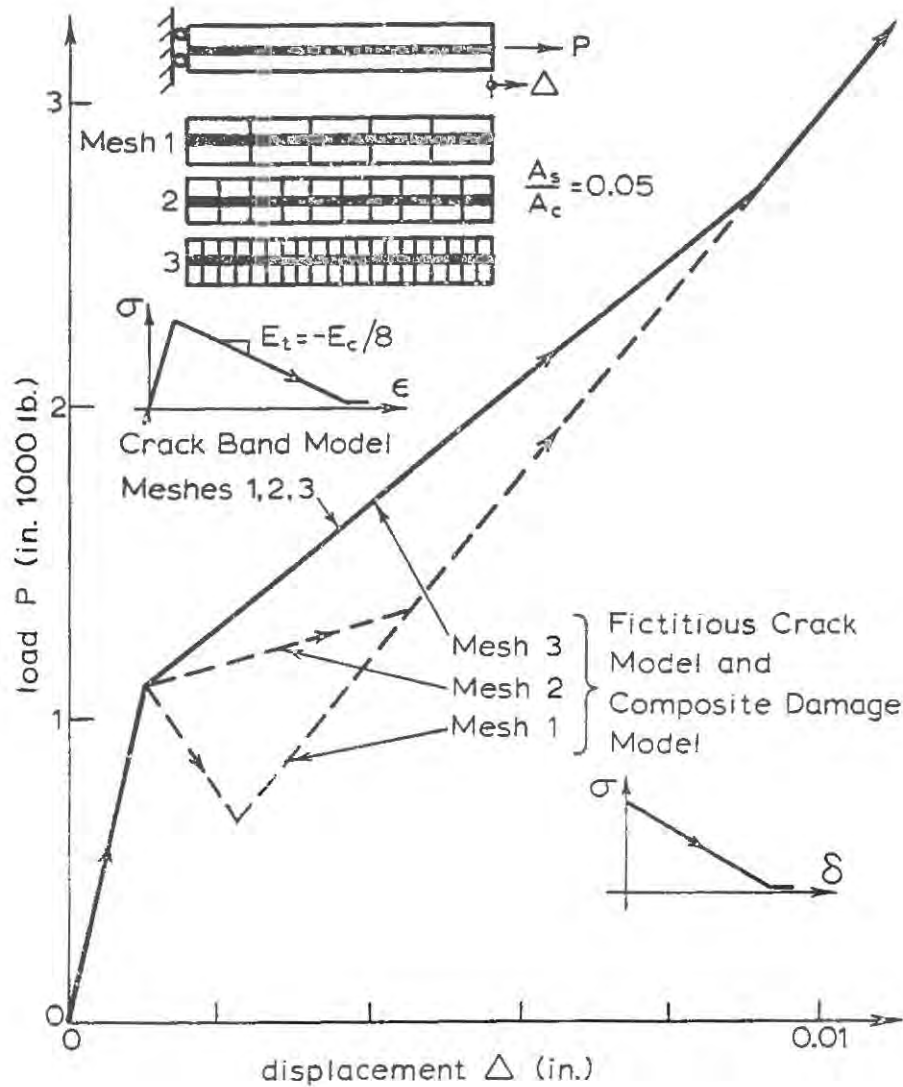


Fig.3.7 Finite Element Results for Different Crack Spacings in a Tensioned Reinforced bar

above).

Along a profile across the fracture process zone, microcracking is manifested by an increase in the average magnitude of the transverse strains. This increase is probably gradual, as shown in Fig. 3.8a, or in a finite element form in Fig. 3.8e. Obviously the width of the fracture process zone obtained by measurements depends on the choice of the cut-off value of the strain. This might explain the differences in interpretation of various types of observations.

To sum up, there seems to be no compelling reasons for rejecting either the crack band model, characterized by softening stress-strain relations, or the line crack model, characterized by softening stress-displacement relations. The choice is essentially a matter of convenience of analysis.

### 3.4 Nonlinear Triaxial Constitutive Models for Strain-Softening

The stress-strain or stress-displacement relations for the fracture process zone which have been described so far take into account only tensile cracking in one direction. However, the fracture process zone may undergo multiple cracking in many directions and may be subjected to high compressive stresses parallel to the crack plane, as well as shear stresses. To handle such situations, finite element analysis needs to be based on a general nonlinear triaxial model. In the fracture process zone, the material undergoes degradation of its mechanical properties, which is basically of two kinds:

- (1) degradation of material stiffness due to damage such as cracking, which is described by continuum damage mechanics (or the fracturing material theory of Dougill, 1976), and is characterized by unloading according to the secant modulus; and
- (2) degradation of the strength or yield limit, which is described by modern adaptations of plasticity.

The real behavior is a combination of both. Such combined behavior has been described for concrete, e.g., by the endochronic theory, plastic-fracturing theory or the damage theory of Ortiz. For a review, see Bažant (1986).

General nonlinear, triaxial constitutive models cannot be accommodated in the stress-displacement relations for sharp line cracks, which are basically counterparts of uniaxial stress-strain relations. The crack band model can be extended to accommodate such models, but for a proper treatment, the nonlocal approach seems to be necessary.

A very general constitutive model, which can handle both the process zone of tensile fracture, as well as compression and shear damage, and describes well the nonlinear triaxial behavior in general, is the microplane model. That this model gives the correct response for fractures is evidenced by the fact that it yields a correct transitional size effect; see Fig. 3.9 taken from Bažant and Ozbolt (1989).

When there is a larger compressive stress  $\sigma_x$  parallel to the crack, at least simple adjustment of the softening stress-displacement curve of  $\sigma_y$  vs.  $\delta_c$  or stress-displacement curve of  $\sigma_y$  vs.  $\epsilon_y$  needs to be made. Biaxial failure envelope data indicate that the tensile strength limit should be scaled down from  $f_t^*$  approximately to the value  $f_t^*$  given already in Eq. 3.9.

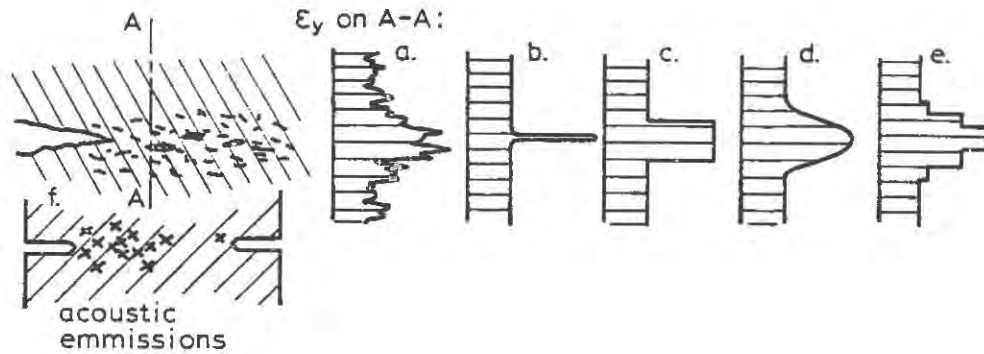


Fig.3.8 Fracture Process Zone, and Stress Profiles Across It: (a) Actual, (b)-(c) Various Representations

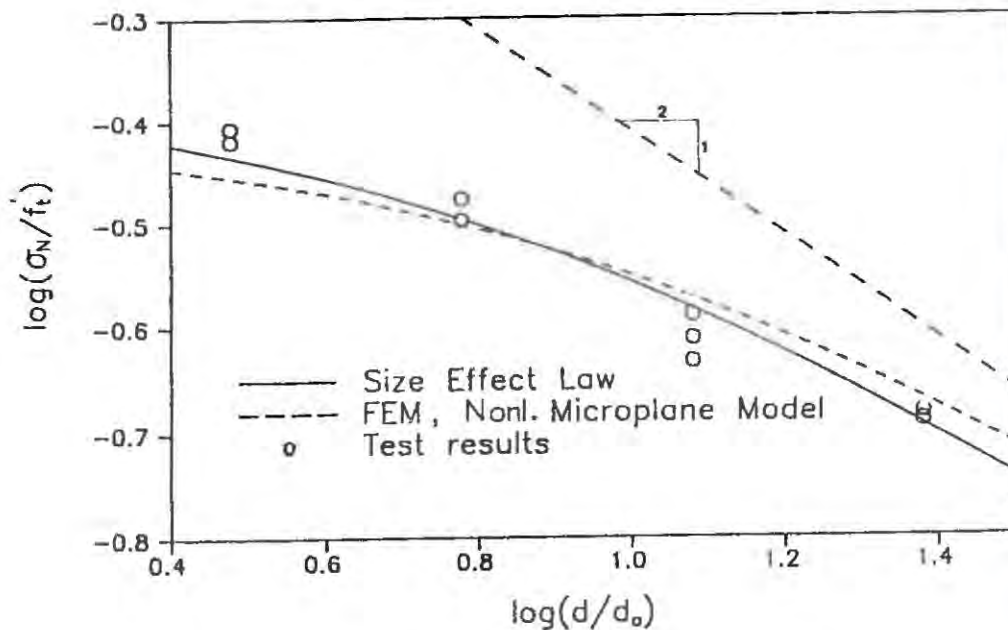


Fig.3.9 Maximum Loads of Notched Beam Specimens Calculated by Nonlocal Microplane Model, Compared to Size Effect Law and to Test Data (Bažant and Ozbolt, 1989)

Whether the  $\sigma_y(\delta_c)$  curve or  $\sigma_y(\epsilon_y)$  curve should be scaled down proportionally, or shifted down, or subjected to some more complex transformation to reflect the effect of  $\sigma_x$  is not known at present. When  $\sigma_x < 0$  and Fig. 3.9 is observed, then, of course, the area under the  $\sigma_y(\delta_c)$  curve does not represent the fracture energy  $G_f$ , but is less than  $G_f$ , i.e. Eq. 3.2 is invalid.

### 3.5 Random Particle Simulation of Microstructure

The most realistic, yet computationally extremely demanding, model for nonlinear fracture behavior of concrete is provided by the random particle simulation. Extensive investigations of this type have been carried out by Wittmann et al., (1984); see also Roelfstra et al., (1985), and Roelfstra (1987). Crack formation and propagation in computer generated composite structures was studied numerically. These investigators used standard finite element techniques, subdividing each aggregate piece and the mortar regions into many finite elements, and also considering weaker aggregate-mortar interfaces. The calculations provided valuable insights but are extremely demanding on computer time and storage which made it impossible to model very large structures.

In the simplest version of random particle simulation, also called the interface element model (Zubelewicz and Bažant, 1987; Bažant, Tabbara, Kazemi and Pijaudier-Cabot, 1989), the aggregate pieces are considered as rigid discs or spheres. An important aspect is that their configuration is generated randomly by the computer. A method to do this so as to satisfy the prescribed mix ratios of aggregates of various sizes has been successfully formulated (Bažant, Tabbara, Kazemi and Pijaudier-Cabot, 1989).

These models represent an adaptation of an earlier model of Cundall (1971), Serrano and Rodriguez-Ortiz (1973), Cundall and Strack (1979), Kawai (1980), and Plesha and Aifantis (1983) for granular materials such as rock, sand or gravel. In contrast to Cundall's model, the simple frictional tension-resisting connection between particles must be replaced by an inelastic interaction with fracture. This has been done by assuming all the interparticle deformations to be concentrated at a point at the middle of the interparticle contact layer of the matrix (mortar). In the original version of this model, both the normal and shear interactions (but not moments) were taken into account, the shear interaction being elastic, and the normal interaction exhibiting a sudden loss of strength after achieving the prescribed strength limit for the interparticle force. A simpler version, in which the shear interaction between particles is neglected and the normal (axial) interaction is characterized by a force-displacement curve with post-peak gradual softening in tension, has been developed by Bažant, Tabbara, Kazemi and Pijaudier-Cabot (1989) and shown to be sufficient for most purposes, except that it tends to give a fracture process zone that is narrower and shorter than that obtained when interparticle shear stiffness is taken into account (and also than that expected from size effect data from concrete fracture tests). This version of the model is equivalent to a random truss with softening members and represents a generalization of the model of Burt and Dougill (1977). The programming is quite similar to nonlinear finite element programs.

The random particle model has been shown to exhibit the size effect on the maximum load which agrees with fracture mechanics; see the results of Bažant, Tabbara, Kazemi and Pijaudier-Cabot (1989) in Fig. 3.10a, obtained with the random particle system for the fracture specimens in Fig. 3.10b. The random particle model seems to represent realistically the pattern of cracking in front of a notch or continuous fracture; see the results of Zubelewicz and Bažant (1987) in Fig. 3.10c, from which it appears that the width of the band of microcracks ahead of the continuous fracture tends to be about three maximum aggregate sizes.

So far the random particle simulations have been done only in two dimensions. Properly, of course, the simulation should be three-dimensional, but this would at present be preposterously demanding for computer time.

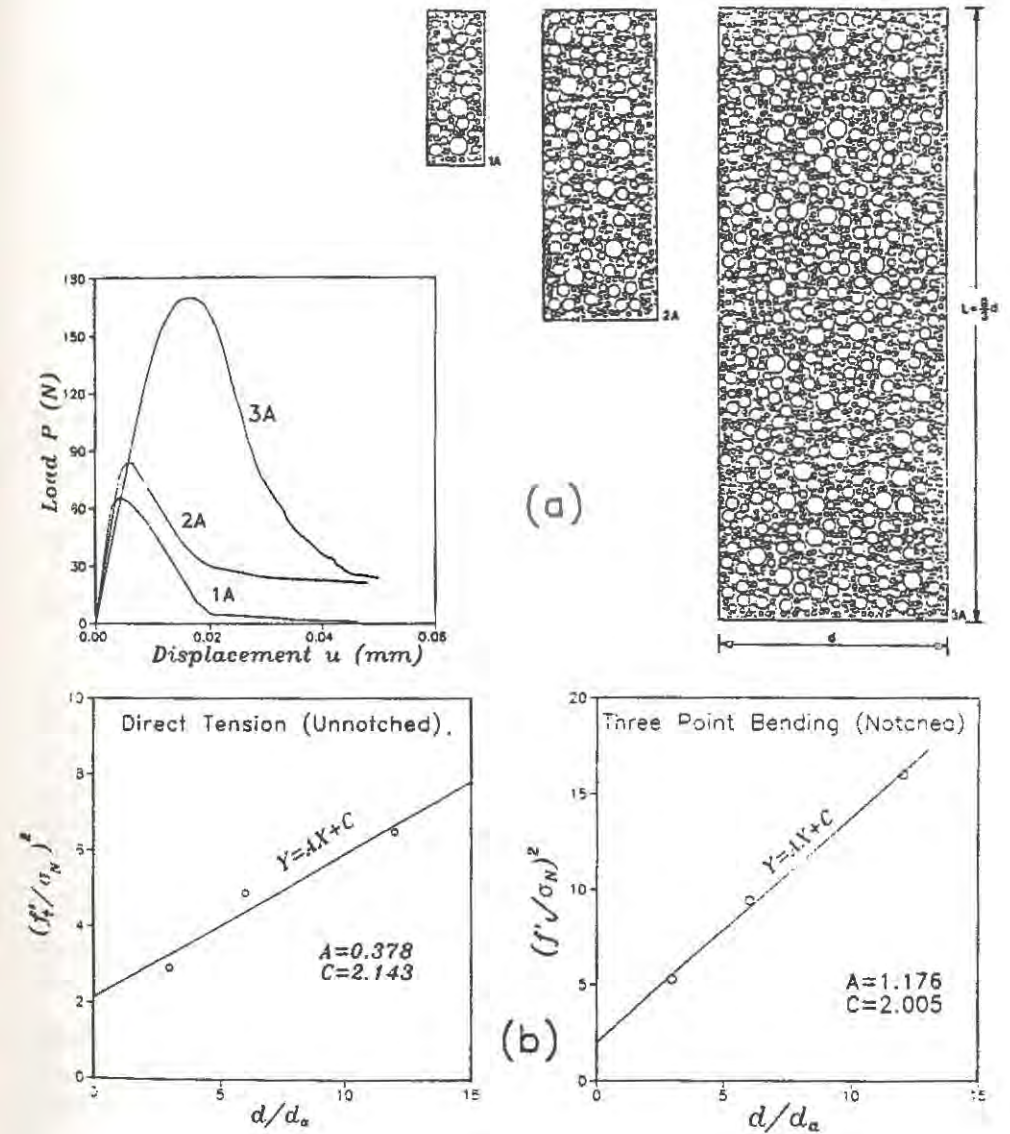


Fig.3.10 Random Particle Simulation of Concrete (a), Resulting Load-Deflection Curves and Size Effect (b), and Cracking Pattern (c)

(continued)

(c)

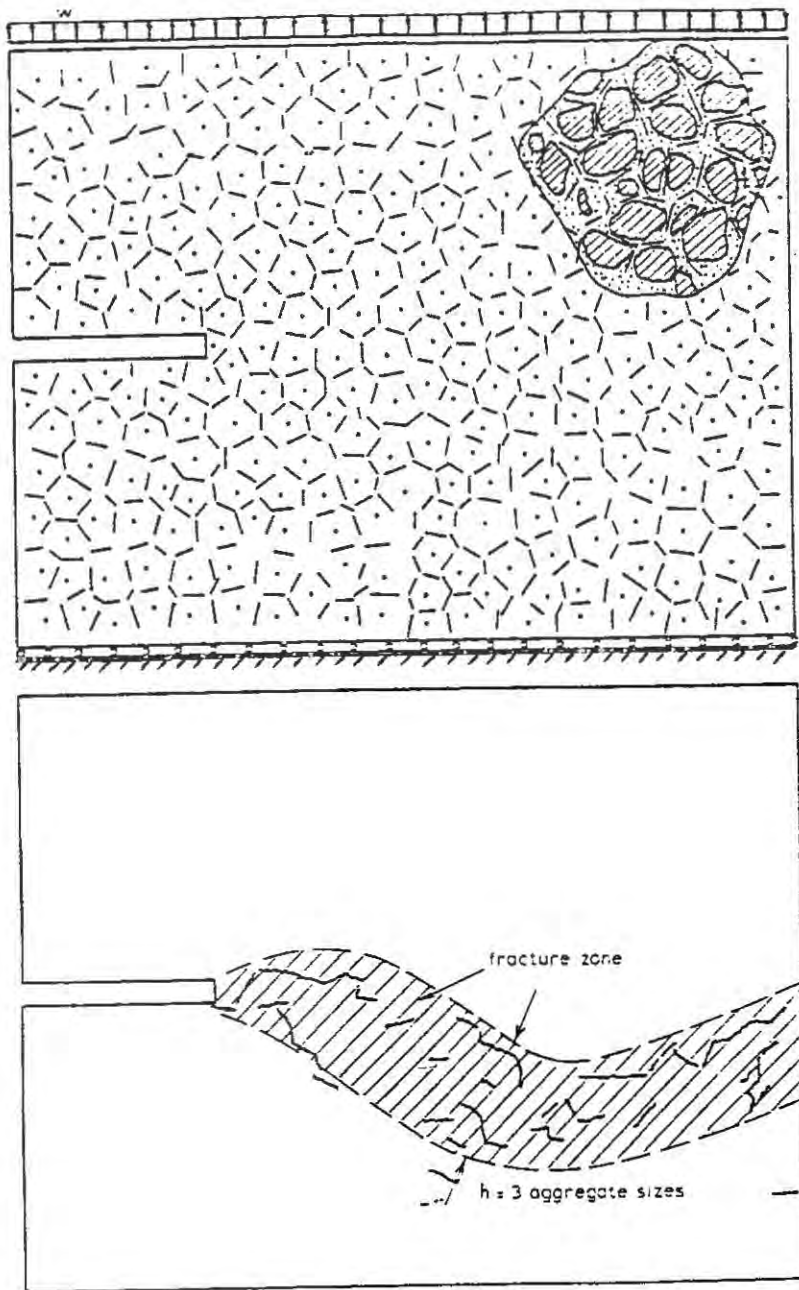


Fig. 3.10 continuation

## Chapter 4. SPECIAL NONLINEAR FRACTURE MODELS BASED ON ADAPTATIONS OF LEFM

Special nonlinear fracture models do not attempt to model the behavior of the fracture process zone through stress-displacement or stress-strain relations. Instead, they introduce some adaptations of linear elastic fracture mechanics (LEFM) which approximately reflect the nonlinearity of fracture behavior.

### 4.1 Effective Crack Models

The effect of a large-size fracture process zone at the tip of the notch or continuous crack is to reduce the stresses near the crack tip and push the peak stress farther ahead. Consequently, the specimen behaves roughly as an elastic specimen with a longer, effective crack length,  $a_e$ . This length can be defined in various ways, giving somewhat different results. In Dugdale-Barenblatt-type models for ductile metals, the effective crack length is calculated usually from the condition that the sum of the stress intensity factors at the tip of the effective crack due to the far field stresses and to the yield stresses in the fracture process zone be zero (Dugdale, 1960; Barenblatt, 1959).

But this definition seems neither quite appropriate nor too convenient for brittle materials. For these materials, an elastically equivalent (Griffith-type) effective crack has been defined as the crack for which the elastically calculated compliance of the specimen is the same as the measured unloading compliance  $C_u$  for unloading of the specimen from the peak-load point (critical state). Effective crack models for concrete using this definition have been proposed by Nallathambi and Karihaloo (1986a) and Swartz and Refai (1989). The effective crack length,  $a_e$ , depends on the microstructure, as well as the geometry of the specimen. When  $K_{Ic}$  is calculated using the effective crack, the results seem to be approximately size independent. Thus it appears that  $a_e$  and  $K_{Ic}$  might be used as two fracture parameters. To this end, empirical relations for relating the effective crack length to the notch length in a fracture specimen have been developed on the basis of experimental data by Nallathambi and Karihaloo (1986a).

The need for empirical equations relating the effective crack length to the notch length reduces the scope of applicability of this method. In addition, one needs empirical equations for each specimen geometry. These limitations are overcome in the two-parameter model proposed by Jenq and Shah. This model is described next.

### 4.2 Two-Parameter Model of Jenq and Shah

This model (Jenq and Shah, 1985a, 1985b; Shah, 1988), which appears to give a rather realistic prediction of concrete fracture behavior, involves two fracture parameters: (1) the critical stress intensity factor  $K_{Ic}$  at the tip of an effective crack of length  $a_e$  at  $P_u$ , and the critical value  $\delta_{CTOD}$  of the crack tip opening displacement, which is calculated at the tip of the pre-existing crack or notch, whose length is denoted as  $a_0$ , and at  $P_u$ . The effective crack

length, as mentioned before, can be calculated from the compliance  $C_u$  recorded at unloading when the specimen is loaded to the critical state (Fig. 4.1). Jenq and Shah experimentally observed that when  $a_e$  was calculated from the compliance measurements for notched beam specimens, the calculated values of  $\delta_{CTOD}$  were more or less independent of the size as well as geometry of the specimens. This indicated that  $\delta_{CTOD}$  and  $K_{Ic}$  may be fundamental material parameters. Using these two parameters, Jenq and Shah also predicted the uniaxial tensile strength, the split cylinder strength, the size effect on conventional  $K_{Ic}$ , and the size effect on the modulus of rupture.

The effective crack length,  $a_e$ , calculated on the basis of these two fracture parameters is found to depend on the size of the specimen, on the compressive strength of concrete, and on the strain rate. The value of  $a_e$  decreases with increasing strength and with increasing strain rate. For the case of an elastic perfectly brittle material,  $\delta_{CTOD}$  approaches zero and  $a_e$  approaches  $a_0$ .

The value of  $K_{Ic}$  from this model has been shown to be essentially independent of the geometry of the specimens. Results obtained using compact tension tests, wedge splitting cube tests and large, tapered, double cantilever beams conducted under the auspices of RILEM Committee FMT 89 showed that the two fracture parameters ( $K_{Ic}$  and  $\delta_{CTOD}$ ) might be considered as geometry-independent material parameters (Jenq and Shah, 1988a), although a later study (Jenq and Shah, 1988b) indicated a significant influence of geometry. It should be noted that this model can be applied to specimens and structures with or without notches. The model has been extended to mixed-mode loading and to impact loading (John and Shah, 1985, 1986, 1989).

### 4.3 Geometry-Dependent R-Curve Determined from Size Effect Law

A quasi-elastic analysis of nonlinear fracture can be accomplished by considering the energy required for crack growth,  $R$ , to be variable rather than constant. The curve of  $R$  vs. the crack extension  $c$  is called the R-curve (or resistance curve). The crack propagation condition is  $G = R(c)$  rather than  $G = G_f$ , and if the value of  $R(c)$  is known, the response is calculated according to linear elastic fracture mechanics, replacing  $G_f$  with  $R(c)$ . Alternatively, but equivalently, one can define the R-curve in terms of the critical stress intensity factor  $K_{Ic}$  with  $K_{IR} = (E'G_f)^{1/2}$ , and use the crack propagation condition  $K_I = K_{IR}$  instead of  $K_I = K_{Ic}$ . The physical reason that the energy release rate,  $R$ , required for crack growth increases with  $c$  is that it is determined by the size of the fracture process zone, which grows. A larger process zone dissipates more energy. How the zone grows, of course, depends also on interaction with the boundaries.

The concept of R-curves was suggested by Irwin (1958) and formulated for metals in detail by Krafft et al. (1961). For certain types of concrete specimens, R-curves were measured by Wecharatana and Shah (1980, 1982) and Jenq and Shah (1985a). For a long time it was thought that the R-curve measured experimentally on a specimen of one geometry can be used universally, as a material property applicable approximately to other geometries. But

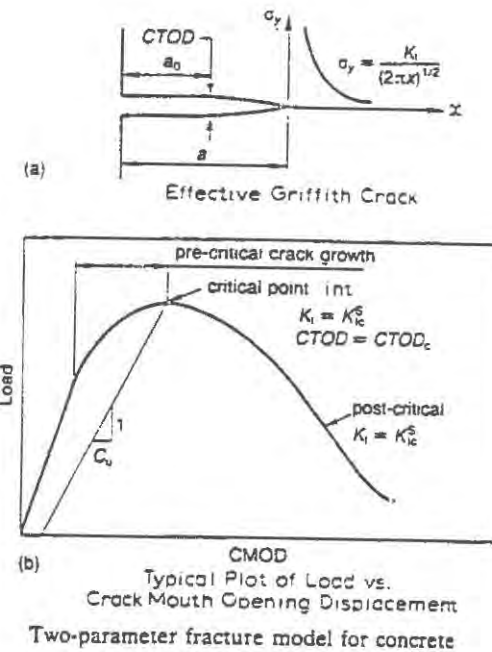


Fig.4.1 Two Parameter Fracture Model of Jenq and Shah (1985)

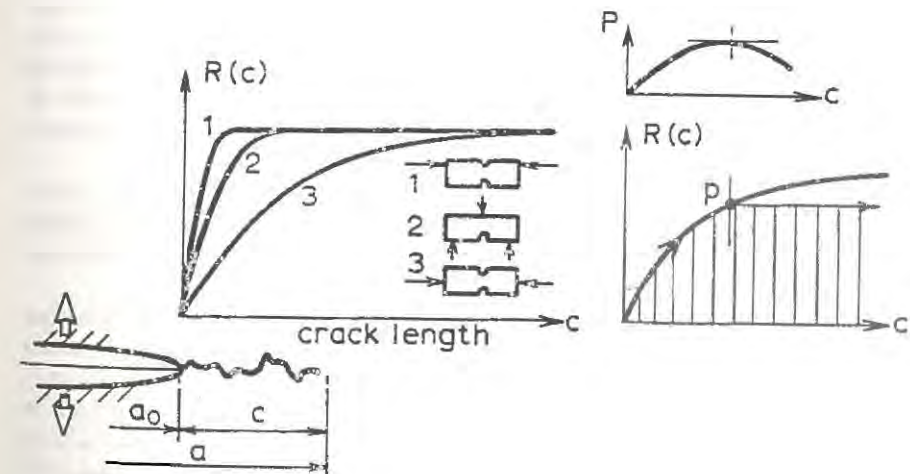


Fig.4.2 R-Curves for Different Specimen Geometries and Their Post-Peak Adjustments

this has not turned out to be the case. Today we know (e.g. Wecharatana and Shah, 1983a; Bažant, Kim and Pfeiffer, 1986) that for concrete, R-curves depend strongly on the shape of the structure or specimen. Therefore, to enable the use of R-curves which certainly represent a very simple approach, one needs some method to obtain the R-curve for a given specimen geometry from some basic fracture characteristics.

As proposed by Bažant and Cedolin (1984), and Bažant, Kim and Pfeiffer (1986), the R-curve for any given geometry may be determined on the basis of the size effect law (Sec. 5.1). This law (Eq. 1.4) appears adequate for that purpose since (unlike the R-curve) it is applicable, in the same form, to most geometries within a size range up to about 1:20, which suffices for most applications. The R-curve is then obtained as the envelope of the fracture equilibrium curves for geometrically similar specimens of various sizes. An easy calculation of the R-curve is possible once the parameters of the size effect law have been determined. In particular, the R-curve, giving the fracture energy required per unit crack growth, can be obtained (according to Bažant and Kazemi, 1988) as follows (for derivation, see Appendix I):

$$R(c) = G_f \frac{g'(\alpha)}{g(\alpha_0)} \frac{c}{c_f} \quad (\alpha = \frac{a}{d}, \alpha_0 = \frac{a_0}{d}, c = a - a_0) \quad (4.1)$$

$$\text{in which } \frac{c}{c_f} = \frac{g'(\alpha)}{g(\alpha_0)} \left( \frac{g(\alpha)}{g'(\alpha)} - \alpha + \alpha_0 \right) \quad (4.2)$$

where  $G_f$  = fracture energy (obtained from the size effect law),  $c = a - a_0$  = crack extension from the notch or initial crack tip,  $g(\alpha)$  = nondimensional energy release rate defined by the total energy release rate  $G$  in the form  $G = g(\alpha)P^2/(Eb^2d)$  (using  $G = K_I^2/E'$ ,  $g(\alpha)$  can be found from the  $K_I$  - values which are available in handbooks such as Tada et al., 1985, and Murakami, 1987, for the basic specimen geometries, and can always be obtained by elastic analysis);  $\alpha_0 = a_0/d$ , and  $c_f = d_0g(\alpha_0)/g'(\alpha_0)$  where  $d_0$  is a constant from the size effect law;  $c_f$  is the effective length of the fracture process zone in an infinitely large specimen (see Eq. 5.5), defined as the distance from the notch tip to the tip of the equivalent elastic crack. The actual process zone length (defined as the distance from the notch tip to the point of maximum tensile stress) is about  $2c_f$ , as indicated by comparisons with various models of the process zone (e.g., Horii, 1988; Horii, et al., 1987, 1988; Planas and Elices, 1988a; Bažant and Kazemi, 1988).

Eqs. 4.1 and 4.2 define the R-curve parametrically. Knowing  $G_f$  and  $d_0$ , one may choose a series of  $\alpha$ -values, and for each of them calculate first  $c$  from Eq. 4.2 and then  $R(c)$  from Eq. 4.1. The R-curves which are obtained from Eqs. 4.1-4.2 for very different specimen geometries are very different from each other, as illustrated in Fig. 4.2a.

Recently it was found (Bažant, Gettu and Kazemi, 1989) that if the post-peak softening load-deflection curve is to be correctly predicted, the increase of  $R$  must be arrested at the peak-load point (point  $p$  in Fig. 4.2), as indicated by the horizontal line 13 in Fig. 4.2. The reason the critical energy release rate  $R$  cannot exceed that for the peak load state is that: (1) the increase of  $R$  is due to an increase of the fracture process zone size (a large zone dissipates more energy), and (2) in the post-peak response, the fracture process zone

detaches itself from the tip of the notch or initial crack and travels forward without growing in size. This behavior has previously been experimentally identified, e.g., from measurements on aluminum (Bažant, Lee and Pfeiffer, 1987) and was verified especially by tests of rock (Bažant, Gettu and Kazemi, 1989) and high-strength concrete (Gettu, Bažant and Karr, 1989).

The study of the R-curves indicates that the concept of elastically equivalent effective crack length cannot give very good results if a constant fracture energy value is associated with the effective crack. Calculation according to Eqs. 4.1-4.2 implies that not only the crack length,  $a = a_0 + c$ , differ from  $a_0$ , but also the energy release rate required for crack growth must be considered to increase with the crack length if a solution that is approximately equivalent to nonlinear fracture mechanics should be obtained. This is not done in some recently proposed models (e.g. Karihaloo's model, Sec. 4.1 and 6.6).

## Chapter 5. SIZE EFFECT AND BRITTLENESS OF STRUCTURES

The size effect is the most important consequence of fracture mechanics theory. Therefore, it is logical to determine fracture properties from it. Knowledge of the size effect is needed for the design of structures, which generally involves extrapolation from laboratory-size to real-size structures. We have already explained the size effect in Chapter 1, and now we review its formulation and consequences in further detail.

### 5.1 Size Effect Law for Maximum Nominal Stress

We consider geometrically similar structures or specimens with geometrically similar notches or cracks. We will now illustrate the analysis for similarity in two dimensions, although the results are the same for similarity in three-dimensions (Bažant, 1987a). The nominal stress at failure (maximum load) may be defined as

$$\sigma_N = c_n \frac{P_u}{bd} \quad (5.1)$$

in which  $P_u$  = ultimate load,  $b$  = thickness of the structure,  $d$  = certain chosen characteristic dimension of the structure, and  $c_n$  = coefficient introduced for convenience. (For example, in the case of bending of a simply supported beam of span  $\ell$  and depth,  $d$ , with concentrated load at midspan, we may introduce  $\sigma_N$  as the maximum bending stress, i.e.  $\sigma_N = 3P_u\ell/2bd^2 = c_n P_u/bd$ , where  $c_n = 1.5\ell/d = \text{constant}$ ; but we can equally well take the characteristic dimension as  $d = \ell = \text{span}$ , and denoting  $h$  = beam depth we then have  $\sigma_N = c_n P_u/bh$  where  $c_n = 3\ell^2/2h^2 = \text{constant}$ , provided the beams are similar).

Noting that  $\sigma_N^2/2E$  represents the nominal strain energy density, the strain energy is  $U = V(\sigma_N^2/2E)\varphi(\alpha)$ , where  $V = c_0bd^2 = \text{volume of the structure}$  ( $c_0 = \text{constant}$ ) and  $\alpha = a/d$ . The energy release rate is given by  $bG = -\partial U/\partial a = -(\partial U/\partial \alpha)/d$ . Now with the notation  $-\varphi'(\alpha)c_n^2c_0/2 = g(\alpha)$ , the energy release rate of the structure is found to have the form

$$G = \frac{P^2g(\alpha)}{Eb^2d} = \frac{\sigma_N^2d}{c_n^2E}g(\alpha) \quad (5.2)$$

in which  $g(\alpha)$  is a known function of the relative crack length  $\alpha = a/d$ . Because  $G = K_I^2/E$ , function  $g(\alpha)$  may be obtained from the expressions for the stress intensity factors, which are always of the form  $K_I = Pk(\alpha)/\sqrt{d}$  where  $k(\alpha) = \text{non-dimensional function}$ . For typical specimen geometries, function  $k(\alpha)$  can be determined from the  $K_I$  values available in handbooks and textbooks, and for other geometries it can be obtained by linear elastic analysis.

Nonlinear fracture with a softening cohesive (fracture process) zone is approximately equivalent to linear elastic fracture of an increased crack length

$$a = a_0 + c \quad \text{or} \quad \alpha = \alpha_0 + (c/d) \quad (5.3)$$

where  $a_0$  = the actual length of the continuous crack or notch, and  $c$  = distance of the tip of the equivalent elastic crack from the tip of the initial crack or notch (Fig. 4.2).

Assuming that  $g'(\alpha) > 0$ , which applies to the majority of specimen geometries, the fracture process zone first grows in size while remaining attached to the tip of notch or initial crack. Since the value of  $G$  must depend on the length of the fracture process zone, it must depend on  $c$ . The fracture energy  $G_f$  may be considered to be the value of  $G$  reached for crack lengths  $c \geq c_f$  where  $c_f$  is a material constant. The value of  $c$  at maximum load is equal to  $c_f$  only for an infinitely large specimen ( $d \rightarrow \infty$ ), but is smaller than  $c_f$  in finite size specimens. Based on Taylor series expansion, we have

$$g(\alpha_f) \simeq g(\alpha_0) + g'(\alpha_0)(c_f/d) \quad (5.4)$$

where  $\alpha_f = c_f/d$  and  $g'(\alpha_0) = dg(\alpha_0)/d\alpha$ . It is reasonable to assume that the  $G$ -value at the peak-load is not constant but is proportional to the  $g(\alpha)$ -value at the peak load, i.e.  $G = G_f g(\alpha)/g(\alpha_f)$ . Substituting this and Eq. 5.4 into 5.2, setting  $P_u = (\sigma_N bd/c_n)^2$ , and solving for  $\sigma_N$ , one obtains

$$\sigma_N = c_n \left( \frac{EG_f}{g'(\alpha_0)c_f + g(\alpha_0)d} \right)^{1/2} \quad (5.5)$$

This represents the size effect law expressed in terms of material parameters (Bažant and Kazemi, 1988). Eq. 5.5 is equivalent to the size effect law  $\sigma_N = Bf'_i(1 + \beta)^{-1/2}$ ,  $\beta = d/d_0$  (Eq. 1.4) if one makes the notations:

$$B = \frac{c_n}{f'_i} \left( \frac{EG_f}{g'(\alpha_0)c_f} \right)^{1/2}, \quad d_0 = c_f \frac{g'(\alpha_0)}{g(\alpha_0)} \quad (5.6)$$

It may be noted that a more general size effect law has been derived;

$$\sigma_N = Bf'_i(1 + \beta^r)^{-1/2r},$$

but  $r$  depends on geometry, and for all geometries combined the value  $r \simeq 1$  was found to be approximately optimum (Bažant and Pfeiffer, 1987).

It is further useful to rewrite the size effect law in the form

$$\tau_N = \left( \frac{EG_f}{c_f + D} \right)^{1/2} \quad (5.7)$$

in which

$$\tau_n = \sqrt{g'(\alpha_0)} \frac{P_u}{bd}, \quad D = \frac{g(\alpha_0)}{g'(\alpha_0)} d \quad (5.8)$$

Here  $\tau_N$  and  $D$  may be interpreted as the shape-independent nominal stress at failure and the shape-independent characteristic dimension of the structure (Bažant and Kazemi, 1988; Bažant, Gettu and Kazemi, 1989).

In the case of three-dimensional similarity, we have  $U = V(\sigma_N^2/2E)\psi(\alpha)$ ,  $V = c_0d^3$  and  $c_1dG = -\partial U/\partial a = -(\partial U/\partial \alpha)/d$  in which  $c_0$  and  $c_1$  are some constants. Denoting  $-\psi'(\alpha)c_0/2c_1c_n^2 = g(\alpha)$  we obtain again Eq. 5.2, and all the remaining derivation is the same. Therefore, the results are again the same as Eq. 5.5 - 5.8.

The size effect law (Eq. 1.4, 5.5, 5.7) can also be derived very generally by means of dimensional analysis and similitude arguments (see Bažant, 1984a, 1985b, for two dimensions; and Bažant, 1987a, for three dimensions) if the following hypothesis is adopted:

The total energy release from the structure of any size  $d$  into the fracture process zone depends on both: (1) the length,  $a_0$ , of the continuous crack or notch, and (2) a length constant of the material  $\ell_0$ . Here  $\ell_0$  may represent the material constant combination  $\ell_0 = E'G_f/f_t^2$  (Irwin's characteristic size of nonlinear near-tip zone), or the effective length  $c_f$  of the fracture process zone in an infinitely large specimen, or the effective width  $w_c$  of this zone. If only part (1) of this hypothesis is adopted, one obtains the size effect of linear elastic fracture mechanics ( $\sigma_N \propto d^{-1/2}$ ), and if only part (2) is adopted, one obtains that of plastic limit analysis (i.e. no size effect).

From this hypothesis it appears that the size effect law is restricted neither to the crack band model nor to the line crack model but is valid for any nonlinear fracture model with a large process zone. Since the length or width of the fracture process zone is related to the characteristic length  $\ell$  of a nonlocal continuum, the size effect law also applies for the nonlocal continuum approach to fracture. This has been demonstrated by finite elements for a simple nonlocal smeared cracking model in Bažant and Lin (1988b) (see Fig. 3.6) and for the nonlocal microplane model (which also describes well nonlinear triaxial behavior in compressive states) by Bažant and Ožbolt (1989) (Fig. 3.9). Particle simulation of random microstructure (Bažant, Tabbara, Kazemi and Pijaudier-Cabot, 1989) also shows good agreement with the size effect law.

A basic criterion for acceptability of nonlinear finite element codes for concrete structures is that they must describe the transitional size effect (Eq. 1.4).

An extensive comparison of the size effect law with fracture test data for different specimen geometries for concrete as well as mortar is found in Bažant and Pfeiffer (1987); see Fig. 5.1 (where  $\lambda_0 = d_0/d_a$ ). These tests have shown that very different types of specimens (bending, centric tension, eccentric compression) yield about the same fracture energy (even though the other parameter values in Fig. 5.1 differ considerably).

### 5.2 Brittleness Number

Eq. 5.6 expresses the size effect law in terms of material fracture parameters,  $G_f$  and  $c_f$  (conversely, their definition and measurement may be based on the size effect law, Eq. 1.4). This fact was exploited by Bažant (1987a) to define the so-called brittleness number,  $\beta$ , which approximately describes the brittleness of the structural response regardless of the structure shape. Based on Eq. 5.7, the brittleness number is expressed as (Bažant and Kazemi, 1988):

$$\beta = \frac{D}{c_f} = \frac{g(\alpha_0) d}{g'(\alpha_0) c_f} \tag{5.9}$$

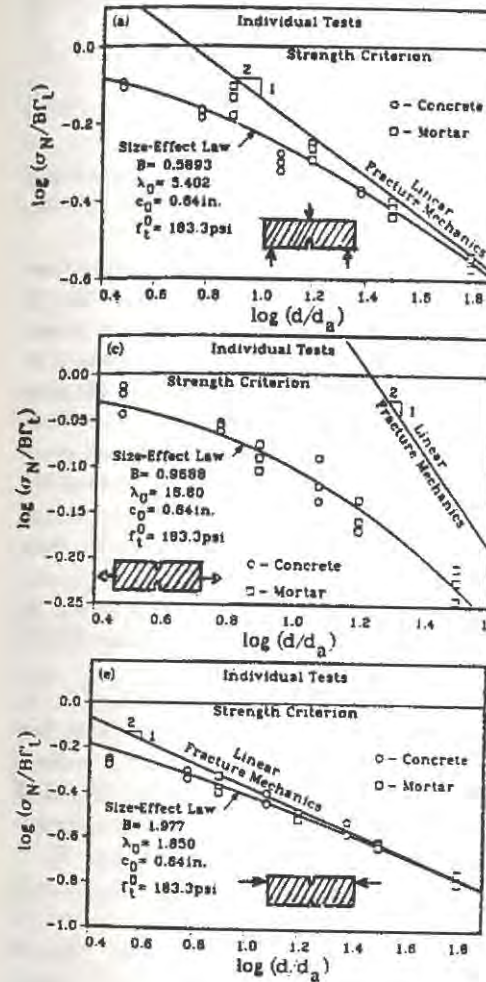


Fig.5.1 Comparison of Size Effect Law Eq. 4.1) with Test Results on Specimens of Various Geometries, for both Concrete and Mortar (after Bažant and Pfeiffer, 1987)

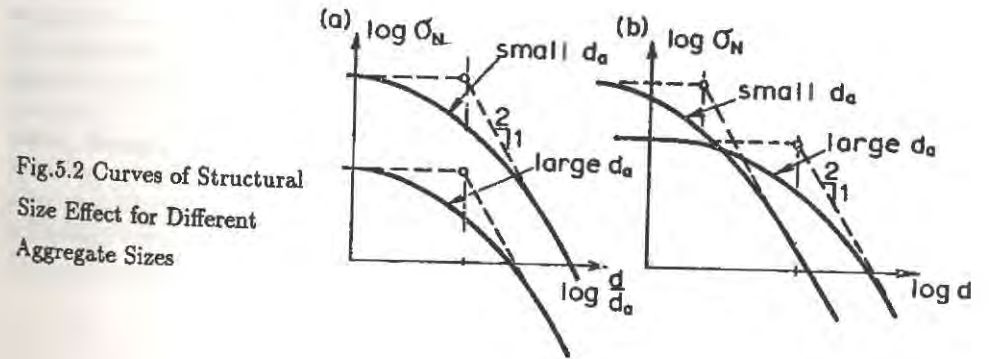


Fig.5.2 Curves of Structural Size Effect for Different Aggregate Sizes

while on the basis of the size effect law expression in Eq. 1.4 it is equivalently expressed as (Bažant, 1987a; Bažant and Pfeiffer, 1987):

$$\beta = \frac{d}{d_0} = B^2 g(\alpha_0) d \frac{f_t'^2}{EG_f} = AB^2 f_t'^2 d \quad (5.10)$$

Eq. 5.9 makes it possible to calculate  $\beta$  solely on the basis of a linear elastic fracture mechanics solution, for which the shape and the length of the continuous crack at ultimate load (or the notch length in a fracture specimen) must be known.

Eq. 5.10 yields the brittleness number which exactly agrees with the transition of the size effect law to the plastic analysis solution when the structure size is very small. Coefficient  $B$  can be determined as  $B = c_n P_u / bdf_t'$  where  $P_u$  = ultimate load stress according to a plastic limit analysis formula for the structural failure, such as employed in the current codes for diagonal shear failure, punching shear failure, torsional failure, etc. Eq. 5.10 is more accurate for small  $\beta$ , while Eq. 5.9 is more accurate for large  $\beta$ .

As a third method for determining  $b$ , if the maximum loads for a given structural geometry are known for significantly different sizes, e.g., on the basis of laboratory tests or on the basis of finite element analysis based on some method of nonlinear fracture mechanics, then regression of the test results by means of the size effect law yields the parameter  $d$ , from which  $b = d/d_0$ .

Alternatively, it also suffices to obtain the failure load  $P_u$  for a very small size ( $\beta \rightarrow 0$ ) by plastic limit analysis, which yields  $B = c_n P_u / bdf_t'$ , and then determine  $\sigma_N$  from the LEFM solution, which yields  $d_0/d = (\sigma_N / Bf_t')^2$ .

The value  $\beta = 1$  (or  $d = d_0$ ) corresponds in the size effect plot of  $\log \sigma_N$  vs.  $\log d$  to the point where the horizontal asymptote for the strength criterion and the inclined asymptote for the linear elastic fracture mechanics intersect; Fig. 1.4. For  $\beta < 1$ , the behavior is closer to plastic limit analysis, and for  $\beta > 1$  it is closer to linear elastic fracture mechanics. If  $\beta \ll 1$  or  $\beta \gg 1$ , nonlinear fracture mechanics is not necessary. The method of analysis may be chosen as follows (Bažant, 1987; Bažant and Pfeiffer, 1987):

$$\begin{aligned} \beta < 0.1 & \quad \text{plastic limit analysis} \\ 0.1 \leq \beta \leq 10 & \quad \text{nonlinear fracture mechanics} \\ \beta > 10 & \quad \text{linear elastic fracture mechanics} \end{aligned} \quad (5.11)$$

For  $\beta < 0.1$ , the error of the plastic limit analysis is less than 4.7% of  $\sigma_N$ , and for  $\beta > 10$  the error of linear elastic fracture mechanics is also less than 4.7%, compared to the nonlinear fracture mechanics solution. If an error under 2% is desired, then the nonlinear range must be expanded to  $1/25 \leq \beta \leq 25$ .

Other definitions of the brittleness number of a structure have been proposed before. Beginning with Irwin (1958), researchers in metals knew that structural brittleness is basically characterized by the ratio of the structure size to Irwin's size of the nonlinear zone, Eq. 2.10. This definition was co-opted for concrete structures by Hillerborg (1985b) (cf. also Elfgren, 1989) who proposed to characterize the structural brittleness by the ratio  $d/\ell_0$

where  $\ell_0 = EG_f/f_t'^2$  (he called  $\ell_0$  the "characteristic length"; but this conflicts with previous terminology in nonlocal continuum theory). Therefore we will call  $\ell_0$  the characteristic process zone size. Carpinteri (1982) proposed the brittleness number  $s = G_f/f_t'd$ . Similar definitions were earlier proposed for ceramics by Gogotsi et al. (1978) and Homeny et al. (1980). The brittleness numbers of Hillerborg, Carpinteri, Gogotsi and Homeny, however, are not independent of the structure geometry and thus cannot be used as universal, absolute characteristics (e.g.,  $\beta = 3$  could then mean a very brittle behavior for one structure geometry and a very ductile behavior for another geometry).

Although Eqs. 5.9 and 5.10 define the brittleness number in relation to the size effect on the ultimate load, the brittleness number also determines the nature of the post-peak response, particularly the steepness of the post-peak softening (load decrease at increasing displacement). That was already illustrated by the series model in Fig. 1.13.

In view of the universality of the brittleness number proposed by Bažant, it appears that a simple adjustment of the current limit-analysis-based code formulas, taking into account nonlinear fracture mechanics, can be made by replacing the nominal stress at ultimate load,  $v_u$ , as given without consideration of size effect, by the expression

$$\sigma_N = \frac{v_u}{\sqrt{1+\beta}} \quad (\geq v_u^{\min}) \quad (5.12)$$

However, the method to calculate  $d_0$ , on which  $\beta$  depends, still needs to be researched. Eq. 5.12 indicates that there might be a lower limit  $v_u^{\min}$  on the nominal strength, due to a possible transition to some non-brittle frictional failure mechanism. An example of such a limit is seen in Brazilian split-cylinder tests (see e.g. Bažant, 1987a).

## 5.3 Other Size Effects and Limitations

### 5.3.1 Effect of Residual Ductile or Frictional Limit

In Brazilian tests of split cylinder strength, Hasegawa et al. (1985) observed that the nominal stress at failure (i.e., the split cylinder strength) decreased with increasing diameter of the cylinder, however, beyond a certain large size of cylinder, no further decrease of the strength was observed (this behavior has now been confirmed by tests of Bažant, Kazemi, et al (1990)). This suggests that for a certain sufficiently large size, there is a transition to some non-brittle failure mechanism at the maximum load. The reason might be that for large sizes the maximum load is decided by friction on a small wedge-shaped region under the load application points. For small specimen diameters, the load to cause the splitting crack is much higher than the load to cause frictional slip of the wedge-shaped region, and therefore the brittle mechanism of cracking decides. However, if the size is very large about  $100 d_a$ , the nominal stress at which the splitting fracture occurs becomes very small, smaller than the nominal stress  $\sigma_N^Y$  which causes the frictional slip of the wedge; see Fig. 5.2. Thus, at least for this type of failure, it seems appropriate to put a lower limit on the size effect law,  $\sigma_N^Y$ , beyond which  $\sigma_N$  cannot be decreased. This might also be true for some other

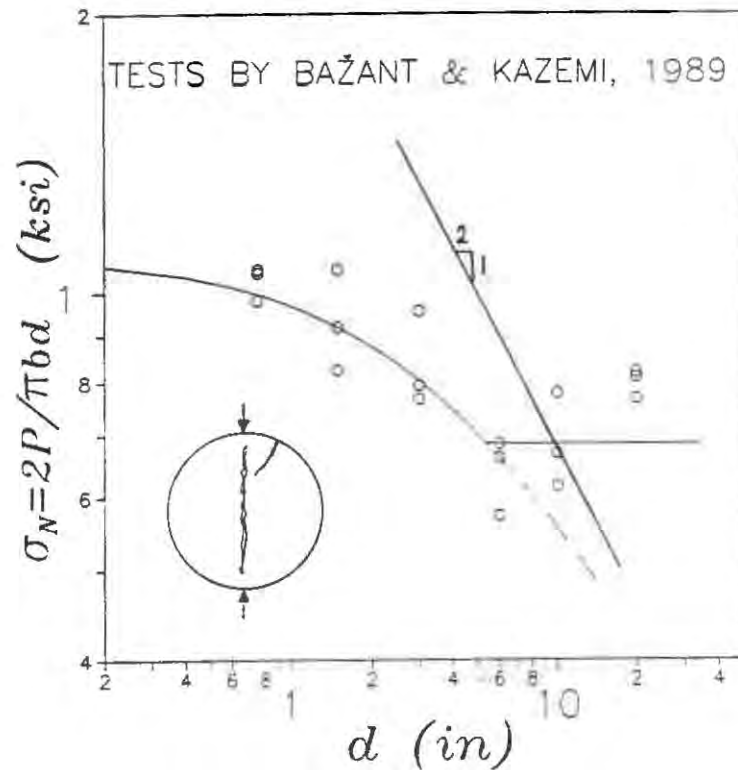
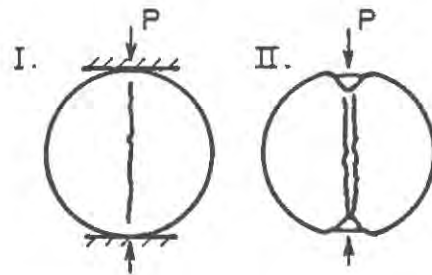


Fig.5.3 Deviation from the Size Effect Law (Eq. 4.1) Observed in Brazilian Compression Splitting Tests

failure mechanisms, especially those involving splitting cracks in compression.

### 5.3.2 Statistical Size Effect Due to Random Strength

Statistical heterogeneity of the material no doubt plays an important role in the micromechanisms determining the material strength. It describes the effect of the size distribution of the flaws in the microstructure on the material strength. However, for reasons already explained in Chapter 1, the randomness of strength due to the heterogeneity of the material, as described by Weibull-type probabilistic models, does not seem to have a major influence on the size effect observed in brittle failures of most concrete structures, except those where the maximum stress is uniform over a large part of the structure (e.g., a long uniformly stressed specimen in tension), or where the structure fails at first macrocrack initiation.

### 5.3.3 Diffusion-Type Size Effects

It must be kept in mind that significant structural size effects can be obtained due to the diffusion process of drying of concrete in structures, the conduction of heat produced by hydration, and the non-uniformities of creep produced by differences in temperature and moisture content throughout the structure.

### 5.3.4 Wall Effect as a Source of Size Effect

Still another type of size effect is caused by the fact that a boundary layer near the surface of concrete inevitably has a different composition and strength than the interior of concrete structure. This layer, whose thickness is about one aggregate size, contains a lower percentage of large aggregates and a higher percentage of mortar. This phenomenon is known as "wall effect". In a small structure, the effect of this layer is larger than in a large structure because the boundary layer thickness is independent of structure size. For very thick cross sections, this effect becomes negligible.

### 5.3.5 Size Effect Due to 3D Singularity at the Ends of the Crack-Edge

According to three dimensional linear elastic solutions, the stress intensity factor of a crack in a plate with a straight orthogonal front edge is not constant along the edge (i.e. across the thickness of the plate) but drops to zero at the intersections with the surfaces of the plate (Bažant and Estenssoro, 1979) (except if the Poisson's ratio were zero). The consequence is that the front edge of a propagating crack must be curved, such that the surface end points of the crack edge must be trailing behind the interior of a propagating crack. This engenders an effect of plate thickness on the average value of the stress intensity factor over the entire plate thickness. This size effect might not be large but can be completely

eliminated if the thicknesses of specimens of all sizes are the same.

### 5.3.6 Effect of Aggregate Size

The fracture parameters as well as the size effect law are valid only for structures made for one and the same concrete, which implies the same aggregate size. If the aggregate size is changed, the fracture parameters and the size effect law parameters change. As proposed by Bažant, the size effect law needs to be adjusted as follows (see also Bažant and Kim, 1984):

$$\sigma_N = \frac{Bf'_t}{\sqrt{1+\beta}}, \quad f'_t = f_t^0 \left( 1 + \sqrt{\frac{c_0}{d_a}} \right), \quad \beta = \frac{d}{d_0} \quad (5.13)$$

in which  $f_t^0$  is the direct tensile strength for a chosen reference concrete,  $f'_t$  is the direct tensile strength for maximum aggregate size  $d_a$ , and  $c_0$  = empirical constant. This formula is analogous to the Petch formula for the effect of grain size on the yield strength of polycrystalline metals, which is derived by the dislocation theory. Eq. 5.13 has been shown to agree reasonably well with the fracture test data of Chana (1981), Taylor (1972) and Iguro et al. (1985), and coefficient  $c_0$  has been calibrated.

Fig. 5.2 (Bažant, 1986) compares the size effect plots according to Eq. 5.13 for specimens with different maximum aggregate sizes  $d_a$ . The comparison is made under the assumption that  $d_0 = nd_a$  where  $n$  = constant, which is only approximate (and might be invalid if very different aggregate types, e.g. round and very elongated aggregates, or crushed and river aggregates are used. According to Eq. 5.13, the size effect curves in the plot of  $\log \sigma_N$  vs  $\log d$  have the same shape for any  $d$ , i.e., one transforms to another by translation. An increase of  $d_a$  not only shifts the size effect curve vertically downward (due to the term  $c_0/d_a$ ) but also to the right (because  $d_0 = nd_a$  is contained in the brittleness number  $\beta$ ).

Consequently, the size effect curves for different  $d_a$  may intersect, as shown in Fig. 5.2 (this must happen unless the material constant  $c_0$  is large enough). Thus, for a sufficiently small specimen size, a higher nominal strength is obtained with smaller aggregate sizes  $d_a$ , while for a sufficiently large specimen size, a higher nominal strength is obtained with larger aggregate sizes. For intermediate structure sizes, the aggregate size makes little difference.

Since the intersection point of the two curves in Fig. 5.2 is not known very accurately, there may be a large range of structure sizes in which the effect of the maximum aggregate size is uncertain. For small beams and slabs, this fracture analysis would suggest using a small aggregate. Concrete dams are so large that the larger the aggregate the better, as far as the dam strength is concerned. However, recent fracture tests of dam concretes of Saouma et al. (1989) indicate a surprisingly small effect of aggregate size as compared to the effect of aggregate shape.

Aggregate size and gradation effects have also been studied for polymer concretes (Vipulanandan and Dharmarajan, 1987, 1988, 1989a,b,c; Dharmarajan and Vipulanandan, 1988). For example, they found that a polymer concrete with well graded sand has 20% higher  $K_{Ic}$

than that with a uniform sand.

### 5.3.7 Effect of Matrix Strength and High Strength Concretes

The recent spectacular advances in the strength of concrete have been achieved mainly by increasing the strength of the matrix and the aggregate-matrix bond. In high strength concretes, the differences between the strength and elastic modulus of the aggregate and the matrix (mortar) are much smaller than they are for normal strength concrete. Consequently, high strength concrete behaves as a more homogeneous material, and the result is that the fracture process zone becomes smaller (John and Shah, 1989b; Gettu, Bažant and Karr, 1989). In view of the discussion of the size effect (especially the fact that coefficient  $d_0$  in the size effect law is related to the size of the fracture process zone), it is clear that, for the same structural size, the behavior of high strength concrete is closer to linear elastic fracture mechanics, i.e., more brittle, than the behavior of the same structure made of normal concrete. Therefore, fracture mechanics analysis and size effects are much more important for high strength concretes than for normal strength concretes (e.g., Shah, 1988).

### 5.3.8 Suppression of Size Effect by Yield of Reinforcement

Aside from providing an additional ductile mechanism which carries part of the load, the effect of reinforcement is to spread the fracture process zone. Therefore, reinforced concrete is generally less susceptible to fracture effects and the accompanying size effects than unreinforced concrete. Further studies are needed in this regard.

It must be kept in mind though, that despite reinforcement, many failures of concrete structures are brittle. According to the current philosophy, the ultimate load is a sum of that due to yield mechanisms (e.g., the yielding of stirrups in diagonal shear) and that due to concrete alone, without reinforcing bars. This might often be a conservative approach, which in fact implies that the concrete contribution to the ultimate load should be analyzed according to fracture mechanics. It is likely, however, that the presence of steel and its yielding alters the fracture behavior of concrete, increasing the contribution to failure load due to concrete alone (Bažant and Sun, 1987). These problems need to be studied further.

## Chapter 6. EXPERIMENTAL OR ANALYTICAL DETERMINATION OF MATERIAL FRACTURE PARAMETERS

After a slow start, made as early as 1961 (Kaplan, 1961), fracture testing of concrete has developed tremendously during the 1980's. A number of experimental testing techniques and specimen types have been tried, and the developments crystalized into some effective methods.

### 6.1 Notched Beam Tests

#### 6.1.1 Notched Beam Tests Using LEFM

Beam tests have been most popular; probably because of similarities with the standard modulus of rupture test and because the first LEFM test standard for metals used this (ASTM, 1983). In addition, testing procedures are simpler than for other geometries and alignment errors are minimal. A typical beam geometry and three-point loading are presented in Fig. 6.1a. The span to depth ratio frequently is 4:1 which conforms with the requirements of the ASTM standard E399 (1983). This is because formulas for opening mode stress-intensity factors for beams are given for  $S/d = 4$  or 8 - Tada et al., (1984) and Murakami (1987) are typical sources - although formulas can also be obtained for other  $S/d$  ratios (e.g., Go, Swartz and Hu, 1986).

The test usually consists of the following steps.

1. Notch the beam to depth  $a_0$  at midspan. This could be done by a sawcut or by an insert cast into the beam and later removed.
2. Using a constant rate, about 1 to 10 min. to failure, increase the load, deflection or crack opening until failure. Record the load-deflection ( $\delta_{LPD}$ ) or load-crack mouth opening displacement ( $\delta_{CMOD}$ ) response continuously.
3. The peak load  $P_u$  or the load  $P_Q$  at the intersection with a secant of slope 95% of initial slope, see Fig. 6.1b, is then used to calculate the fracture toughness from the relationship (ASTM, 1983; Tada et al., 1985; Go, Swartz and Hu, 1986; Murakami, 1987)

$$K_{Ic} = F(S, d, b, a_0, P_u \text{ or } P_Q) \quad (6.1)$$

The value of  $K_{Ic}$  so determined is presumed to be the critical, opening mode stress intensity factor associated with unstable crack growth and is a material property.

If  $K_{Ic}$  is, in fact, a material property obtainable from the unmodified use of LEFM, the following should be true: (1)  $K_{Ic}$  should be invariant with respect to beam size and notch depth or crack depth. (2) Any zone of "plasticity" or "micro-cracking," i.e., the fracture process zone, should be very small compared to the notch depth. ASTM E399 (1983) gives

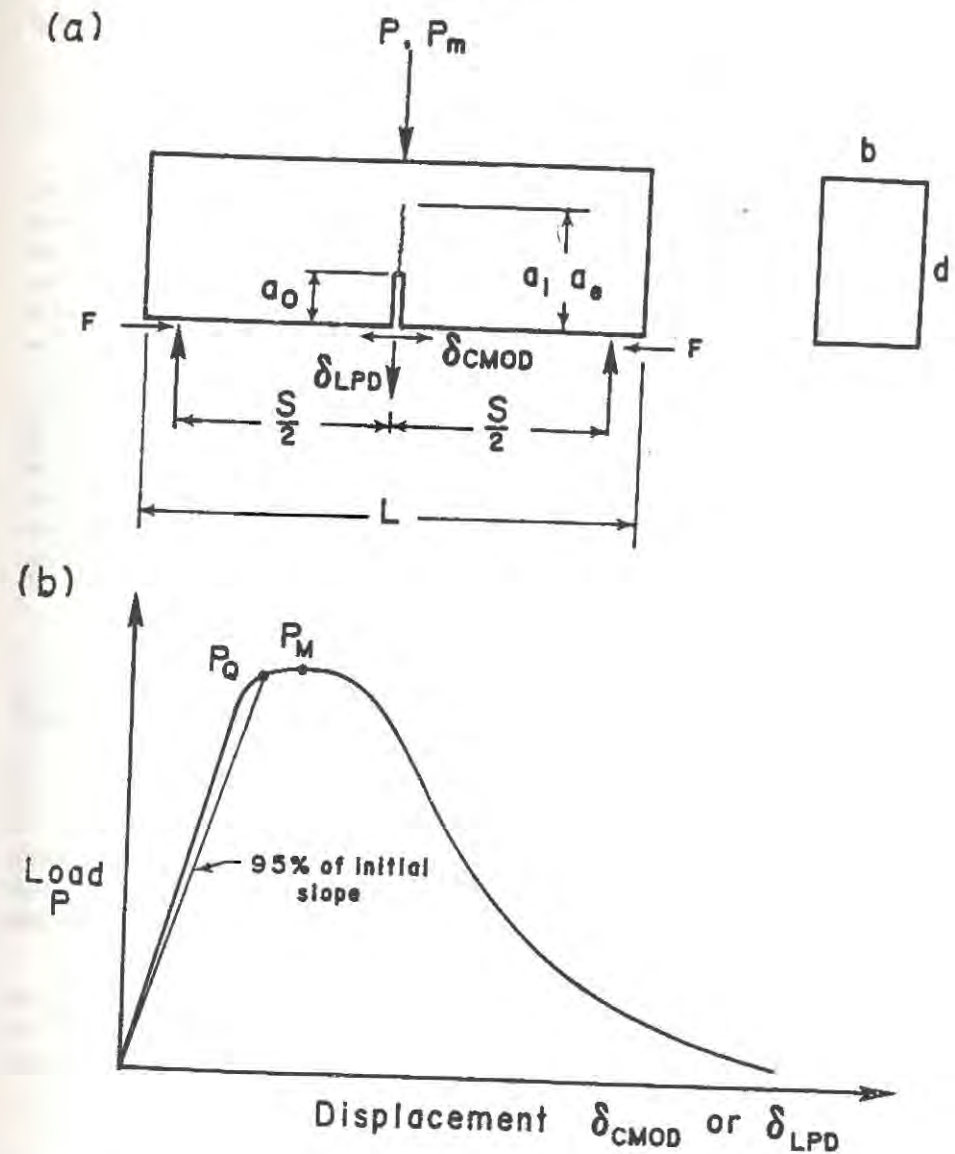


Fig.6.1 (a) Notched Beam in Three-Point Bending and (b) Load-Displacement Curve

a formula to determine if this requirement is satisfied. This has been adapted to concrete (Sec. 6.8). (3) The critical energy release rate is related to  $K_{Ic}$  by

$$G_{Ic} = \frac{K_{Ic}^2}{E} \quad (6.2)$$

In which the (slight) influence of Poisson's ratio is neglected and  $E$  is the modulus of elasticity.

The early researchers found that  $K_{Ic}$ , or  $G_{Ic}$ , was constant with respect to neither beam size (Walsh, 1972, 1976) nor notch depth (Swartz, Hu, Fartash and Huang, 1982) for concrete beams. One possible explanation for this was provided by Shah and McGarry (1971) who noted that cracks are arrested by the aggregate particles. Additional energy is required to propagate the cracks through and/or around these particles. Another possible reason for the variation in  $K_{Ic}$  measured by LEFM was suggested by Swartz and co-workers (Swartz, Hu, Fartash and Huang, 1982; Swartz, Hu and Jones, 1978; Swartz and Go, 1984). They noted that the data evaluations in the early tests (Naus and Lott, 1969; Walsh, 1972, 1976) were referenced to the original notch depth,  $a_0$ . This violates one of the requirements of the ASTM method for metals, namely that a true crack - not a notch - is to be used. Of course, measuring the actual crack length in concrete is quite difficult and, in fact, a precise result is impossible, since the crack front is strongly non-uniform through the specimen thickness.

### 6.1.2 Compliance Calibration Method

In an attempt to estimate the crack length in plain concrete beams subjected to three-point bending, an indirect method based on the compliance of notched beams was proposed by Swartz, Hu and Jones (1978). This test procedure is as follows:

1. Notch a beam at midspan.
2. Mount a displacement gage to measure the crack-mouth-opening displacement  $\delta_{CMOD}$  (see Fig. 6.1a) and cycle the load on the beam three times while plotting load  $P$  versus  $\delta_{CMOD}$ . The maximum load is selected to be less than 1/3 the expected failure load for that notch depth.
3. Measure the inverse slope of the  $P$  versus  $\delta_{CMOD}$  plot. This is the compliance  $C$  for the notch depth. (This is, of course, only an apparent indirect measure of compliance. The true compliance would be obtained by measuring the vertical load-point displacement  $\delta_{LPD}$ , or by loading the specimen at the crack mouth.)
4. Repeat steps a-c for different notch depths using the same beam.
5. Plot  $C$  versus  $a_0/d$ . A typical plot is shown in Fig. 6.2.

Subsequently, the experimentally determined compliance plot is used to estimate the initial crack length of precracked beams loaded to failure (Swartz, Hu and Jones, 1978). The use of precracked beams was felt to be necessary in order to obtain valid fracture

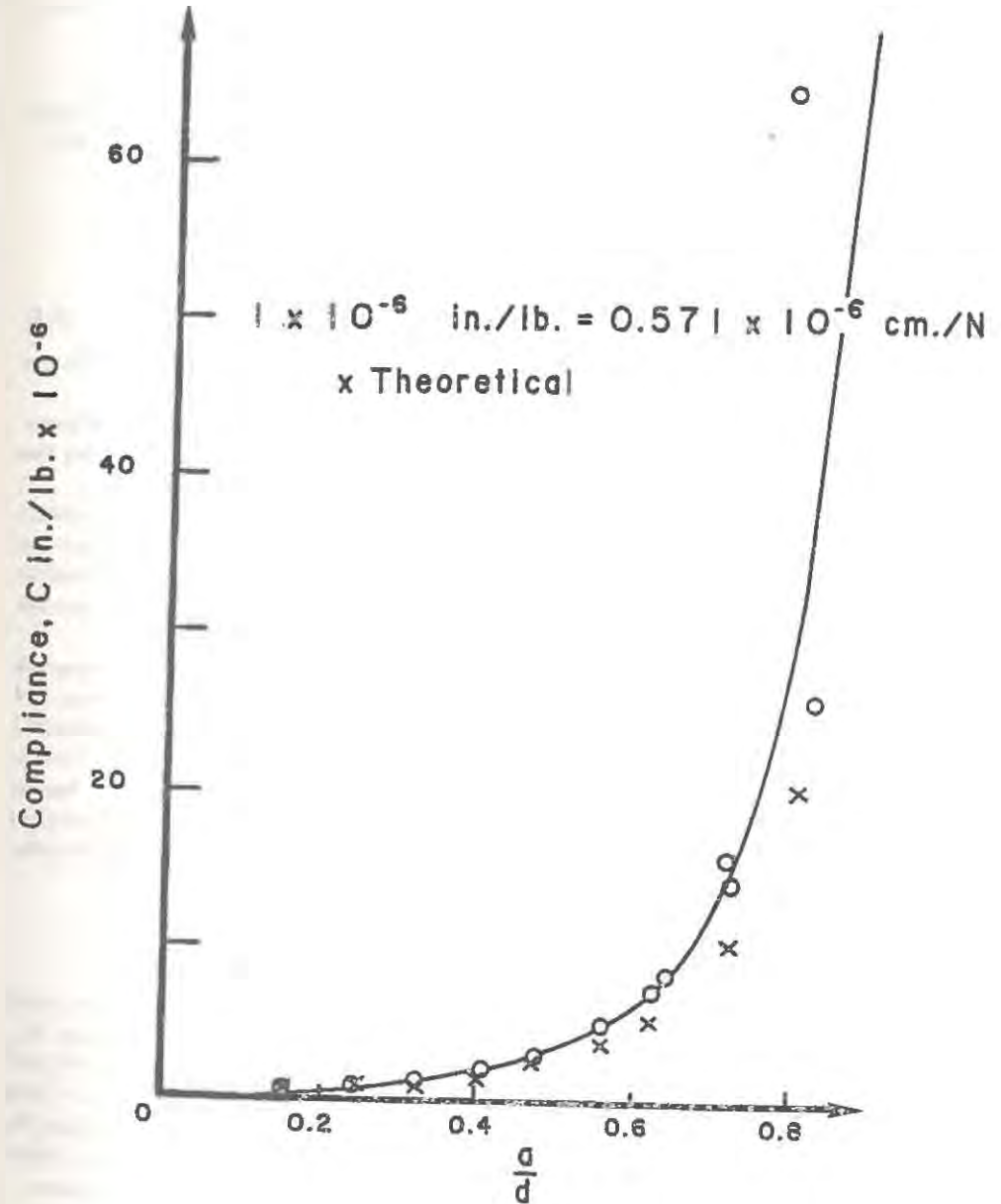


Fig.6.2 Compliance Calibration Curve for Notched Beam

data because the phenomenon of crack closing stresses makes it impossible to model a real crack with a notch.

The procedure to precrack a (different) beam for a subsequent load test was as follows:

6. Cut a small, starter notch at midspan. This was typically  $a_0/d \leq 0.10$ .
7. Load the beam to a load beyond  $P_u$  to grow a crack from the notch until the  $P - \delta_{CMOD}$  unloading or re-loading slope matches that associated with the desired crack length. After the beam is precracked, then
8. Load the beam to failure and measure  $P_u$  or  $P_Q$ . Calculate  $K_{Ic}$  from

$$K_{Ic} = F(S, d, b, a_i, P_u, \text{ or } P_Q) \quad (6.3)$$

Notice that the only difference between this and the earlier LEFM procedure is the use of  $a_i$  instead of  $a_0$ .

Using the relation of compliance to crack length calculated from LEFM, one can determine the initial crack length  $a_i$  from the slope of the  $P - \delta_{CMOD}$  curve (Fig. 6.3) after the initial crack closure stresses are overcome.

This method of testing requires the use of a closed-loop electro-hydrodynamic system in which the controlled, feedback variable is the output of the transducer used to measure the  $\delta_{CMOD}$ . This has traditionally been called "strain control." This term may approximately apply if the controlled variable is the  $\delta_{CMOD}$  or some other beam displacement, but not the stroke displacement of the testing system.

A test was made to show a direct comparison between notched beams and precracked beams following the procedures described above and using Eq. 6.1 for the notched beams and Eq. 6.3 for the precracked beams. It was found that the computed  $K_{Ic}$  for the precracked beams was always higher than for the notched beams (Swartz, Hu, Fartash and Huang, 1982). However, this approach was criticized because notched - not precracked - beams were used to construct the compliance calibration curves (see steps a-e). A further criticism was that, due to slow crack growth, the initial crack length  $a_i$  might not be appropriate for determining  $K_{Ic}$ . Therefore this method was modified.

### 6.1.3 Modified Compliance Calibration Method

The modification was to use precracked beams which are impregnated by a dye to reveal the shape of the crack front, and then use the extended crack length  $a_e$  to determine  $K_{Ic}$ . The method was first proposed by Go (Swartz and Go, 1984; Go and Swartz, 1986) and subsequently refined by Refai (Swartz and Refai, 1989). Precracked beams are used both for the creation of a compliance calibration curve and for failure tests. The method has the disadvantage that it is quite time-consuming and a number of beams are required to obtain a calibration curve instead of just one beam. The procedure for each beam is as follows:

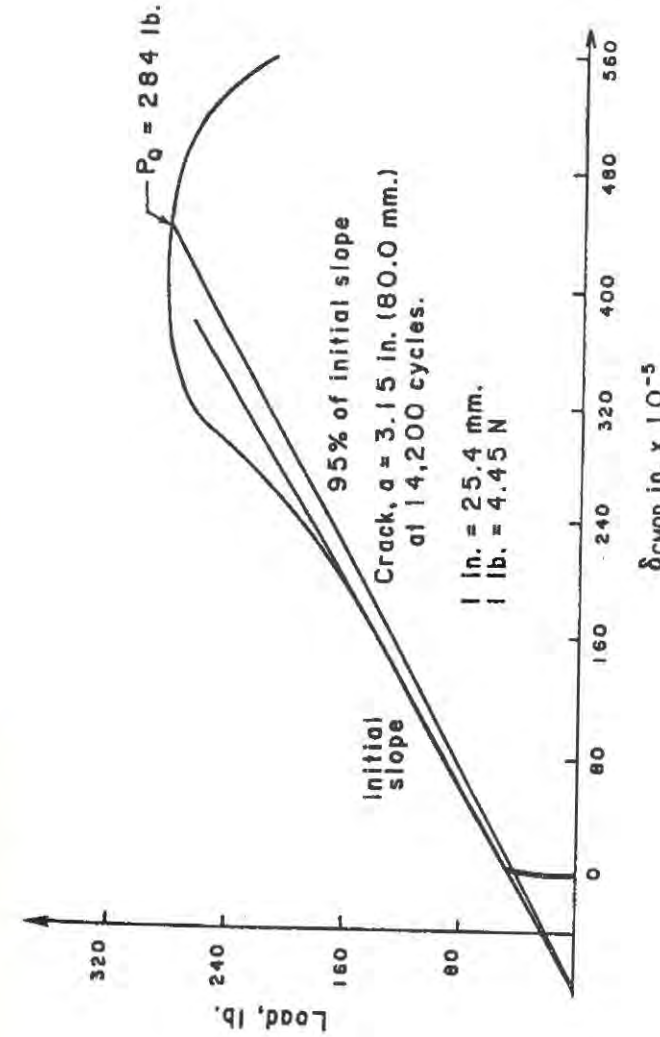


Fig.6.3 Load versus  $\delta_{CMOD}$

1. Cut a small starter notch at midspan.
2. Using a ramping function and strain control, load the beam beyond  $P_u$ , grow a crack and then remove the load. Subsequently, plot  $P$  versus  $\delta_{CMOD}$  using a maximum load  $\leq 1/3$  the maximum load associated with the crack.
3. Introduce the dye and cycle the load to work the dye into the cracked surface. The beam must be loaded with the crack proceeding from the top surface downward. The load must be greater than that needed to overcome crack closure stresses and must be less than about  $1/3$  of  $P_u$ .
4. Dry the dyed surface and load the beam to failure. Plot  $P$  and  $\Delta_{CMOD}$ . The initial slope after crack closure is overcome gives the initial compliance  $C_i$ .
5. After failure, measure the dyed surface area. The initial crack length is

$$a_i = (\text{area of dyed surface})/b \quad (6.4)$$

Typical dyed surfaces are shown in Fig. 6.4.

6. Repeat steps 1-5 for different crack depths and establish calibration curves relating  $C_i$  and  $a_i$ ,  $P_u$  and  $a_i$ . The latter relationship allows one to obtain an estimate of the crack length associated with any load on the softening part of the load-displacement plot.
7. At the point on the unloading plot corresponding to the onset of unstable crack growth - taken to be at  $0.95 P_u$  determine the extended crack length  $a_e$  from the  $P_u - a_i$  plot (step 6). The extended length must not be greater than  $a_e/d = 0.65$ . Using  $0.95 P_u$  and  $a_e$  compute  $K_{Ic}$  from

$$K_{Ic} = F(S, d, b, a_e, 0.95 P_u) \quad (6.5)$$

The validity of the procedure to estimate the extended crack length  $a_e$  may be argued by referring to a load-unload-reload diagram (Fig. 6.5). The objective is to determine the crack length at some point on the softening branch - say point  $C$  (which may be any point). If the actual unloading trace is available, the unloading compliance  $C_u$  can readily be measured and used with a compliance calibration curve to determine the extended crack length  $a_e$ . Alternatively, the  $P_u - a_i$  relationship may be used where the load at point  $C$  is used for  $P_u$ . In constructing the  $P_u - a_i$  curve, it is noted from Fig. 6.5 that an approximation exists in that  $P_u$  and  $a_i$  imply the use of the slope of line  $OB$  instead of the actual line  $OA$ . The error in determining the crack length from this approximation was determined to be less than 6% with a coefficient of variation of 8.5% (62 samples) (Swartz and Refai, 1989).

The results obtained by using this method on 8 in. and 12 in. deep beams with  $a_e/d \leq 0.65$  show  $K_{Ic}$  to be invariant with respect to the crack length and beam size, with a coefficient

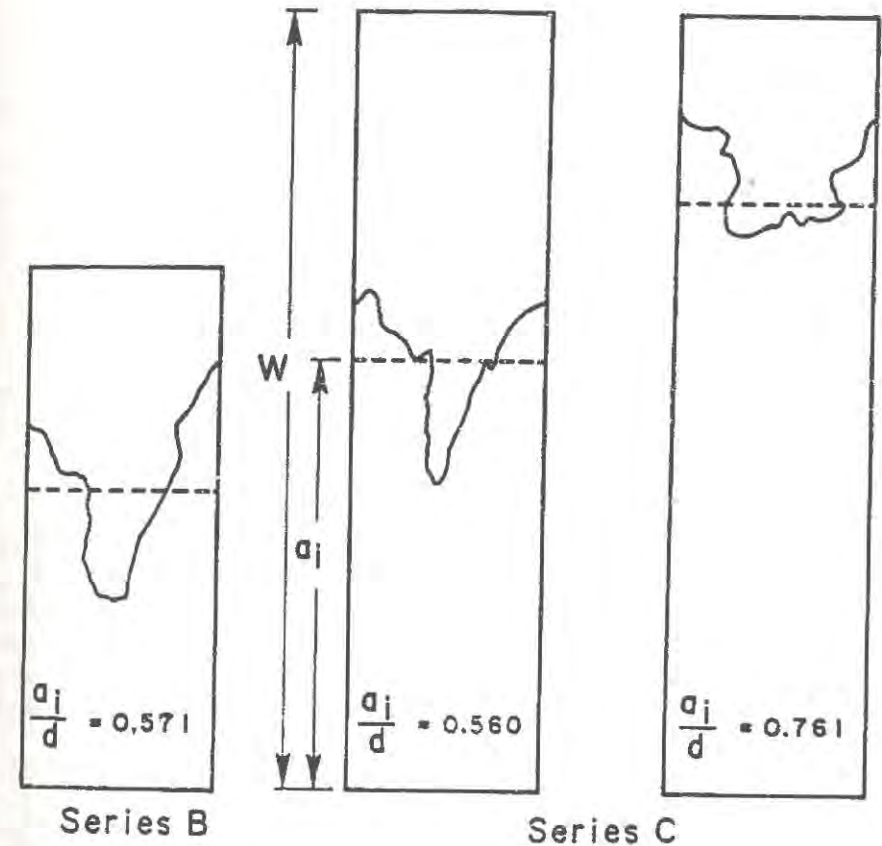


Fig.6.4 Dyed Cracked Surfaces

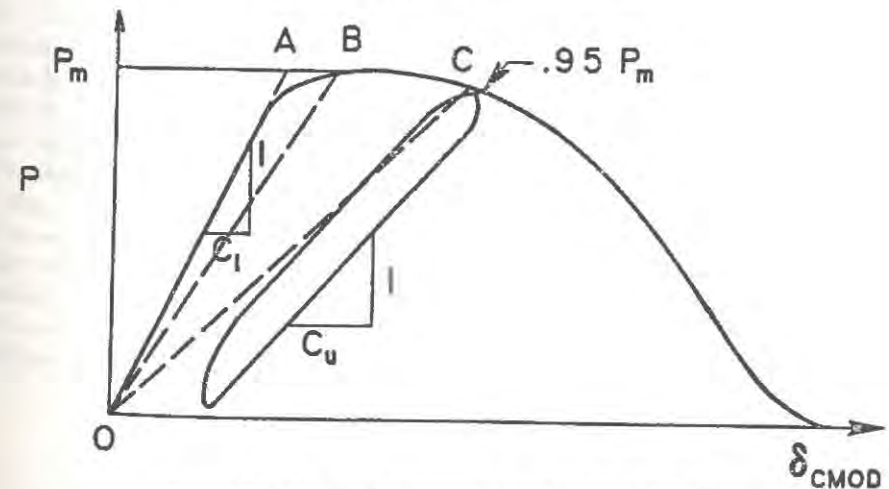


Fig.6.5 Load versus  $\delta_{CMOD}$  with Reload at  $0.95 P_u$

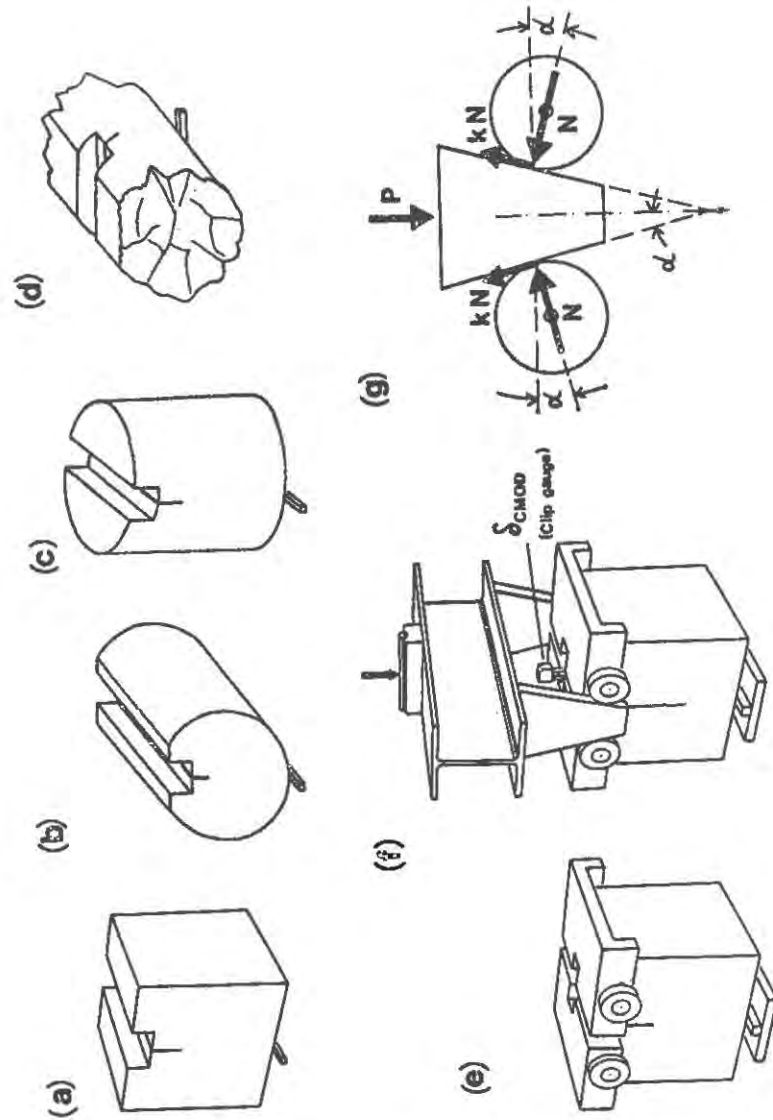


Fig. 6.6 (a) Wedge-Splitting Specimen Shape, (b-c) Alternative Shapes, (e-f) Loading Devices, (g) Forces Acting on the Wedge.

of variation of 5.5% ( $N = 19$ , 8 in. beams) and 3.5% ( $N = 19$ , 12 in. beams) (Refai and Swartz, 1988; Swartz and Refai, 1989).

### 6.1.4 Effect of Friction

An advantage of notched beam tests is that friction effect is small. To explain this effect, let  $\eta d$  be the distance from the bottom face (Fig. 6.1) to the point on the crack plane such that an axial force passing through this point would cause no deflection of the beam; obviously  $a_0/d < \eta < 1$  (typically  $\eta = 0.75$ ). If the horizontal friction forces acting at the beam supports are denoted as  $F$ , the bending moment at midspan needed to cause crack propagation is  $M = (P/2)(S/2) - F\eta d$  where  $S = \text{span}$ ,  $P = \text{applied load}$ ,  $F = kP/2$  and  $k$  is the coefficient of friction. Denoting  $P_0 = 4M/S$ , which represents the force needed to cause the crack to propagate if there were no friction ( $k = 0$ ) one gets  $P_0 = P - \Delta P_f$  where  $P = \text{measured applied force}$  and (according to Bažant):

$$\Delta P_f = \frac{2\eta d}{S} kP$$

This represents the portion of the applied force needed to overcome the friction. The larger the  $S/d$  ratio, the smaller is  $\Delta P_f$ . For  $\eta = 0.75$  and  $k = 0.005$  for roller bearings (manufacturers give an upper value of  $k = 0.01$ ) and for  $S/d = 2.5$  (used by Bažant and Pfeiffer, 1987),  $\Delta P_f = 0.003P$ . Thus, we see that the notched beam tests are relatively insensitive to friction, which is their advantage compared to some other tests (as pointed out by Planas and Elices, 1988b).

### 6.2 Wedge-Splitting Test

Another useful test for fracture of concrete is the wedge-splitting test (Fig. 6.6). It is similar to the compact tension test used for metals. Wedge splitting tests were studied for concrete by Hillemier and Hilsdorf (1977) and the present shape of the test specimen, characterized by a starter notch and a guiding groove which can be either moulded or sawn, was proposed by Linsbauer and Tschegg (1986). The test was subsequently refined by Bruhwiler (1988), and Bruhwiler and Wittmann (1989) who conducted (at the Swiss Federal Institute of Technology) over 300 such tests on normal concrete, dam concrete and other cementitious materials. Very large wedge splitting specimens, of sizes up to 1.5 m (5 ft.), have recently been tested by Saouma, Broz, Bruhwiler and Boggs (1989) at the University of Colorado, to study the size effect in dam concrete.

Fig. 6.6 (a-d) shows various possible wedge-splitting specimen shapes. Specimen (Fig. 6.6 (c)) requires either a deep notch or a longitudinal groove on both sides, in order to prevent shear failure of one of the cantilevers. Fig. 6.6 (e,f) illustrates the method of testing. The assembly of two wedges is pressed between two low-friction roller or needle bearings (on each side) which develop a pair of forces  $N$  that tend to split the specimen (Fig. 6.6g). The wedge assembly is loaded in a statically determinate manner so that each wedge receives the

same load. The dimensions of the notch and the groove must be chosen so that the crack propagates symmetrically.

During the test, the splitting force  $N$  (Fig. 6.6g) must be measured with sufficient accuracy. The crack mouth opening displacement  $\delta_{CMOD}$  is measured by a transducer or a clip gage (Fig. 6.6f) which should be attached at the level of the splitting forces, in which case  $\delta - CMOD$  represents the load-point displacement  $\delta_{LPD}$  associated with the horizontal component of the splitting force  $N$ . The test is controlled by  $\delta_{CMOD}$  in a closed-loop servo-hydraulic testing machine. However, a stable test can also be performed under actuator stroke control or under crosshead displacement control using conventional testing machines. In that case, the appropriate notch length necessary to ensure stability must be identified by considering the interaction between testing machine stiffness, specimen stiffness and material properties (Bruhwiler, 1988; Bruhwiler and Wittmann, 1989).

The advantages of the wedge splitting test are as follows:

1) The specimens are compact and light, since the ratio of fracture area to the specimen volume is larger than for other tests (e.g., 5.2-times larger than that for the three-point-bend test according to RILEM, 1985). This is especially useful for the study of size effect, since larger fracture areas can be obtained with smaller specimen weight. Due to lesser weight, larger specimens are easier to handle, and there is a lesser risk of breaking them during handling.

2) The cubical or cylindrical specimens (Fig. 6.6 a-c) can be easily cast at the construction site using the same molds as for strength tests, and the cylindrical shapes (Fig. 6.6 b-d) can also be obtained from drilled cores from existing structures.

3) The use of wedges for inducing the load increases the stiffness of the test set-up and thus enhances stability of the test, making it possible to conduct the test even in a machine that is not very stiff.

4) the effect of selfweight is negligible in contrast to notched beam tests (where the bending moment due to own weight can be over 50% of the total bending moment).

On the other hand, it must be noted that the wedge loading has also a disadvantage as it intensifies frictional effects. Let  $P$  = applied vertical load,  $N$  = specimen reactions needed to propagate the cracks which are normal to the wedge surface inclined by angle  $\alpha$  (Fig. 6.6g), and  $k$  = friction coefficient of the bearings. Then, the equilibrium condition of vertical forces acting on the wedge yields  $P = 2(N \sin \alpha + kN \cos \alpha) = P_0(1 + k \cot \alpha)$ , where  $P_0 = 2N \sin \alpha$  is the force needed to propagate the crack if there were no friction ( $k = 0$ ). Since  $k \cot \alpha \ll 1$ , we have  $P_0 \simeq P/(1 + k \cot \alpha) = P(1 - k \cot \alpha)$  or  $P + o = P - \Delta P_f$  where (according to Bazant):

$$\Delta P_f = PK \cot \alpha \quad (6.6)$$

$P$  is the measured load and  $\Delta P_f$  represents the portion of the load needed to overcome the friction. If  $\alpha < 45^\circ$ ,  $\Delta P_f$  is larger than  $kP$ , which means that frictional effects are enhanced by the wedge loading.

For the typical wedge angle  $\alpha = 15^\circ$ ,  $\Delta P_f = 3.73kP$ . The manufacturers of roller bearings give  $k$ -values ranging from 0.001 to 0.005 (and guarantee 0.01 as the limit). Assuming  $k = 0.005$ ,  $\Delta P_f = 0.019P$ . This frictional effect is significant and is about 6-times larger

than for the short notched beams of Bazant and Pfeiffer (1987), and about 20-times larger than for the longer notched beams recommended by RILEM, for the same value of  $k$  (see Sec. 6.1.4.). This disadvantage of the wedge splitting test is surmountable, and frictional effects can be reduced by (1) attaching hardened steel inserts along the inclined wedge surface, (2) using needle bearings, and (3) carefully polishing the wedge surface as shown by Hillemeier and Hilsdorf (1977) who experimentally determined a  $K$ -value = 0.00031 for their wedge loading set-up with needle bearings.

If the value of  $k$  is nearly constant and well reproducible, one may introduce the correction  $\Delta P_f$  in the analysis. However, since the value of friction coefficient is often quite uncertain, it is better to measure the splitting force  $N$  directly by instrumenting the wedges and the shafts that carry the bearings with strain gages.

The foregoing analysis shows that a very small wedge angle  $\alpha$  is unfavorable from the viewpoint of friction. On the other hand, the smaller the angle, the stiffer is the specimen-machine assembly. The angle  $\alpha = 15^\circ$  is a reasonable compromise.

Also, a large wedge angle ( $\alpha > 30^\circ$ ) is undesirable because it leads to a significant normal stress parallel to the crack plane in the fracture process zone. The presence of such stresses may affect the softening curve for the fracture process zone, as described by Eq. 3.9. The area under the softening curve is then not longer equal to the fracture energy,  $G_f$ ; nor is the area under the load-displacement curve.

The apparent fracture toughness,  $K_{Ic}$  is obtained by the same method as described in Section 6.1 for notched beam tests. The effective crack length, which accounts for the fracture process zone, is determined by the compliance method, based on finite element calibration. For that purpose, unload-reload cycles are performed during the test. Other methods such as the evaluation of fracture energy from the area under the load-displacement diagram and the size effect method are applicable, as described in the sequel.

### 6.3. Work-of-Fracture Method (RILEM, Hillerborg)

This method, which was originally developed for ceramics (Nakayama, 1965; Tattersall and Tappin, 1966), is the first method of testing for fracture properties of concrete to be proposed as a standard (RILEM, 1985). The basis for applying this method to concrete was developed by Hillerborg and his co-workers (Hillerborg, 1985b). Their method uses the "fictitious crack" concept (Hillerborg et al., 1976; Hillerborg, 1980; Petersson, 1981) (Fig. 6.7) implicitly and thus is not an LEFM method.

In order to contrast this with LEFM on the basis of energy parameters, recall that the critical energy release rate  $G_{Ic}$  is the energy required per unit crack extension in a material in which there is no process zone, that is, all the energy is surface energy and no energy is dissipated away from the crack tip. In fact, a process zone does exist and therefore the total energy of fracture includes all the energy dissipated per unit propagation distance of the fracture process zone as a whole. This is called the fracture energy  $G_f$  (Fig. 6.7).

Conceptually, the method can be applied to a variety of test specimen geometries but the proposed standard uses a beam specimen loaded in three point bending with a central

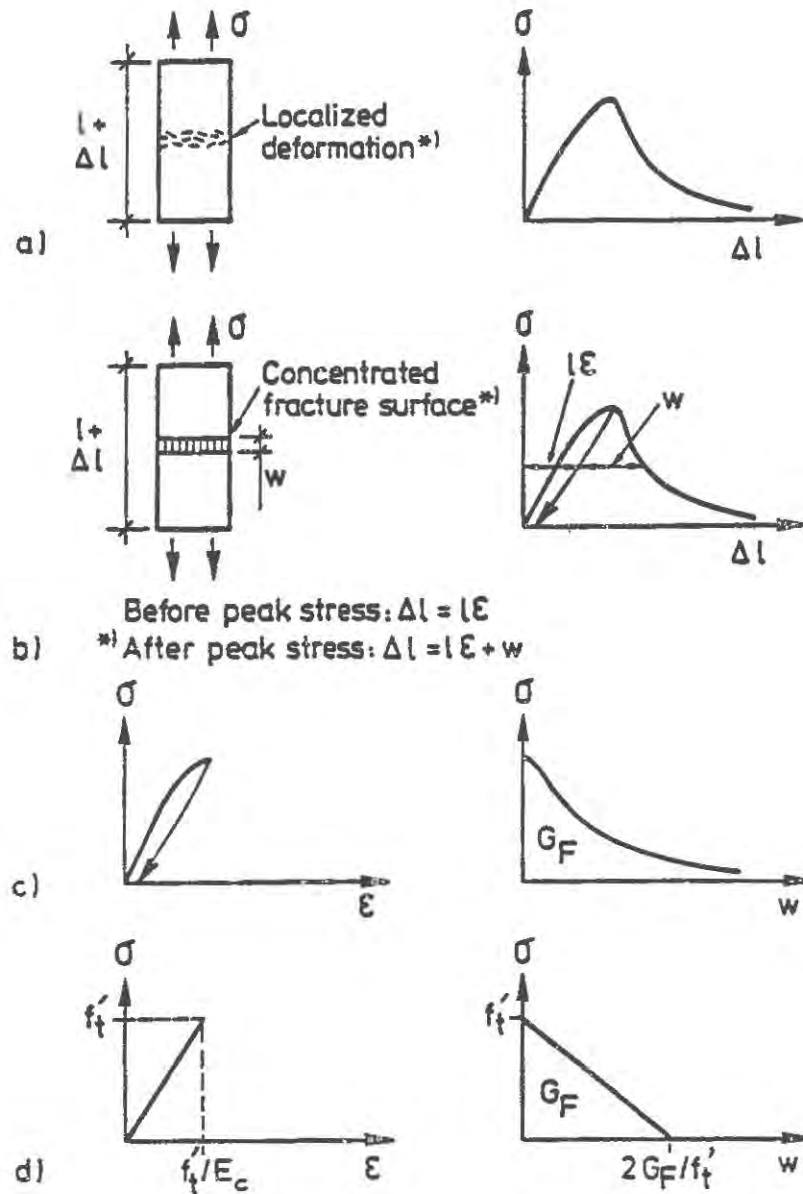


Fig.6.7 Fictitious Crack Model Description of Tensile Fracture

edge notch (Fig. 6.1a). Complete details of the proposed standard are given in the RILEM Recommendation (1985) and are not repeated here. Briefly, the test procedure consists of the following steps.

1. The beam proportions are selected in relation to maximum aggregate size. The minimum depth  $d$  is approximately six times the size of the aggregate. The ratios of  $S/d$  vary from 8 to 4. See Table 6.1. The beam specimen is notched to a depth  $a_0/d = 0.5$ .
2. The vertical load-point deflection of the beam (called  $\delta_{LPD}$  in Fig. 6.1a) is to be measured and plotted continuously along with the applied load  $P$ . The resulting trace is shown in Fig. 6.8.
3. The test is to be conducted in a manner to produce stable crack growth. If closed-loop testing is used then strain control should be selected. If a closed-loop system is not available, then a stiff testing machine is required (stiffness recommendations are given in RILEM, 1985.)
4. The fracture energy is calculated as

$$G_f^R = \frac{W_0 + mg\delta_0}{A_{lig}} \quad (6.7)$$

in which  $W_0$  = area under  $P - \delta_{LPD}$  curve up to  $\delta_0$ ;  $\delta_0$  = displacement when  $P$  returns to 0;  $mg = (m_1 + 2m_2)g$  and  $m_1g$  = beam weight between supports,  $m_2g$  = weight of fixtures which is carried by the beam; and  $A_{lig}$  = original, uncracked ligament area =  $b(d - a_0)$ .

This formula is valid if the movement of load and  $\delta_{LPD}$  are downward. If the beam is tested "on its side" so that the applied load  $P$  is normal to the beam's self weight vector, then the term  $mg\delta_0$  is neglected. Also, if the dead weight is otherwise compensated, this term is neglected.

Further, if the movements of load and  $\delta_{LPD}$  are upward - thus opposing the self weight vector - then it is shown that (Swartz and Yap, 1988)

$$G_f^R = \frac{W_0 - \frac{1}{2}mg\delta_0}{A_{lig}} \quad (6.8)$$

in which  $\delta_0$  = displacement at the point on the unload portion of the plot when  $P = (m_1/2 + m_2)g$ .

Eqs. 6.6 and 6.7 were derived by Swartz and Yap (1988). The self weight term may be quite significant, especially if young concrete is being tested or the specimen is large.

Extensive round-robin tests from 14 laboratories incorporating about 700 beams were reported by Hillerborg (1985c). With regard to variation of results within a given tests series, the coefficient of variation ranged from about 2.5% to 25% with most results around 10 to 15%. It was noted that "... the sensitivity of the strength of a structure with regard to changes in  $G_f^R$  is normally less than 1/3 of the sensitivity with regard to changes in normal

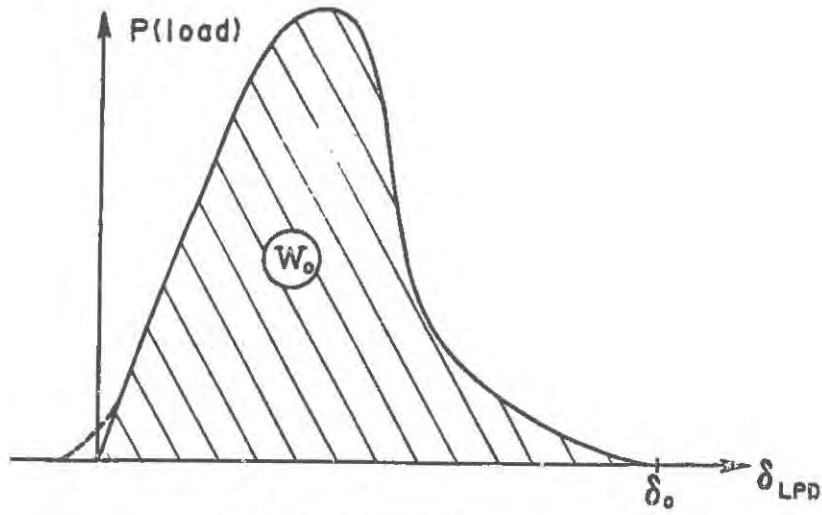


Fig.6.8 Load Versus  $\delta_{LPD}$

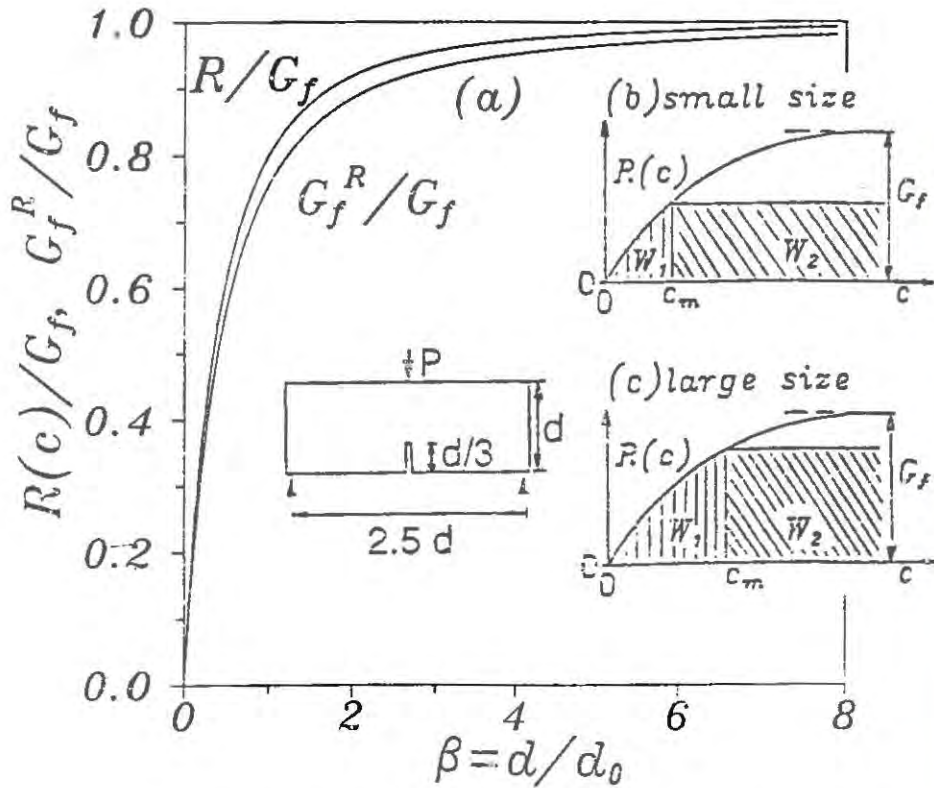


Fig.6.9 Theoretical Size Dependence of RILEM Fracture Energy  $G_f^R$

TABLE 6.1. Specimen Sizes Recommended for Hillerborg's Method (RILEM, 1985)

Maximum Aggr. Size mm	Depth d mm	Width b mm	Length L mm	Span S mm
1-16	100 ± 5	100 ± 5	840 ± 10	800 ± 5
16.1-32	200 ± 5	100 ± 5	1190 ± 10	1130 ± 5
32.1-48	300 ± 5	150 ± 5	1450 ± 10	1385 ± 5
48.1-64	400 ± 5	200 ± 5	1640 ± 10	1600 ± 5

TABLE 6.2. Regression Coefficients  $A_i, C_i, B_j, D_j$  for Karihaloo and Nallathambi's Method ( $i = 0, \dots, 4; j = 0, \dots, 5$ )

i/j	$A_i$	$C_i$	$B_j$	$D_j$
0	3.6460	1.5640	0.4607	1.9560
1	-6.7890	-8.3200	0.0484	0.3982
2	39.2400	52.9500	-0.0063	-0.0553
3	-76.8200	-124.9000	-0.0003	0.0027
4	74.3300	122.9000	-0.0059	0.0202
5	.	.	0.0003	-0.0055

strength values, and that therefore the acceptable error and standard deviation of a  $G_f^R$  test are about 3 times as high as in most strength tests (Hillerborg, 1985c)." It was concluded on this basis and by examining the changes in  $G_f^R$  values associated with changes in beam depth that the spurious influence of specimen size on measured values of  $G_f^R$  is acceptable. (However, the size effect method discussed later eliminates this influence.)

Thus, even though there was an undesirable size dependency in the test results for  $G_f^R$  it was considered to be of no greater importance on the calculated strength of the structure than the similar size dependency in ordinary strength tests.

Results from another series of tests (Swartz and Refai, 1989; Refai and Swartz, 1988) show a similar size effect and also a variation of  $G_f^R$  with notch depth.

In summary, the RILEM work-of-fracture method is a practical approach, which is suitable for use in laboratories which do not have very elaborate equipment and incorporates a number of compromises in order to simplify testing while still obtaining useful results (Hillerborg, 1985b). The method is based on a theory which has had wide acceptance, the fictitious crack model (Hillerborg et al., 1976). The fracture energy concept also has a very simple meaning, without using LEFM.

There are, however, certain aspects in which the RILEM work-of-fracture method needs to be further improved. This method does not give results independent of the size of the cracked area for a given beam depth even if precracked beams are used, and thus the value of  $G_f^R$  must be considered to be only an approximation of the true energy parameter which characterizes the surface energy and the energy of process zone formation. It is simplified but not unreasonable to consider this sum also to be constant with respect to the crack length. This implies that the shape and size of the process zone do not change. Furthermore, refinement of the RILEM method is needed as a result of the size effect, which will be discussed next.

#### 6.4 Size Effect in Work-of-Fracture Method

The size dependence of fracture energy  $G_f^R$  obtained according to the existing RILEM recommendation on the work of fracture method has been investigated by Planas and Elices (1988b) on the basis of solution of an integral equation and by Bazant and Kazemi (1989b) on the basis of the size effect law. The premise of the latter analysis was that the law is applicable to size ranges up to about 1:20 and has the same form (for this size range) for all specimen geometries (with only negligible errors). The analysis utilizes the method for calculating the R-curve from size effect and load-deflection curve from the R-curve as already explained (Sec. 5.1). The R-curve obtained in this manner is strongly dependent on the geometry of the specimen. The basic relation (Fig. 6.9b,c)

$$G_f^R = \frac{W_1 + W_2}{b\ell}, W_1 = b \int_0^{c_m} R(c)dc, W_2 = bR(c_m)(1 - c_m) \quad (6.9)$$

where  $b$  = specimen thickness,  $\ell = d - a_0$  = ligament length ( $d$  = beam depth), and  $c_m$  = crack length  $c$  at peak load.  $W_1$  and  $W_2$  represent the works of fracture before and after the

peak load. Note from Fig 6.9b,c that  $W_2$  depends strongly on specimen size, because the value of  $c_m$  depends on the size.

The results of this investigation show that  $G_f^R$  is not size-independent, as one might desire, but depends strongly on the specimen size as shown in Fig 6.9a. This dependence is seen to be even stronger than that of the R-curve. When the specimen size is extrapolated to infinity,  $G_f^R$  coincides exactly with Bazant's definition of fracture energy  $G_f$  obtained by the size effect method.

This investigation also showed that the pre-peak contribution of the work of the load to the fracture energy  $G_f$  is relatively small (generally under 6%). This conclusion basically agrees with that obtained by Planas and Elices (1988b) in a different manner.

#### 6.5 Two-Parameter Fracture Model of Jenq and Shah

Unlike the fictitious crack model, the two-parameter model of Jenq and Shah (1985a, 1985b), already explained in Sec. 4.2, does not require a post-peak (strain softening) constitutive law, yet it can describe the nonlinear slow crack growth prior to peak load. The two parameters are the critical stress intensity factor  $K_{Ic}^S$  and the critical crack tip opening displacement  $\delta_{CMOD}$  relationship shown in Fig. 6.10. This relationship is essentially linear on the ascending portion of the curve from  $P = 0$  up to about the load corresponding to half the maximum load  $P_u$ . At this stage, the crack tip opening displacement is negligible and  $K_I$  is less than  $0.5K_{Ic}^S$  (Fig. 6.10a). As the load  $P$  exceed the value of  $0.5P_u$ , inelastic displacement and slow crack growth occur during the nonlinear range (Fig. 6.10b). At the critical point (Fig. 6.10c), the crack tip opening displacement reaches a critical value and  $K_I = K_{Ic}^S$ . For standard plain concrete beams tested in three-point bending, the critical point can be approximated between the point of  $P_u$  and the point of  $0.95P_u$  on the descending branch of the  $P - \delta_{CMOD}$  plot. The concept is also shown for a beam in bending in Fig. 6.11.

Depending upon the geometry of the specimen, the rate of loading, and the method of loading, further crack growth may occur at a steady-state value of  $K_{Ic}^S$ . Denoting the crack length  $a$ , the load  $P$  will have a value equal to  $P_u$  when  $K_I$  reaches  $K_{Ic}^S$  if  $dK_I/da > 0$ . If  $dK_I/da$  at this loading stage is negative, then beyond the critical point the crack will propagate at a constant value of  $K_{Ic}^S$  and the applied load will increase until  $dK_I/da = 0$ .

In the majority of practical cases, the value of  $dK_I/da$  is positive, i.e.,  $K_I$  is a monotonically increasing function of  $a$ . Three- and four-point bent, and single-edge notched and double-edge notched specimens subjected to tensile loading are found to satisfy this condition (Jenq and Shah, 1985b). For this case, the values of  $K_{Ic}^S$  and  $\delta_{CTOD}$  can be obtained from the measured peak load and from the knowledge of an associated effective crack length  $a_e$ .

The method has been proposed to RILEM (Karihaloo and Nallathambi, 1987) as a standard test method for determination of  $K_{Ic}^S$  and  $\delta_{CTOD}$  in plain concrete using beam specimens. The following dimensions are suggested if a maximum aggregate size not exceeding one inch (25.4mm) is used; see Fig. 6.1, in which  $b \times d \times L = 3\text{in.} \times 6\text{in.} \times 28\text{in.}$  (76.2 mm  $\times$  152.4 mm  $\times$  711.2 mm);  $S = 24\text{ in.}$  (609.6 mm);  $a_0/d = 1/3$ ;  $S/d = 4$ .

For larger maximum aggregate sizes the dimensions should increase proportionately.

A closed-loop testing system with strain control using the  $\delta_{CMOD}$  gage or else a stiff machine (a machine that is at least 10-times stiffer than the test specimen) is recommended to achieve stable failure. The rate of loading should be such that peak load is reached in about 5 min.

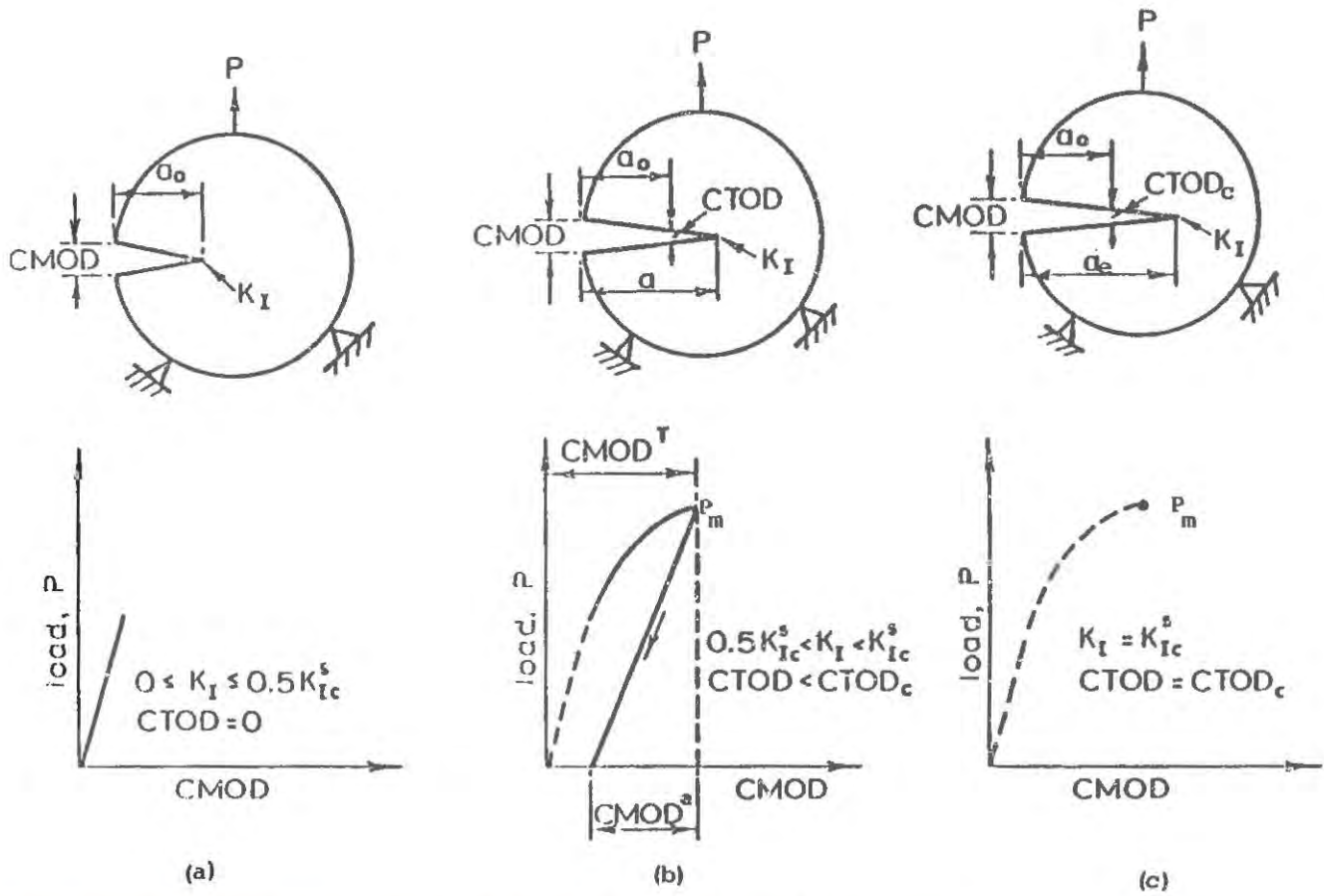


Fig.6.10 Fracture Resistance Stages of Plain Concrete

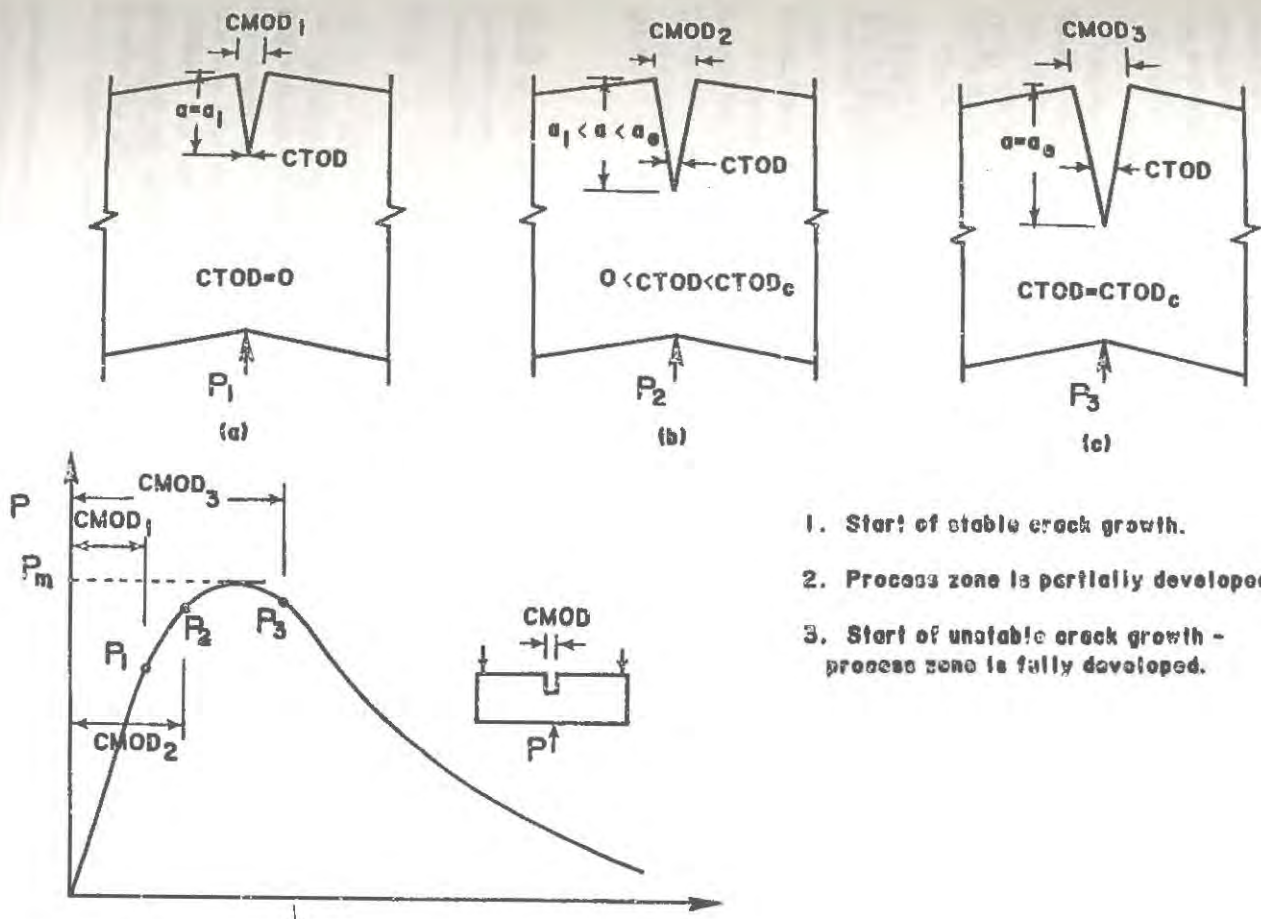


Fig.6.11  $\delta_{CMOD}$  and  $\delta_{CTOD}$  Behavior at Different Loading Stages

To determine the two fracture parameters  $K_{Ic}^S$  and  $\delta_{CTOD}$  for plain concrete, the maximum  $P_u$  and the corresponding elastic component of the  $\delta_{CMOD}$ , denoted  $\delta_{CMOD}^e$  are measured. These values are then used to estimate the effective elastic crack length  $a_e$  such that the calculated  $\delta_{CMOD}^e$  (based on LEFM equations) is equal to the measured value. For a given initial notch length  $a_0$  and depending upon the type of test, the two fracture parameters are determined as follows (see Fig. 6.2 and 6.11):

The modulus of elasticity  $E$  is determined using initial compliance  $C_i$  from

$$E = \frac{6 S a_0 V_1(\alpha_0)}{C_i b d^2} \quad (6.10)$$

$$V_1(\alpha_0) = 0.76 - 2.28\alpha_0 + 3.87\alpha_0^2 - 2.04\alpha_0^3 + \frac{0.66}{(1 - \alpha_0)^2} \quad (6.11)$$

and  $\alpha_0 = (a_0 = h_0)/(d + h_0)$ ,  $h_0$  = clip gage holder thickness.

The effective crack length is determined from Eq. 6.8 by replacing  $a_0$  with  $a_e$ ,  $\alpha_0$  with  $\alpha_e$  and  $C_i$  with  $C_u$  where  $\alpha_e = (a_e + h_0)/(W + h_0)$  and  $C_u$  is the unloading compliance at 0.95  $P_u$ . Thus,

$$a_e = a_0 \frac{C_u V_1(\alpha_0)}{C_i V_1(\alpha_e)} \quad (6.12)$$

which may be solved fairly easily by iteration.

Then the critical stress intensity factor is

$$K_{Ic}^S = \frac{3 P_u S}{2 b d^2} \sqrt{\pi a_e} F(\alpha) \quad (6.13)$$

and

$$F(\alpha) = \frac{1}{\sqrt{\pi}} \frac{1.99 \alpha(1 - \alpha)(2.15 - 3.93\alpha + 2.7\alpha^2)}{(1 + 2\alpha)(1 - \alpha)^{3/2}} \quad (6.14)$$

with  $\alpha = a_e/d$ . The critical crack-tip opening displacement is

$$\delta_{CTOD} = \frac{6 P_u S a_e}{b d^2 E} V_1(\alpha) [(1 - \bar{\beta})^2 + (-1.149\alpha + 1.081)(\bar{\beta}^2)]^{1/2} \quad (6.15)$$

where  $\bar{\beta} = a_0/a_e$ .

In using this method for precracked - instead of notched - beams, replace  $a_0$  by  $a_i$ .

In Jenq and Shah (1985b) it is shown that this method gives  $K_{Ic}^S (= K_{Ic}^e)$  results which are independent of specimen size when notched beams are used. As shown in Swartz and Refai (1989) the same invariance is obtained when precracked beams are used and also  $K_{Ic}^S$  is independent of crack length for  $a_e/d < 0.65$ . It is also shown that the modified compliance method (section 6.1.3) gives virtually the same result for  $K_{Ic}$  for precracked beams as the Jenq-Shah method. For example, for  $d = 12$  in., and  $a_e/d \leq 0.65$ , the average  $K_{Ic}^S = 1206 \text{ kNm}^{-3/2}$  (C.V. = 9.2%, N = 11) and the compliance method average  $K_{Ic} = 1151 \text{ kNm}^{-3/2}$  (C.V. = 3.5%, N = 19).

It is further shown by Jenq and Shah (1985b) that the results for  $\delta_{CTOD}$  are relatively constant with respect to beam size. This result was also obtained for beams tested by Refai and Swartz (1987) but a variation with  $a_i$  was found.

## 6.6 Effective Crack Model of Karihaloo and Nallathambi

This method (Nallathambi and Karihaloo, 1986a, 1986b) has also been proposed to RILEM as a standard (Karihaloo and Nallathambi, 1987). In this approach a simple technique is used where the critical stress intensity factor  $K_{Ic} (= K_{Ic}^e)$  and critical energy release rate  $G_{Ic} (= G_{Ic}^e)$  are found for beam specimens by LEFM methods after the crack has grown from a notch  $a_0$  to an effective length  $a_e$ .

The formulas which follow later were developed for certain ranges of specimen dimensions. These ranges, which are to be used for maximum aggregate sizes  $d_a$  ranging from 5 to 25 mm, with no critical dimension being less than five times  $d_a$ , are:  $b = 40 - 80$  mm ( $\geq 3d_a$ );  $d = 50 - 300$  mm ( $\geq 3d_a$ );  $S = 200 - 1800$  mm ( $\geq 3d_a$ ); with  $4 \leq S/d \leq 8$ . Also  $a_0/d = 0.2 - 0.6$  (0.3 or 0.4 is preferred).

The loading setup which is idealized in Fig. 6.1 is shown in Fig. 6.12 where the  $\delta_{LPD}$  is measured by an LVDT. In addition, the  $\delta_{CMOD}$  could be measured by adding a clip gage across the notch. Preferably a closed-loop testing system should be used with strain control feedback from either the  $\delta_{LPD}$  or  $\delta_{CMOD}$  gage. Otherwise, a stiff testing machine should be used. In any event, a continuous record of  $P$  and  $\delta_{LPD}$  is made up to peak load which should be reached in 1-10 minutes. The softening response is not required with this method.

If it is not possible to obtain a continuous load-displacement record, the method can still be used but the modulus of elasticity,  $E$ , must be determined from uniaxial tests on other specimens.

If a continuous record of  $P$  vs.  $\delta_{LPD}$  is available, determine  $E$  from

$$E = \frac{P_i}{\delta_i} \frac{S^3(1 + \frac{5w}{8P_i})}{4b d^3(1 - \frac{a_0}{d})^3} \lambda \quad (6.1)$$

where  $P_i$ ,  $\delta_i$  are measured at any intermediate location on the initial ascending portion of the curve and  $w$  is the self-weight of the beam. The term  $\lambda$  is a correction factor relating deflections of a notched to an unnotched beam and is obtained from finite element calculations as

$$\lambda = \eta_1 \exp\{\eta_2(a_0/d)^2 + \eta_3(S/d)^2 + \eta_4(a_0/d)(S/d) + \eta_5(S/d)^3\} \quad (6.2)$$

and  $\eta_1 = 1.379$ ,  $\eta_2 = -1.463$ ,  $\eta_3 = -0.036$ ,  $\eta_4 = -0.201$ , and  $\eta_5 = 0.004$  (Karihaloo and Nallathambi, 1987). Then the effective crack length  $a_e$  is obtained from  $P_u$  and the corresponding displacement  $\delta_u$  as

$$a_e/d = 1 - \left[ \frac{P_u S^3(1 + \frac{5w}{8P_u})}{4b d^3 \delta_u E_c} \right] \lambda \quad (6.3)$$

If  $S/d$  is "small," the effect of shear deformation can be considered by using

$$E = \frac{P_i}{\delta_i} \left[ \frac{S^3(1 + \frac{5w}{8P_i})}{4b d^3(1 - \frac{a_0}{d})^3} + \frac{(1 + \nu)S}{2\kappa b d(1 - \frac{a_0}{d})} \right] \lambda \quad (6.4)$$

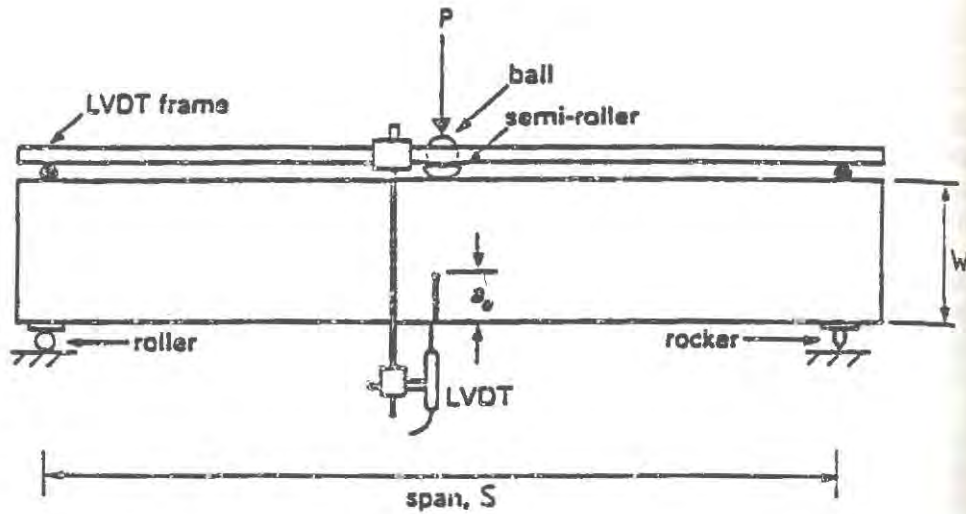


Fig.6.12 Loading Apparatus and Fixing Arrangement of LVDT

NORMAL SIZE

INFINITE SIZE

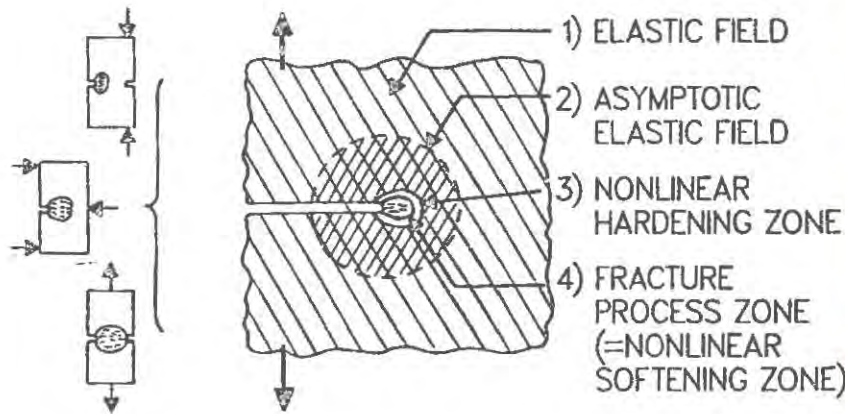


Fig.6.13 Fracture Process Zones in Different Specimens and Extrapolation to Infinite Size

where  $\kappa = \text{shear constant} = 10(1 + \nu)/(12 + 11\nu)$  for a rectangular section and  $\nu$  is Poisson's ratio. This value of  $E$  is then substituted into Eq. 6.16 to obtain  $a_e$ . Karihaloo and Nallathambi (1987) contains regression formulas to determine  $a_e$  instead of using Eq. 6.16.

The critical stress intensity factor is then given as

$$K_{Ic}^e = \sigma_n \sqrt{a_e} F(\alpha) \tag{6.5}$$

where  $F(\alpha)$  is given by Eq. 6.16,  $\alpha = a_e/d$  and  $\sigma_n = 6M/bd^2$ . The midspan moment  $M$ , including self-weight effects is

$$M = (P_u + w/2) S/4 \tag{6.6}$$

The critical energy release rate is

$$G_{Ic}^e = \frac{(K_{Ic}^e)^2}{E} \tag{6.7}$$

Improved (but more complicated expressions for  $K_{Ic}^e (= \bar{K}_{Ic}^e)$  and  $G_{Ic}^e (= \bar{G}_{Ic}^e)$  are obtained by use of finite element methods which consider the tensile stress normal to the crack faces, the tensile stress in the plane of the crack and the shearing stress. The formulas of  $\bar{K}_{Ic}^e$  and  $\bar{G}_{Ic}^e$  are

$$\bar{K}_{Ic}^e = \sigma_n (a_e)^{1/2} Y_1(\alpha) Y_2(\alpha, \beta) \tag{6.8}$$

$$\bar{K}_{Ic}^e = \left( \frac{s_n^2 a_e}{E_c} \right) Z_1(\alpha) Z_2(\alpha, \beta) \tag{6.9}$$

In these equations again

$$\alpha = a_e/d, \beta = S/d;$$

$$Y_1(\alpha) = A_0 + A_1\alpha + A_2\alpha^2 + A_3\alpha^3 + A_4\alpha^4, Y_2(\alpha, \beta) = B_0 + B_1\beta + B_2\beta^2 + B_3\beta^3 + B_4\alpha\beta + B_5\alpha\beta^2,$$

$$Z_1(\alpha) = C_0 + C_1\alpha + C_2\alpha^2 + C_3\alpha^3 + C_4\alpha^4,$$

and

$$Z_2(\alpha, \beta) = D_0 + D_1\beta + D_2\beta^2 + D_3\beta^3 + D_4\alpha\beta + D_5\alpha\beta^2.$$

Regression coefficients  $A_i, B_j, C_i, D_j (i = 0, 1, \dots, 4; j = 0, 1, \dots, 5)$  are given in Table 6.2.

A very extensive testing program was carried out by Karihaloo and Nallathambi (Nallathambi and Karihaloo, 1986a; Karihaloo and Nallathambi, 1987) using this method to evaluate data from more than 950 beams in which maximum aggregate size, beam size, and relative notch crack depth were varied. The test results were generally very consistent with the calculated values; the coefficient of variation generally ranged between 6% and 10%. Test data from other investigators were also used, with generally excellent agreement between the results of this method and Jenq and Shah's method for  $K_{Ic}$ . For example, the data from Refai and Swartz (1987) for  $d = 304 \text{ mm}$  gave  $\bar{K}_{Ic}^e = 1074 \text{ kNm}^{-3/2}$ ,  $K_{Ic}^s = 1206 \text{ kNm}^{-3/2}$  (Jenq and Shah) and  $K_{Ic} = 1151 \text{ kNm}^{-3/2}$  (compliance method).

## 6.7 Determination of Material Parameters by Size Effect Method

### 6.7.1 Asymptotic Definition for Infinite Size

Since the size effect is the most important practical consequence of fracture mechanics, it

is not illogical to exploit it for determining the material fracture properties, as proposed by Bažant. In principle, the size effect provides the only means for an unambiguous definition of material fracture properties. The fracture energy as well as other nonlinear fracture parameters may be uniquely defined by their values extrapolated to a specimen of infinite size. The reason is that, in an infinitely large specimen, the fracture process zone occupies an infinitely small fraction of the specimen volume (Fig. 6.13). Hence, nearly all of the specimen is in an elastic state. Now, from linear elastic fracture mechanics it is known that the near-tip asymptotic field of displacements and stresses (Fig. 6.13) is the same regardless of the specimen or structure geometry (Eq. 2.1). Therefore, the fracture process zone in an infinitely large specimen is exposed on its boundary to the same stress field regardless of structure geometry, and so it must behave in the same manner. In particular, it must dissipate the same energy and have the same length and width. Therefore, as proposed by Bažant (1987a), an unambiguous definition is as follows:

The fracture energy  $G_f$  and the effective fracture process zone length  $c_f$  are the energy release rate required for crack growth and the distance from the notch tip to the tip of the equivalent LEFM crack in an infinitely large specimen of any shape.

With this asymptotic definition, determination of the fracture properties is reduced to the calibration of the size effect law. If we knew the size effect law exactly, we would get exact results. Unfortunately, the exact size effect law, applicable up to infinite size, is not known. Therefore, this method, like others, yields in practice only approximate results. Nevertheless, the validity of the size effect law proposed by Bažant (Fig. 6.14, Eq. 1.4) is rather broad, covering a range of sizes of perhaps 1:20, which is sufficient for most practical purposes; see Planas and Elices (1988a).

### 6.7.2 Basic Relations

In Eq. 5.2 we gave the expression for the energy release rate in terms of the applied load or nominal stress. Setting  $P = P_u$ , we have  $G = R =$  specific energy required for crack growth, and by extrapolation to infinite size we have

$$G_f = \lim_{d \rightarrow \infty} R = \lim_{d \rightarrow \infty} \frac{P_u^2(\alpha)}{Eb^2d} = \frac{B^2 f_t^2}{c_n^2 E} \lim_{d \rightarrow \infty} \frac{d}{1 + d/d_0} \lim_{d \rightarrow \infty} g(\alpha) \quad (6.10)$$

in which we have expressed  $P_u$  according to Eq. 1.2. Taking the limit  $d \rightarrow \infty$ , for which  $\alpha \rightarrow \alpha_0 = a_0/d$ , we obtain the expression

$$G_f = \frac{B^2}{c_n^2 E} f_t^2 d_0 g(\alpha_0) = \frac{g(\alpha_0)}{AE} \quad (6.11)$$

proposed by Bažant (1985b) in which  $A$  is the slope of a linear regression plot of test data (Fig. 6.14) obtained by algebraically rearranging the size effect law (Eq. 1.4) in the form  $Y = AX + C$ , in which

$$X = d, \quad Y = (c_n/\sigma_n^2), \quad B = C^{-1/2}, \quad d_0 = C/A \quad (6.12)$$

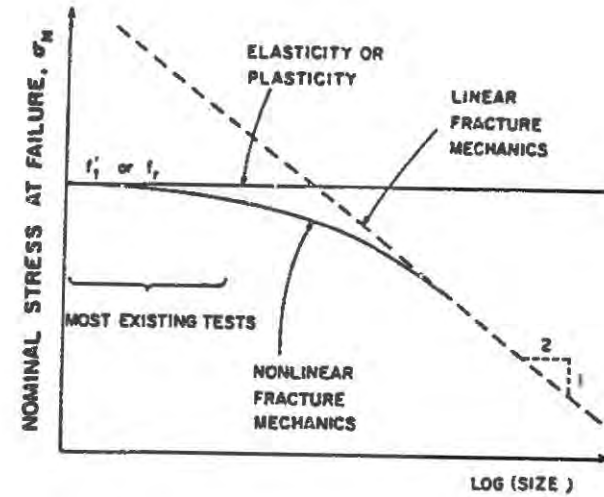


Fig.6.14 The Size Effect Law (Eq. 1.4; Bažant, 1984)

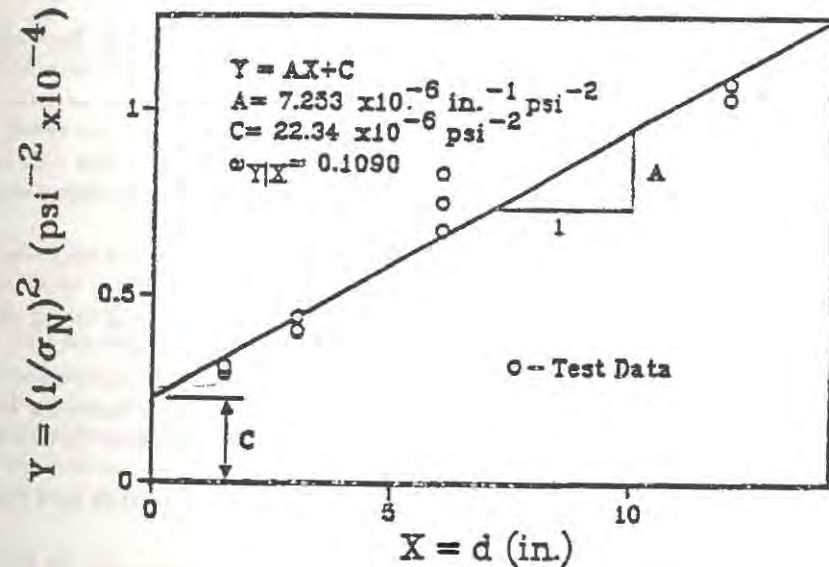


Fig.6.15 Regression Plot for Size Effect Method

The second nonlinear fracture parameter, namely the effective length  $c_f$  of the fracture process zone, defined for an infinitely large specimen, is obtained from Eq. 5.6 as follows:

$$c_f = \frac{g(\alpha_0)}{g'(\alpha_0)} d_0 = \frac{g(\alpha_0) C}{g'(\alpha_0) A} \quad (6.13)$$

Again, we see that  $c_f$  can be determined from the linear regression parameters  $A$  and  $C$  (Bažant and Kazemi, 1988). An important point is that the test data must cover a sufficiently broad range of sizes, so that the statistical scatter and other influences would not overshadow the size effect.

Eqs. 6.24 and 6.26 form the basis for the determination of the fracture energy and effective process zone length from the size effect. Bažant and Pfeiffer (1987) verified that very different types of specimens (Fig. 5.1), including three-point bend specimens, edge-notched tension specimens and eccentric compression specimens, yield approximately the same values of the fracture energy for the same concrete. Studies of Karihaloo and Nallathambi (1987), Swartz and Refai (1987) and Planas and Elices (1988b) further established that this method yields approximately the same results for the fracture energy as Jenq and Shah's two-parameter method. On the other hand, the value of fracture energy obtained by these methods is generally quite different from that obtained from the RILEM work-of-fracture method (i.e. Hillerborg's method). Planas and Elices (1988b) and Planas et al. (1989) analyzed these differences exhaustively and concluded that the reason why Hillerborg's method yields different values is mainly the assumed shape of the softening stress-displacement curve. By modifying the shape of this curve (steeper initial decline, extended tail), a better agreement in the values of  $G_f$  could apparently be obtained.

It must be noted that Eq. 6.26 fails if  $g'(\alpha_0)$  approaches 0. This happens, e.g., for a certain crack length in a center-cracked specimen loaded on the crack. In that case according to Eq. 6.26,  $C$  would have to vanish if  $c_f$  is constant, and then also  $d_0 \rightarrow 0$ . Due to statistical scatter, the ratio  $C/g'(\alpha_0)$  in Eq. 6.26 becomes meaningless when  $g'(\alpha_0)$  is too small. For still shorter cracks in this kind of specimen, one obtains  $g'(a_0) < 0$ , and in that case again Eq. 6.26 cannot be used. However, for typical fracture specimens such situations do not arise.

In contrast to Eq. 1.4, the size effect law in the form of Eq. 5.6 involves only material parameters,  $G_f$  and  $c_f$ . Therefore, these parameters can be obtained directly by optimum fitting of Eq. 5.6 to the measured values of  $\tau_N$  for various values of  $D$ . Such fitting can be accomplished easily by nonlinear regression or any optimization subroutine.

The specimen shapes do not need to be geometrically similar if Eq. 5.6 (rather than Eq. 1.4) is used. However, the parameter that takes into account the specimen shape, namely the ratio  $g'(\alpha_0)/g(\alpha_0)$ , is only approximate and involves some error. To avoid this error, it is preferable to use specimens which are geometrically similar.

The size effect method has also been proposed by RILEM Committee TC 89 for a RILEM Recommendation.

As for the specimen shape, in principle any suitable fracture specimen can be used. In view of the popularity and certain practical advantages of the three-point bend specimens,

the proposal has been worked out in detail for this type of specimen. (See Fig. 6.1, which also explains the notations.)

All the prescribed details for specimen preparation, testing and data evaluation are given in Karihaloo and Nallathambi (1987) and will not be repeated here. Briefly, the testing program uses specimens of at least three - but preferably more - sizes characterized by beam depths  $d_1, d_2, \dots$  and spans  $S_1, S_2, \dots$ . The smallest depth  $d_1$  must not be larger than  $5 d_n$  and the largest depth  $d_n$  must not be smaller than  $15 d_1$ . The ratio  $d_n/d_1$  must be at least 4. The beam width  $b$  should be kept constant as should the span/depth ratio  $S_j/d_j$ . A minimum of three samples per given size should be tested.

One of the advantages of the method is that an ordinary uniaxial testing machine without servo-control or high stiffness may be used. The only measured responses needed are the peak loads  $P_j$  for all specimens,  $j = 1, 2, \dots, n$ . The loading rate should be selected so that the maximum load would be reached in one to ten minutes.

### 6.7.3 Calculation Procedure of Size Effect Method:

If the length  $L_j$  of specimen  $j$  is almost the same as  $S_j$  its span, then compute

$$P_j^0 = P_j + \frac{1}{2} m_j g \quad (6.14)$$

in which  $m_j g$  is the weight of the specimen and the specimen is loaded downward. If  $L_j$  is much larger than  $S_j$  then

$$P_j^0 = P_j + \frac{2 S_j - L_j}{2 S_j} m_j g \quad (6.15)$$

If the specimens are geometrically similar set  $P_j^* = P_j^0$ . If not

$$P_j^* = P_j^0 \frac{d_m S_j}{d_j S_m} \quad (6.16)$$

where  $m$  refers to the mid-size specimen. Next, plot  $Y_j$  (ordinate) versus  $X_j$  (abscissa) where

$$Y_j = \left( \frac{b d_j}{P_j^*} \right)^2, \quad X_j = d_j \quad (6.17)$$

and determine the slope of the line  $A$  as shown in Fig. 6.15 as well as the  $Y$ -intercept  $C$ . The fracture energy  $G_f$  is calculated from Eq. 6.24 and the effective length of the fracture process zone from Eq. 6.26. The value of  $E$  for Eq. 6.26 needs to be determined from companion tests or estimated from  $f'_c$  using established empirical formulas. The expression for  $g(\alpha_0)$  may be obtained by using standard references for LEFM formulas. The following are from Tada et al. (1985): For  $S/d = 4$ :

$$F(\alpha) = \frac{1}{\sqrt{\pi}} \frac{1.99 - \alpha(1 - \alpha)(2.15 - 3.93\alpha + 2.7\alpha^2)}{(1 + 2\alpha)(1 - \alpha)^{3/2}} \quad (6.18)$$

For  $S/d = 8$ :

$$F(\alpha) = 1.106 - 1.552\alpha + 7.71\alpha^2 - 13.53\alpha^3 + 14.23\alpha^4 \quad (6.19)$$

Linear interpolation is acceptable provided  $3 \leq S/d \leq 10$ . Finally,

$$g(\alpha_0) = \frac{S_m}{d_m} \pi, \alpha_0 [1.5F(\alpha_0)]^2 \quad (6.20)$$

In Bažant and Pfeiffer (1987) and Karihaloo and Nallathambi (1987) there are discussions of calculations needed to verify the result for  $G_f$  and to obtain the standard deviation. It is also pointed out that scattered results can arise from other size effects (Sec. 5.3). This may be of particular concern for very large and thick specimens, since hydration heat will produce different temperatures in thin and thick specimens and thus lead to an additional size effect that is superimposed on that described by the size effect law. In that case this method could fail. Similarly, it could fail due to difference in moisture content, since thin specimens dry faster than thick ones. These effects, as well as the wall effect, are minimized by using the same specimen thickness for all the sizes.

#### 6.7.4 Comparison with Other Methods

Karihaloo and Nallathambi (1987) list most of the known fracture test results, in which Bažant's size effect method is also compared with Karihaloo and Nallathambi's method. For this purpose the values of  $G_f$  were converted to  $K_{Ic}$  by use of the LEFM relationship  $K_{Ic} = (G_f E)^{1/2}$ . For the beam results reported, the  $K_{Ic}$  values were  $0.847 - 0.892kN_m^{-3/2}$  and the values from the Karihaloo and Nallathambi's method were  $K_{Ic}^e = 0.867$  and  $K_{Ic}^{-e} = 1.005kN_m^{-3/2}$ . Similar agreement was found from the data of Bažant and Pfeiffer (1987).

The size effect method was used by Bruhwiler (1988) and Saouma et al. (1989) to measure the fracture energy of dam concrete.

#### 6.8 Size Required for Applicability of LEFM

An early attempt to specify the minimum size of test specimen such that LEFM may be used was that of Walsh (1972, 1976). He argued that, by comparing the nominal stress at the notch tip for a beam specimen (calculated by using an LEFM formula for  $K_{Ic}$ ) with the modulus of rupture of the material, a transition dimension may be found. He stated that the characteristic beam dimension should be at least double this in order for LEFM to be valid. Based on his test data he suggested the notched beam to be tested should have a depth not less than 230 mm (9 in.).

In the light of recent experimental studies on the size effect in fracture, the recommendation for the specimen size analyzable by LEFM now appears to be grossly underestimated. According to the size effect law of Bažant, the brittleness number  $\beta$  must be at least 25 if the deviation from the straight line asymptote for LEFM should be less than 2%. Bažant and Pfeiffer's (1987) tests of various types of specimens shown in Fig. 5.1 indicate that: (1) for eccentric compression fracture specimens  $d_0 = 1.85d_a$ , (2) for three-point bend specimens

$d_0 = 5.4d_a$ , and (3) for centric tension specimens  $d_0 = 16.8d_a$ . Consequently, the minimum cross section depths of these specimens which are needed for applicability of LEFM (with the theoretical error of 2%) are as follows:

$$\begin{aligned} \text{For eccentric compression specimens: } & d \geq 46d_a \\ \text{For three-point bend specimens: } & d \geq 135d_a \\ \text{For concentric tension specimens: } & d \geq 420d_a \end{aligned} \quad (6.21)$$

These dimensions are impracticably large for laboratory tests, and their use would be financially wasteful since knowledge of the size effect can provide adequate information on material fracture parameters using much smaller specimens.

#### 6.9 Identification of Nonlocal Characteristic Length

For the nonlocal continuum model with local strain (or nonlocal damage continuum), the fracture energy  $G_f$  is proportional to the area  $W_s$  under the complete tensile stress-strain curve (with softening) times the characteristic length,  $\ell$ , and  $c_f$  is proportional to the characteristic length. This fact is exploited by a simple method, conceived by Bažant and Pijaudier-Cabot (1988b, 1989). It uses the relation:

$$\ell = \frac{G_f [J/m^2]}{W_s [J/m^3]} \quad (6.22)$$

More precisely, there is a multiplicative empirical coefficient on the right hand side, which is, however, very close to 1 (it slightly depends on the type of the nonlocal model adopted, and for one particular model used it was 1.02). So the only problem is how to measure the energy dissipated per unit volume,  $W_s$ .

To this end, one needs to stabilize the specimen by bonded reinforcing rods so that concrete can deform homogeneously and remain in a macroscopically homogeneous state during the softening behavior, without any localization of cracking. This may be accomplished using the specimen shown in Fig. 6.16, which also shows a companion fracture specimen used for determination of  $G_f$ . The longer sides of the rectangular cross section are restrained by gluing to them, with epoxy, a system of parallel densely spaced thin steel rods. The gaps between the rods, filled partially by epoxy, are quite deformable, so that the system of thin rods cannot develop any significant transverse stresses and thus cannot interfere with the Poisson effect in concrete. By choosing the cross sections of the rods to be much smaller than the maximum aggregate size, the rods cannot affect the nonlocal behavior of the material in the transverse direction. The rectangular cross section is elongated, so as to minimize the influence of the wall effect and of the local stresses near the short sides of the cross section. The thickness of the specimen is chosen to be only three times the maximum aggregate size. The reason is to assure the restraint due to steel rods to be effective through the entire thickness (for much thicker specimens, localization of cracking could occur at mid-thickness).

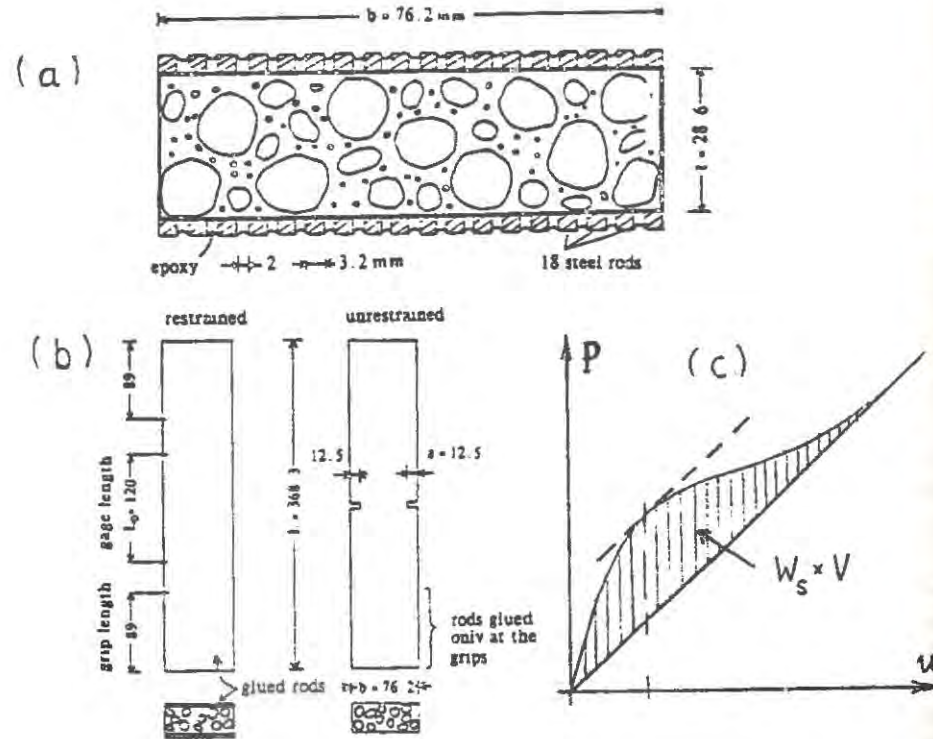


Fig. 6.16 Measurement of Energy Dissipation Due to Cracking per Unit Volume in a Stabilized Specimen According to Bažant and Pijaudier-Cabot (1988)

The combined cross section of all the steel rods is selected so as to assure the tangential stiffness of the composite specimen to be always positive. This guarantees the specimen to be stable, making localization instability impossible. The force in softening concrete, characterizing the true post-peak stress-strain diagram, can thus be obtained after the force in steel rods calculated from the measured strain is subtracted from the measured total force.

The specimen is gripped at the ends, e.g., by metallic plates glued by epoxy to the surface of the steel rods. The specimen is subjected to tension in a closed-loop testing machine, and the plot of force vs. relative displacement over gauge length  $L$  in the middle part of the specimen is recorded; see Fig. 6.16c. The inclined straight line in this plot represents the stiffness of the rods alone, without any concrete. For very large displacements, the response approaches this line asymptotically. Work  $W_s$ , the desired result, is represented by the cross-hatched area between the response curve and the rising straight line for the steel rods alone.

For the particular concrete used by Bažant and Pijaudier-Cabot (a microconcrete with maximum aggregate size  $9.5 \text{ mm}$ ), substitution of the measured value of  $W_s$  into Eq. 6.34 yielded the nonlocal characteristic length  $\ell = 2.7d_s$ . This is rather close to what has been inferred from finite element fitting of the size effect data from fracture tests.

It might be noted that evaluation of the present type of test by means of the fictitious crack model appears problematic. If one takes care to produce a nearly perfect restraint, multiple parallel fictitious cracks with arbitrarily close spacing could be obtained in computations, making the results ambiguous. As already pointed out, this problem can be avoided by enriching the fictitious crack model with a third independent material parameter, the minimum spacing of the line cracks (such spacing of course is equivalent to the nonlocal characteristic length  $\ell$ ).

An interesting point to note is that the characteristic length,  $\ell$ , cannot be identified from uniaxial tests of unrestrained specimens of different lengths (e.g. tests of van Mier, 1984, 1986) or different gage lengths (Shah and Sankar, 1987). Such data can be fitted equally well using any value of  $\ell$ , including  $\ell = 0$  (Bažant, 1989a).

## 6.10 Identification of Tensile Post-Peak Softening Stress-Strain Curves

To identify a strain-softening triaxial constitutive relation from test data, one must in general solve an inverse boundary value problem taking into account strain localization (Ottie, 1988). This is a task of formidable complexity. However, identification of a uniaxial strain softening stress-strain relation is relatively simple, provided that the characteristic length is determined in advance, as already explained. As shown by Bažant's (1989a) analysis of uniaxial test data for specimens of various lengths, localization in uniaxial test specimens can be adequately described by the series coupling model, in which a strain-softening loading zone of length  $\ell$  is coupled in series to an unloading zone. If the value of  $\ell$  is known, the axial strain in the strain-softening zone corresponding to uniaxial stress  $s$  may be approximately

calculated as (Bažant 1989a):

$$\epsilon(\sigma) = \frac{L}{\ell} \bar{\epsilon}(\sigma) - \left( \frac{L}{\ell} - a \right) \epsilon_u(\sigma) \quad (6.23)$$

where  $L \geq \ell$ ,  $\bar{\epsilon}(\sigma)$  = mean axial strain corresponding to  $\sigma$ , obtained from measured displacement over the gage length  $L$ , and  $\epsilon_u(\sigma)$  = axial strain in the unloading part corresponding to  $\sigma$  for an unloading branch emanating from the peak stress point.

### 6.11 Material Parameters for Mode II and Planar Mixed Mode Fracture

For two dimensional stress states, in general it may be presumed that crack propagation would take place under the combined action of Mode I (opening) and Mode II (sliding) deformation. In concrete, however, the effect of aggregate interlock, which leads to volume dilation, tends to resist crack propagation in any mode other than opening (Bažant and Gambarova, 1980). Nevertheless, there has been an extensive amount of experimental work done over the years, and continuing today, in an attempt to cause cracking and fracture in concrete to occur in mode II or at least in mixed mode.

The Iosipescu specimen geometry, shown in a modified form in Fig. 6.17, has been used by various investigators (Barr et al., 1987; Bažant and Pfeiffer, 1985a, 1985b, 1986; Swartz and Taha, 1987) and so has a similar geometry with only one notch (Arrea and Ingraffea, 1981; Swartz, Lu, Tang and Refai, 1988). Beams in three-point bending with off-center notches have been used by Jenq and Shah (1987a, 1987b) and Swartz, Lu and Tang (1988) (see Fig. 6.18). Biaxial testing systems have been developed in which combinations of direct tension and compression are used (Reinhardt et al., 1989) or direct tension and shear (Hassanzadeh et al., 1987).

Numerical modeling of the Iosipescu specimen was done by Arrea and Ingraffea (1981), Ingraffea and Panthaki (1985), Ingraffea and Gerstle (1985), Bažant and Pfeiffer (1985b), Rots and de Borst (1987), and Swenson (1986). Rather interesting was the finding by Bažant and Pfeiffer that if the shear zone in the beam is very narrow, the crack propagates in the cross section plane rather than in an inclined direction. This provided a challenge for numerical modeling. Acceptable fits of test results were obtained (Bažant and Pfeiffer, 1985b) assuming a Mode II state at the crack tip, modelled as a band of inclined Mode I microcracks. Others obtained acceptable fits assuming the crack propagation to occur with only Mode I deformation at the crack tip although Mode II-type deformation (combined with Mode I) exists immediately behind the crack front. The application of Swenson's model to beams tested by Swartz et al. in three-point bending (Fig. 6.18) and four-point bending (Swartz, Lu, Tang and Refai, 1988) (similar to Fig. 6.17, but with only one notch) shows clearly that propagation in their type of test occurs in Mode I. However, alternative explanations of the fracture pattern observed by Bažant and Pfeiffer (1985b, 1986), which require only Mode I type cracking, have been offered by Ingraffea and Panthaki (1985), and Swartz et al. (Swartz and Taha, 1987), while Rots and de Borst (1987) considered the crack

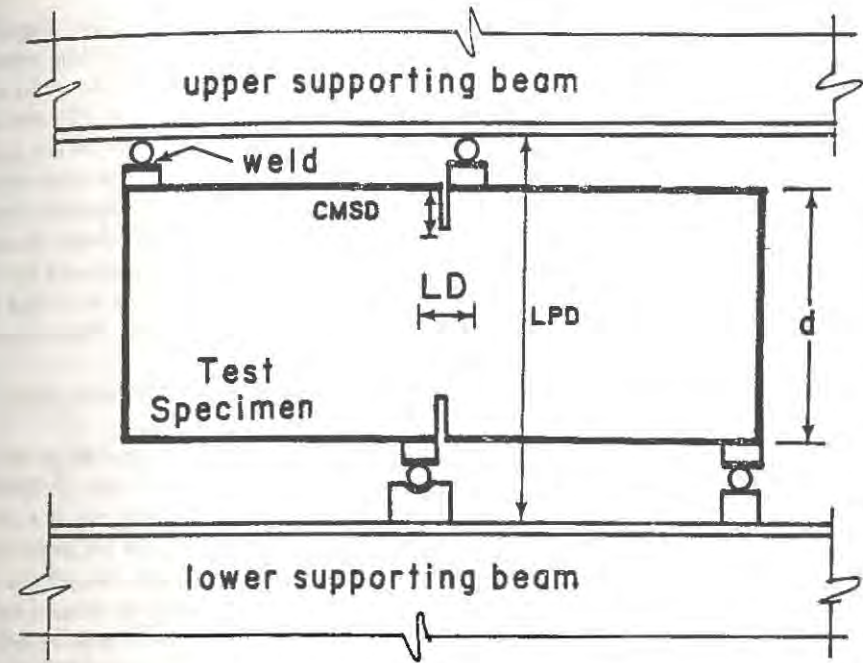


Fig.6.17 Iosipescu-Type Shear Test Geometry

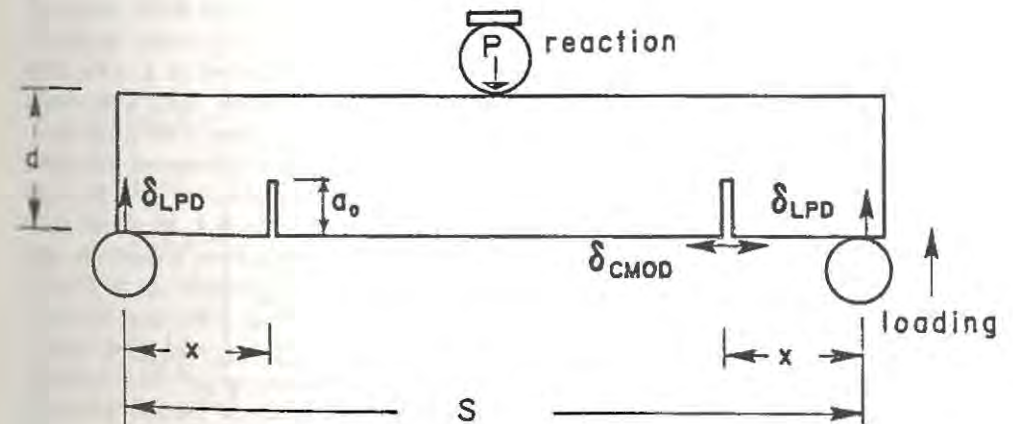


Fig.6.18 Beam with Off-Center Notches

opening to initiate in Mode I and subsequently to respond possibly in Mode II also. Ingraffea and Panthaki have argued that the observed fracture originated from tensile splitting stresses in the region between the notch tips (Fig. 6.17). The existence of these stresses was also shown analytically by Rots and de Borst. Similar experiments by Swartz et al. (Swartz and Taha, 1987) showed the principal fracture originating in this region and not at the notch tips. The finite element analysis of Bažant and Pfeiffer (1985b) confirmed the existence of significant tensile stresses between the crack tips but showed the inclined principal tensile stresses at the crack tips to be even higher. Recent tests at Northwestern University (Kazemi and Bažant, 1988) indicated that if the specimen in Fig. 6.17 is loaded symmetrically by  $P/2$  at each side of each crackmouth rather than antisymmetrically, then it splits at a load not much higher than the maximum load for the antisymmetric loading shown. This suggests that the splitting tensile stress might be important.

From size effect tests, Bažant and Pfeiffer (1986) found the Mode II fracture energy to be many times higher than for Mode I (Bažant and Pfeiffer, 1985a, 1985b).

Clearly, aggregate interlock and shear friction play a major role in providing energy to resist crack propagation even though the driving energy at the tip is due to Mode I deformation. Whether this can indeed be modeled properly by appropriate use of a crack band with inclined microcracks or friction elements is not clear at present. At the same time, there are no good microscopic observations available to indicate the presence, shape and size of a process zone although evidence of this is clear from Mode I bending and tension tests.

With regard to Mode II or mixed mode crack propagation, there is thus a general lack of information and understanding. There is no general agreement as to the suitability of test methods, data evaluation or failure theory to predict mixed-mode crack propagation and fracture in concrete.

## 6.12 Material Parameters for Mode III Fracture

In the Iosipescu type mixed-mode specimens already discussed, a perfect antisymmetry is not achieved. The specimen fails with a planar crack in the cross section plane, although the principal normal stresses were inclined with regard to the cross section plane. However, a perfect antisymmetry, required for Mode III fracture, can be achieved in a cylindrical specimen with a circumferential notch in the middle, subjected to torsion. Such a specimen was introduced by Bažant and Prat (1988a), and Bažant, Prat and Tabbara (1989); Fig. 6.19. Testing geometrically similar specimens of different sizes, they found a pronounced size effect and used it to determine the Mode III fracture energy,  $G_f^{III}$ . For specimens with no axial force, they found it to be about three-times larger than that for Mode I. However, they observed that despite perfectly satisfying the antisymmetry of geometric conditions and loading arrangement required for a Mode III situation, a Mode III field might not have been achieved locally due to volume expansion of the fracture process zone. They also observed that the Mode III fracture energy is apparently very sensitive to the normal stress across the fracture process zone. It appears that Mode III fracture energy cannot be a material constant; but it could be a material function, depending on the transverse normal stress and possibly other variables.

Recently, similar tests of Xu and Reinhardt (1989) indicated only a negligible size effect in torsional Mode III specimens. The reason for this difference is not clear.

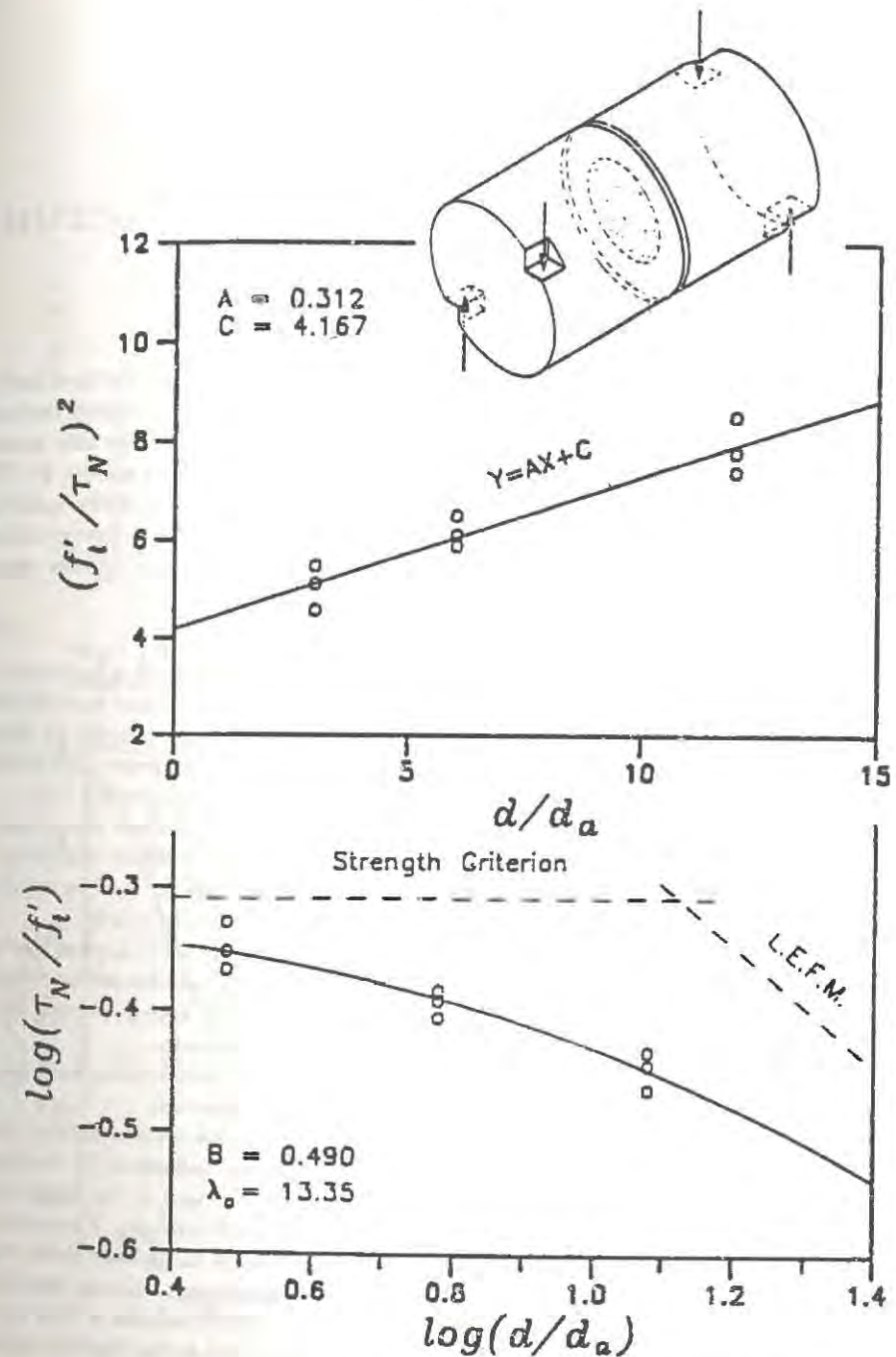


Fig. 6.19 Size Effect Regression Plot for Measurement of Mode III (after Bažant, Prat and Tabbara, 1989)

## Chapter 7. FACTORS INFLUENCING FRACTURE PARAMETERS

### 7.1 Effect of Loading Rate and Creep

In no material can fracture happen instantly. Cracks take a finite time to form and to propagate over a finite distance. The reason is that the process of bond ruptures proceeds at a certain finite rate. The basic physical theory describing the process is the rate process theory, in which the rate of bond ruptures is determined by the activation energy,  $U$ . The probability (or frequency) of bond rupture depends on the microstress level at the crack tip, which in turn is determined by either the stress intensity factor,  $K_I$ , or by the energy release rate,  $G$ . Based on these physical observations, the following approximate relation ensues (Evans, 1974):

$$\dot{a} = \nu_c (K_I / K_{Ic})^n e^{-U/RT} \quad (7.1)$$

in which  $\dot{a}$  = velocity of crack tip propagation,  $T$  = absolute temperature,  $R$  = universal gas constant, and  $\nu_c, n$  = empirical constants. Roughly,  $n \approx 30$ , while  $\nu_c$  can have very different values. According to Eq. 7.1, the relationship between  $\log \dot{a}$  and  $\log K_I$  should be linear. But this is true only approximately. Experiments indicate a mildly nonlinear relationship between  $\log K_I$  and the loading rate, but no clear information exists with regard to  $\dot{a}$ .

There exist other useful relations relating the remote stress to the remote stress rate or remote strain rate, or unloading rate (e.g. Reinhardt, 1984). They are however valid only for certain particular situations and are not generally interpretable. ("Remote" are the locations so far from the crack so that the stress is not significantly affected by the crack).

John and Shah (1985, 1986, 1987, 1989a; also John, Shah and Jenq, 1987) applied the two-parameter fracture model to Mode I and Mixed Mode fracture tests conducted at different strain rates. They concluded that  $K_{Ic}$  is rate-independent but that  $\delta_{CTOD}$ , as well as the effective crack length at peak load, decrease as the loading rate increases.

It should also be observed that the effects of crack growth rate and loading rate are, in their physical mechanism, related to the stress corrosion effect in fracture.

In analyzing the fracture behavior of specimens or structures under various loading rates, the phenomena of fracture and creep are inseparable. The results are influenced by the short-term linear viscoelasticity of concrete, which is quite pronounced, and in the high stress regions near the fracture front, by the additional nonlinear creep of concrete. Furthermore, the strain-softening behavior in the fracture process zone is likely to be even more time-dependent than the nonlinear creep in the hardening high stress range. Recent studies of the size effect at various rates of loading (Bažant and Gettu, 1989) indicate a very strong creep or stress relaxation in the strain-softening range which prevails in the fracture process zone. This phenomenon seems to reduce the size of the fracture process zone as the loading rate diminishes (i.e. the time to failure increases), with the consequence that long-time response might be closer to linear elastic fracture mechanics than short-time response. This is illustrated with recent data of Bažant and Gettu (1989) in Fig. 7.1 in which the results

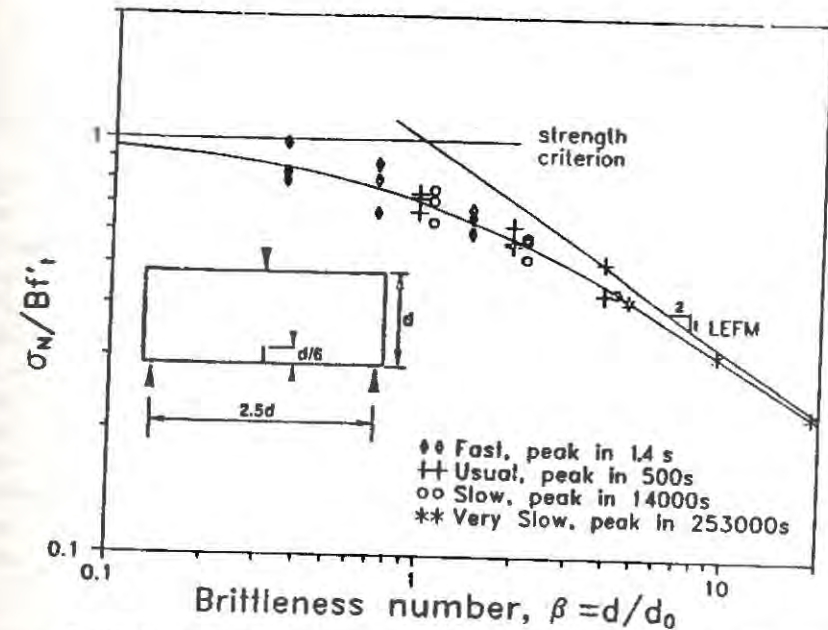


Fig.7.1 Increase of Brittleness Number (Shift to the Right on the Size-Effect Curve) Due to Increasing Time to Failure of Fracture Specimens

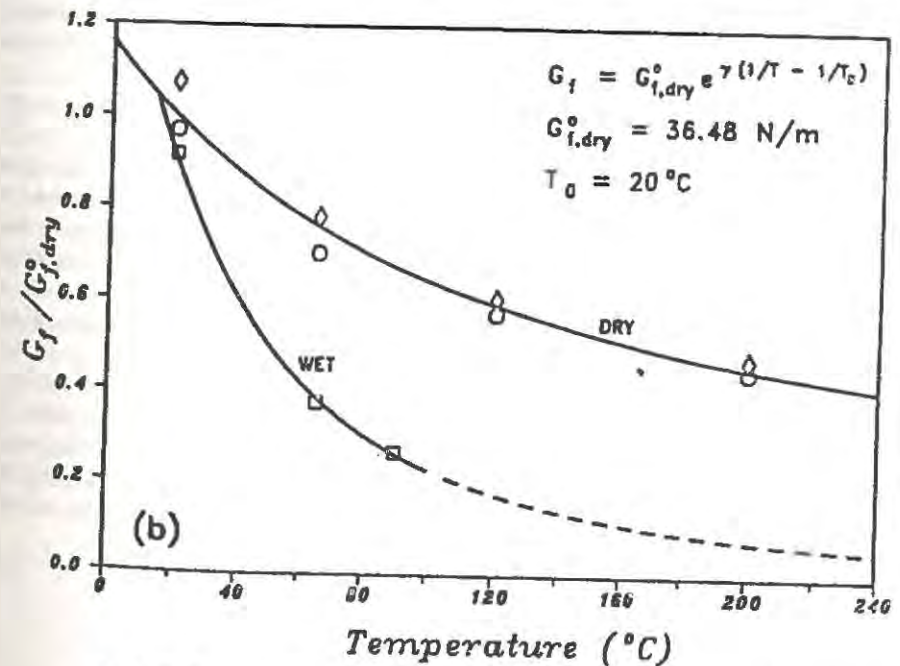


Fig.7.2 Fracture Energy Dependence on Temperature and Moisture Conditions (after Bažant and Prat, 1988)

for different times to failure, plotted as  $\sigma_N$  vs. the brittleness number of Bažant (Sec. 5.1 and 5.2), can be seen to shift to the right as the time increases.

Similar findings, indicating that the process zone size and fracture energy decrease as the time to failure increases, have been recently reported by Wittmann et al. (1987), although this study did not deal with size-independent fracture characteristics.

Lest it be perceived that the aforementioned findings of Bažant and Gettu contradict those of John and Shah, one should realize that John and Shah's method determines basically the reach of the fracture process zone where there is significant displacement due to microcracking. But at the locations where the microcracks are opened most widely, the stress may have already relaxed to zero. This portion of the microcracking zone would not be manifested in the process zone size obtained by the size effect method, which eventually gives the length of the zone over which significant bridging stresses are transmitted. It is quite conceivable that, due to stress relaxation, this length represents only a small part of the length of the microcracking zone, as obtained by John and Shah's method. More rigorous studies are needed, however.

The experimental techniques for measuring fracture properties at high loading rates are discussed by John and Shah (1985), Reinhardt (1984), Mindess (1984), and others.

## 7.2 Effect of Temperature and Humidity on Fracture Energy

This effect is likely to have at least partly the same physical mechanism as the effect of crack velocity on loading rate. The rate of bond ruptures depends not only on the stress level but also on temperature, according to the activation energy theory. Using Eq. 7.1 as the point of departure, Bažant and Prat (1988b) have shown that, according to the activation energy theory, the fracture energy of concrete should depend on the absolute temperature as follows:

$$G_f = G_f^0 \exp\left(\frac{\gamma}{T} - \frac{\gamma}{T_0}\right), \quad \gamma = \frac{2U}{nR} \quad (7.2)$$

in which  $T_0$  = reference temperature,  $G_f^0$  = fracture energy at reference temperature, and  $\gamma$  = constant. Eq. 7.2 agrees well with test results of the size effect method obtained for various temperatures from room up to 200°C; see Fig. 7.2. Some results have also been obtained for temperatures in the freezing range, indicating the trend in Fig. 7.2 to continue down to about -20°C, and then reversing (Maturana et al., 1988).

A similar dependence of  $G_f$  on  $T$  was experimentally determined by Brameshuber (1988, 1989) who, however, used different formulas to describe the observed trend.

The aforementioned size effect tests were conducted at various temperatures on saturated (wet) concrete as well as on concrete which was dried before the test. The difference in humidity conditions appeared insignificant at room temperature, however, at high temperatures the wet concrete had a much lower fracture energy than the dry concrete (Fig. 7.2, after Bažant and Prat, 1988b). Assuming linear dependence on the specific water content, parameter  $\gamma$  was expressed as

$$\gamma = \gamma_0 + (\gamma_1 - \gamma_0) \frac{w}{w_1} \quad (7.3)$$

in which  $w$  = specific water content,  $w_1$  its value at saturation, and  $\gamma_0, \gamma_1$  = value of  $\gamma$  in dry and wet conditions (for the concrete tested, it was found that  $\gamma_0 \simeq 600^\circ K$ , and  $\gamma_1 \simeq 1900^\circ K$ ).

The effect of temperature is quite pronounced in polymer concretes, in which viscoelasticity of the polymer binder is no doubt an important factor (Vipulanandan and Dharmarajan, 1987, 1988, 1989a,b,c).

## 7.3 Effect of Cyclic Loading

Repeated loading tends to gradually increase the crack length even if the maximum stress intensity factor of the cycles is well below its critical value for static loading. The rate of increase of the crack length,  $a$ , with the number of cycles,  $N$ , has been shown for many materials to be approximately described by the Paris law (Paris and Erdogan, 1963):  $da/dN = C(\Delta K_I/K_{Ic})^m$ , in which  $C$  and  $m$  are empirical constants. Although Eq. 7.4 is essentially empirical and does not have a fundamental physical basis such as Eq. 7.1, it is nevertheless an equation of rather general applicability. For concrete, however, it was found (Bažant and Xu, 1989) that deviations from Paris law arise due to the size effect. They can be described by the following generalization (Bažant and Xu, 1989):

$$\frac{da}{dN} = C \left( \frac{\Delta K_I}{K_{Im}} \right)^m, \quad \text{with } K_{Im} = K_{Ic} \left( \frac{d}{\bar{d}_0 + d} \right)^{1/2} \quad (7.4)$$

where  $\bar{d}_0$  is a constant having a similar meaning to  $d_0$  in the size effect law (Eq. 1.4),  $K_{Im}$  is the apparent (size-dependent) fracture toughness calculated from the peak load of the specimen and LEM relations, and  $d$  is the size of the specimen. Test showed that  $\bar{d}_0 \simeq 10d_0$  when the load is cycled between 0 and 80% of the maximum load for monotonic loading. Eq. 7.4, shown in Fig. 7.3 by the three straight lines, is seen to agree quite well with the data for three-point-bend notched beams of sizes 1:2:4. Paris law, by contrast, yields in Fig. 7.3 a single straight line and cannot describe the observed size effect.

An interesting point about Paris law is that the rate of crack extension does not depend on the upper and lower limiting values of the stress intensity factor, but approximately only on their difference,  $\Delta K_I$ . This might be explained by a sort of a shakedown in the fracture process zone, with development of residual stresses after a number of cycles. Various other interesting results on cyclic fracture of concrete, which pertain to particular test conditions, have been obtained, for example, by Swartz, Hu and Jones (1978), Swartz, Huang and Hu (1982), Swartz and Go (1984), Perdikaris and Calomino (1987), and others.

The interpretation of the  $\Delta K_I$ -value which should be substituted in Eq. 7.4 is subject to some question with regard to the size effect on the value of  $K_{Ic}$ . The value of  $\Delta K_I$  should be calculated for the elastically equivalent effective crack length  $a = a_0 + c$ , which means  $\Delta K_I$  should be modified with respect to the length of crack extension from the notch (Fig. 4.2).

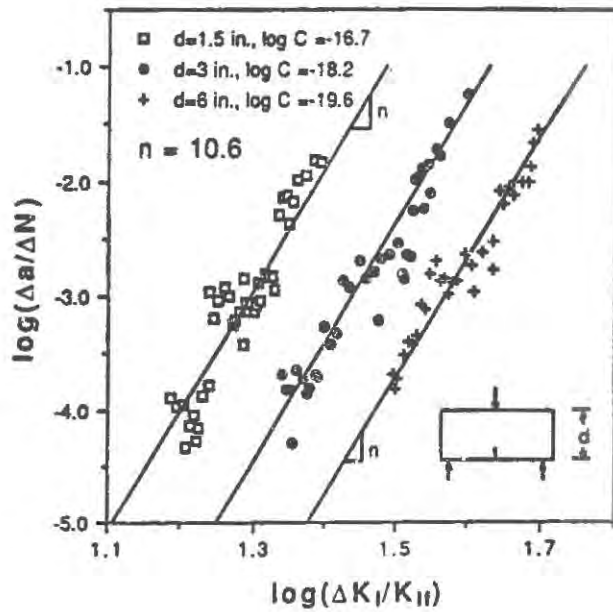


Fig. 7.3 Fracture of Three-Point Bend Specimens under Cyclic Loading

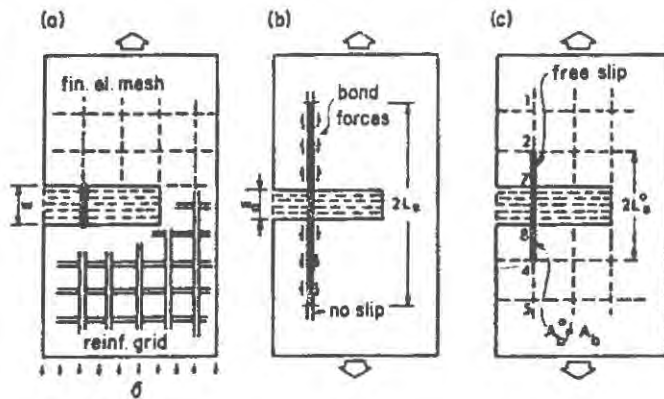


Fig. 8.1 Effect of Bond Slip of Reinforcing Bars Crossing Crack Bands or Cracks

## Chapter 8. EFFECT OF REINFORCEMENT

### 8.1 Effect of Reinforcing Steel Bars

When concrete is reinforced by a regular grid of reinforcing bars, it is often appropriate to consider concrete with the bar grid as one heterogeneous composite material which is macro-homogeneous on a larger scale. Obviously, in such a composite, the bars inhibit the formation and propagation of cracks. If there were no bond slip, then the opposite faces of a crack would not be able to open apart, and so there would be no fracture until the bar breaks. This simple consideration immediately clarifies that bond slip must take place and must be taken into account. The property which matters is the stiffness of the connection provided by the steel bars between the opposite faces of the crack or crack band.

Assuming the ultimate bond stresses  $U_b$  to be approximately constant, the bar stress, which is equal to  $\sigma_s$  at the crack crossing, decreases linearly over the distance of bond slip,  $L_s$ , on each side of the crack. From this stress distribution, one can estimate the relative displacement of the bar against concrete over length  $2L_s$ . Furthermore, in a macroscopically uniform or quasi-uniform field, the force carried by the bar at the crack crossing must equilibrate the force per bar carried jointly by concrete and steel at locations beyond the bond slip length. From these conditions it follows that (Bažant and Cedolin, 1980; Bažant 1985c):

$$L_s = \frac{A_b}{U_b} \frac{1-p}{1-p+np} \sigma_s \quad (8.1)$$

in which  $p$  = steel ratio,  $n$  = steel-to-concrete ratio of the elastic moduli, and  $A_b$  = bar cross section. For the purpose of finite element analysis, one may further imagine an equivalent bar which is anchored to concrete at the nodes of the finite element mesh and has no bond stresses but a shorter equivalent free-slip length. Another simple formula for this length has been devised by Bažant and Cedolin (1980).

A detailed description of cracking in reinforced concrete requires a more sophisticated theory; see e.g. Pijaudier-Cabot and Mazars (1989), and Breyse and Mazars (1988). These studies used damage theory for concrete combined with an elasto-plastic model for steel bars. The results were interesting, giving information on the evolution of damage zones around cracks, development of cracks and the global response of the structure. Bond stresses and slip need to be also included in a detailed analysis; this has been done by Pijaudier-Cabot et al. (1989) in terms of a nonlocal damage model which also yields the size effect.

### 8.2 Fracture in Fiber-Reinforced Concrete

Bond slip of the fibers is a phenomenon similar to the slip of reinforcing bars, and again has a major effect on fracture, along with the phenomenon of fiber pull-out due to short length.

Potentially useful improvements in the mechanical behavior of tension-weak concrete matrices can be effected by the incorporation of fibers. Similar to the behavior of plain

concrete, composite failure under most types of loading is initiated by the tensile cracking of the matrix along planes where the normal tensile strains exceed the corresponding permissible values. This may be followed by multiple cracking of the matrix prior to composite fracture, if the volume fraction of fibers are sufficiently high (or if the fibers are continuous) (Aveston et al., 1971). However, when short fibers are used (steel, polypropylene, glass, etc.), once the matrix has cracked, one of the following types of failure will occur:

- (a) The composite fractures immediately after matrix cracking. This results from inadequate fiber content at the critical section or insufficient fiber lengths to transfer stresses across the matrix crack.
- (b) Although the maximum load on the composite is not significantly different from that of the matrix alone, the composite continues to carry decreasing loads after the peak. The post-cracking resistance is primarily attributed to gradual (rather than sudden) fiber pull-out associated with crack bridging. While no significant increase in composite strength is observed, the composite fracture energy and toughness are considerably enhanced (Fig. 8.2) (Gopalaratnam and Shah, 1987a).
- (c) Even after matrix cracking, the composite continues to carry increasing loads. The peak load-carrying capacity of the composite and the corresponding deformation are significantly greater than that of the unreinforced matrix. During the pre-peak inelastic regime of the composite response, progressive debonding of the interface and distributed microcracks in the matrix may be responsible for the energy dissipation process (Mobasher, Castro- Montero and Shah, 1989). It is clear that this mode of composite failure results in the efficient use of both the constituents (Mobasher and Shah, 1989; Stang, Mobasher and Shah, 1989; Mobasher, Stang and Shah, 1989).

Analytical models used for the prediction of the mechanical behavior of fibrous composites may be suitable for one or more of the above types of failure mechanisms. Based in part on the fundamental approach in their formulation, analytical models can be categorized (Gopalaratnam and Shah, 1987a) as: models based on the theory of multiple fracture, composite models, strain-relief models, fracture mechanics models, interface mechanics models, and micromechanics models. Fairly exhaustive reviews of these models are available elsewhere (Gopalaratnam and Shah, 1987a; Mindess, 1983). Brief reviews of the fracture mechanics based models and the interface mechanics models are given here as these are typically the most suitable for modeling the inelastic processes in short-fiber composites.

Two broad categories of models can be identified from among the fracture mechanics based models. The more fundamental class of models use the concepts of LEFM to solve the problem of crack initiation, growth, arrest and stability in the presence of fibers through appropriate changes in the stress intensity factor (Romualdi and Batson, 1963; Romualdi and Mandel, 1964). Typically these models assume perfect bond between the fiber and the matrix, and are one-parameter fracture models. Unlike the classical LEFM models, some of the later models implicitly account for the inelastic interface response during crack growth through a nonlinear stress- displacement relationship for the fiber-bridging zone (process zone). This approach, which has come to be known as the fictitious crack model (Hillerborg, 1980), is conceptually similar to that described in Sec. 3.1 for the fracture of unreinforced concrete. The major differences in the fictitious crack models (Hillerborg, 1980; Petersson,

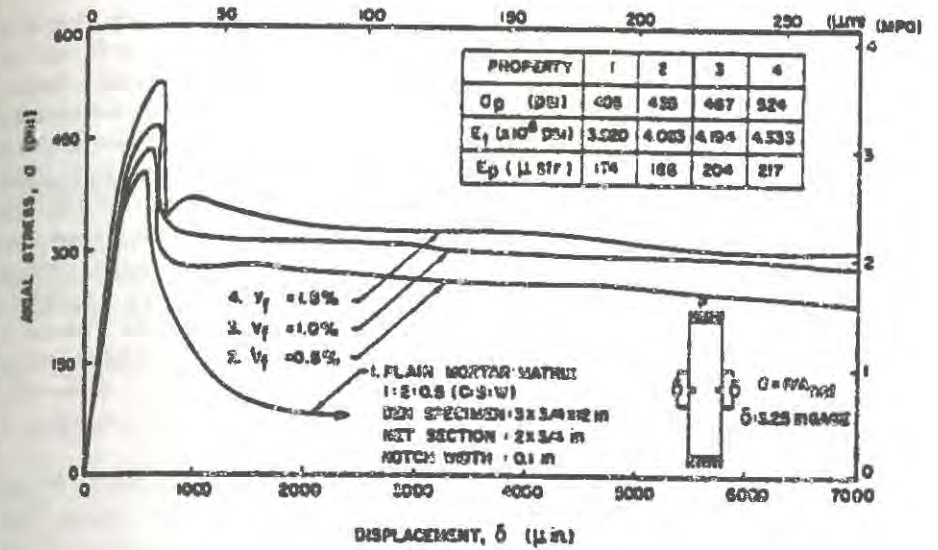


Fig. 8.2 Typical Results of Stress-Displacement Curves Obtained From Direct Tension Tests on Plain Mortar Matrix and Steel Fiber Reinforced Concrete

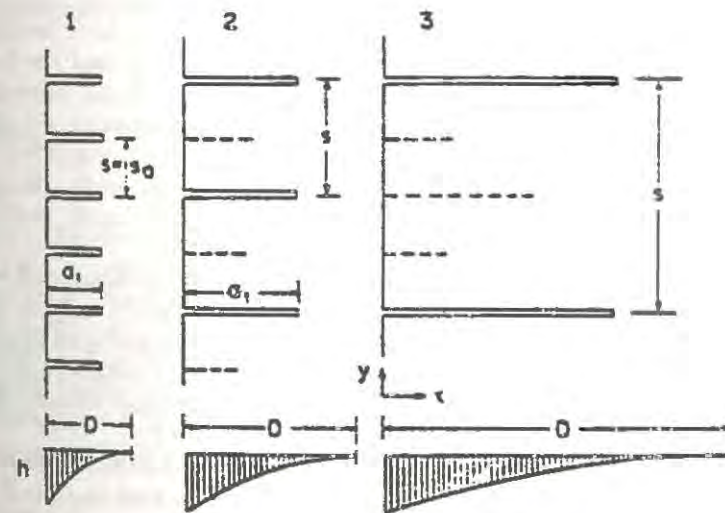


Fig. 9.1 Arrest of Parallel Crack Due to Instability and Change of Spacing for Leading Cracks

1980; Wecharatana and Shah, 1983b; Visalvanich and Naaman, 1982) are the singularity assumptions at the crack-tip, the criteria used for crack initiation and growth, and the stability of the crack growth. More recently, Jenq and Shah (1986) have proposed a fracture mechanics model to predict the crack propagation resistance of fiber reinforced concrete that is somewhat different from either of these two approaches. Fracture resistance in fibrous composites according to this model is separated into four regimes which include: linear elastic behavior of the composite; subcritical crack growth in the matrix and the beginning of the fiber bridging effect; post-critical crack growth in the matrix such that the net stress intensity factor due to the applied load and the fiber bridging stresses remain constant (steady state crack growth); and the final stage where the resistance to crack separation is provided exclusively by the fibers. The model uses two parameters to describe the matrix fracture properties ( $K_{Ic}^*$ , modified critical stress intensity factor based on LEFM and the effective crack length, and  $\delta_{CTOD}$ , the critical crack tip opening displacement, as described earlier for unreinforced concrete), and a fiber pull-out stress-crack-width relationship as the basic input information.

Mobasher, Ouyang and Shah (1989) recently developed an  $R$ -curve approach for fracture of cement-based fiber composites. The parameters of the  $R$ -curve can be uniquely determined according to material properties, such as  $K_{Ic}^*$  and  $\delta_{CTOD}$  defined by Jenq and Shah (1986). Toughening of the matrix by the fibers is incorporated into the  $R$ -curve by fiber-bridging pressure. By incorporating the closing pressure in the equilibrium conditions during the stable crack propagation, the onset of instability of matrix is shown to be dependent on the fibers.

All of the fictitious crack models rely on the stress-crack-width relations obtained experimentally. There have been some attempts at predicting the macroscopic stress-crack-width relations of the composite from a study of the mechanics of the fiber-matrix interface. They can be grouped as models based on the shear-lag theory or modifications thereof (Lawrence, 1972; Laws et al., 1972; Gopalaratnam and Shah, 1987b; Gopalaratnam and Cheng, 1988), fracture mechanics based interface models (Stang and Shah, 1986; Morrison et al., 1988) and numerical models (Morrison et al., 1988; Sahudin, 1987). Many of these models have been successful to varying degrees in predicting the peak pull-out loads and the load-slip response of idealized aligned single fiber pull-out. These models have been tremendously useful in understanding the basic mechanics of stress transfer at the interface and showing that interfacial debonding plays an important role in the fracture of such composites. Significant research efforts will, however, be needed to modify these models to predict the pull-out characteristics of inclined fibers that are randomly oriented at a matrix crack (randomness in both the angular orientation as well as the embedment length).

Stang and Shah (1989) proposed a damage model for the study of distributed microcracking. The compliance of the composite subjected to uniaxial tension was initially derived according to the shear lag theory. A damage variable, which is a function of crack spacing and fiber debonding length at the crack section, was introduced. After specifying the damage evolution law by a damage surface, the stress and strain response of fiber reinforced composites subjected to uniaxial tension can be calculated.

Fracture has also been studied for glass-fiber polymer (polyester) concrete. Such materials show considerable nonlinearity and stable crack growth prior to peak load, and the  $R$ -curves that have been measured reflect this behavior (Vipulanandan and Dharmarajan, 1987, 1988, 1989a,b,c).

## Chapter 9. CRACK SYSTEMS

In contrast to metallic structures, concrete structures contain numerous large cracks which are close enough to interact. Therefore, understanding of crack interaction is more important than it is for metallic structures.

### 9.1 Response of Structures with Interacting Growing Cracks

Consider a structure with cracks of lengths  $a_i (i = 1, 2, \dots, n)$  loaded by a system of forces or boundary displacements, shrinkage or thermal dilation proportional to parameter  $\lambda$ . The energy (under isothermal conditions, more precisely the Helmholtz free energy) of the structural system is the sum of the strain energy  $U$ , which depends on the load parameter as well as the crack lengths, and the energy needed to produce the cracks, i.e.,

$$F = U(a_1, \dots, a_n; \lambda) + \sum_i \int_0^{a_i} R(a'_i) da'_i \quad (9.1)$$

in which  $R$  = specific energy (per unit crack length) required for crack growth and  $a'_i$  are the crack length values between 0 and  $a_i$ . In the case of linear elastic fracture mechanics,  $R = G_f$ . The equilibrium condition of the system is  $\delta F = \Sigma (U_{,i} + R(a_i)) \delta a_i = 0$  for any variation  $\delta a_i$ , which implies that  $-U_{,i} = R(a_i)$ . This is the well-known condition of crack propagation already stated at the beginning. The stability of the structure with the cracks requires that the second variation  $\delta^2 F$  be positive for any admissible  $\delta a_i$  (Bažant and Ohtsubo, 1977, 1978; Bažant and Wahab, 1979). From Eq. 9.1, we have

$$\delta^2 F = \sum_i \sum_j \frac{1}{2} U_{,ij} \delta a_i \delta a_j + \sum_i \frac{\partial R(a_i)^2}{\partial a_i} (\delta a_i)^2 = \sum_i \sum_j \frac{1}{2} A_{ij} \delta a_i \delta a_j \quad (9.2)$$

in which  $A_{ij}$  form a square matrix,

$$A_{ij} = U_{,ij} + 2R_{,i} \delta_{ij} H(\delta a_i) \quad (9.3)$$

Here the subscripts following a comma represent partial derivatives with respect to  $a_i$ ,  $\delta_{ij} = 1$  if  $i = j$  and 0 if  $i \neq j$ ; and  $H(\delta a_i) = 1$  if  $\delta a_i \geq 0$ , and 0 otherwise. Note that  $-U_{,i} = K_i^2/E'$  where  $K_i$  = stress intensity factor of crack  $a_i$  (any mode), and  $-E'U_{,ij} = 2K_i K_{j,i}$ .

As the loading parameter  $\lambda$  increases, the cracks grow. At a certain crack length it can happen that there are more than one solution for the crack increments, i.e., the path of the system plotted in the space with coordinates  $a_i$  bifurcates. It can be shown that the bifurcation condition is

$$\det A_{ij} = 0 \quad (9.4)$$

After bifurcation, the path which is followed is that for which (Bažant, 1988):

$$\begin{aligned} \text{For displacement control: } \delta^2 F &= \min \\ \text{For load control: } \delta^2 F &= \max \end{aligned} \quad (9.5)$$

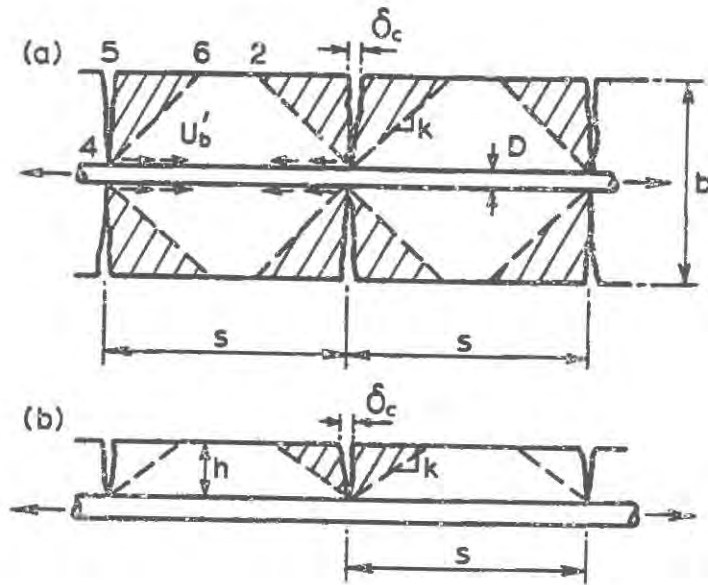


Fig. 9.2 Energy Release Zones Governing Crack Spacing in Tensioned Reinforced bar

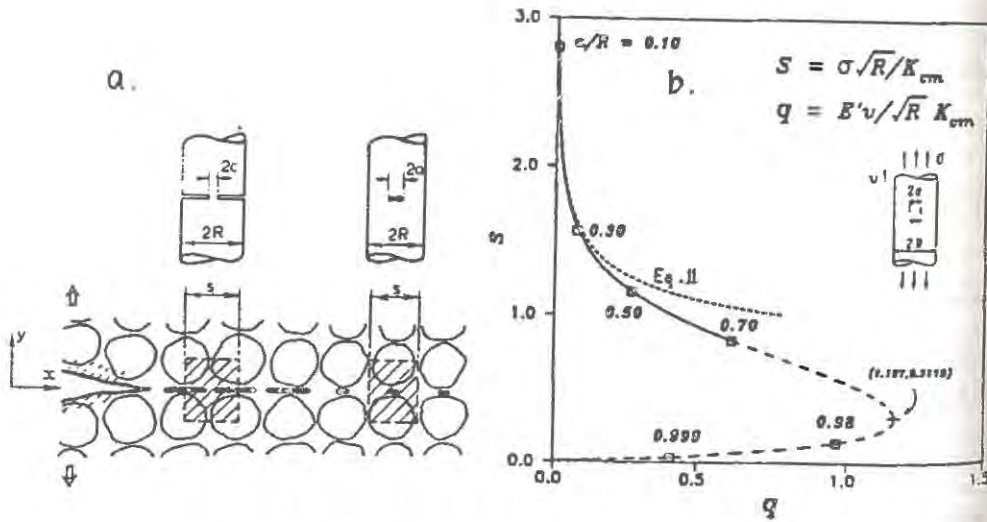


Fig.9.3 Discrete Cracking in Fracture Process Zone and Theoretical Stress-Displacement Diagram for Crack Coalescence

This condition is derived from the fact that the path which occurs must be that with the maximum internal entropy increment.

More recently, Bažant (1989b) and Bažant and Tabbara (1989) have shown that the tangential stiffness matrix containing  $N$  interacting cracks of lengths  $a_i (i = 1, \dots, N)$  is

$$K_{rs}^t = K_{rs}^s - \sum_{k=1}^{\nu} \sum_{m=1}^{\nu} \Psi_{km} \frac{\partial^2 F}{\partial a_m \partial q_r} \frac{\partial^2 F}{\partial a_k \partial q_s} \quad (9.6)$$

where

$q_r =$  displacements ( $r = 1, \dots, N_d, N_d =$  number of displacements);

$K_{rs}^s = \partial^2 F / \partial q_r \partial q_s =$  secant stiffness matrix of cracked structure;

$\nu =$  number of cracks that propagate during loading (cracks  $a_{\nu+1}, \dots, a_N$  remaining stationary,  $\nu \leq N$ );

$\Psi_{km} =$  inverse of the matrix  $\Phi_{km}$ , in which

$\Phi_{km} = \partial^2 F / \partial a_k \partial a_m + \delta_{km} dR_m / da_m$ ; and

$R_m(a_m) =$  given  $R$ -curve of the  $m$ -th crack (in LEFM,  $R_m = G_f, dR_m / da_m = 0$ ).

Eq. 9.6 is valid only if  $\delta a_m = -\sum_k \Psi_{km} \sum_s \delta q_s \partial^2 F / \partial a_k \partial q_s \geq 0$  for all  $m \leq \nu$  and  $\sum_u \partial^2 U / \partial a_m \partial q_k \geq 0$  for all  $m > \nu$ . If not, the set of propagating cracks is different than assumed. Obviously, various sets of propagating cracks must be tried until the foregoing conditions are met for all  $m$ . Based on Eq. 9.6,  $2\delta^2 F = \sum_r \sum_s K_{rs}^t \delta q_r \delta q_s$ , which needs to be used to determine the stable path of evolution of the crack system. For further details, see the textbook by Bažant and Cedolin (1990).

### 9.2 Interacting Parallel Cracks

The preceding formulation has an interesting application to systems of parallel cracks caused, e.g., by drying shrinkage or cooling stresses, or by bending. In the idealized case of a massive wall treated as a half-space, the shrinkage cracks start at some close spacing  $s$  and then, as the drying front advances into the wall, they continue to grow inward. Calculations on the basis of Eq. 9.2 have shown that the system becomes unstable when the crack length reaches the value approximately  $a_i = 1.7s$ , at which point the drying front is approximately at the depth  $2.6s$  (Bažant and Ohtsubo, 1977; Bažant, Ohtsubo and Aoh, 1979; Bažant and Wahab, 1979). At this point there is a bifurcation of the equilibrium path in the space of  $a_i$ . Every other crack stops growing and closes, keeping the length  $a_2$ , while the intermediate cracks of length  $a_i$  continue to grow, their spacing doubled to  $2s$ . The arrest of the growth and closing of every other of the leading cracks is again repeated later, and so on. This produces the crack systems shown in Fig. 9.1.

The spacing of the cracks,  $s$ , is important for determining their width. As is well known, it is desirable to keep the crack width less than about 0.1mm to 0.4mm, mainly because narrow cracks are not really continuous and do not serve as good conduits for moisture or

corrosive agents. If the average shrinkage strain or cooling strain is  $\epsilon^0$ , and the body is restrained, then the opening of the cracks is

$$\delta_c \simeq s \epsilon^0 \quad (9.7)$$

The drying cracks that have stopped growing will gradually close (Fig. 9.1). Thus, one must substitute in Eq. 9.6 the spacing of the leading cracks, which evolves as  $s = s_0, 2s_0, 4s_0, 8s_0, \dots$ . The spacing of the leading cracks generally remains between  $s = a_1/1.7$  and  $2a_1/1.7$ , i.e., on the average  $s \simeq 0.9a_1$ . Thus, in view of Eq. 9.6, the opening width of the shrinkage cracks is, on the average,

$$\delta_c \simeq 0.9a_1 \epsilon^0 \quad (9.8)$$

The behavior is rather similar for parallel cracks caused by cooling, as well as parallel cracks in beams caused by bending or axial force. In reinforced concrete structures, the gradual opening of the shrinkage cracks with the progress of drying or the bending cracks with the progress of loading, is prevented by reinforcement. In fact, it is possible to calculate (provided the bond slip length is known) the minimum reinforcement which is required to keep the cracks propagating with equal lengths at their small initial spacing. Such a reinforcement prevents the opening width of the cracks from exceeding a certain value. The necessary reinforcement has been calculated from the stability condition based on Eq. 9.2 in Bažant and Wahab (1980), and it turned out that, for a typical situation, the minimum reinforcement was about 0.2% of the cross-sectional area of concrete. Thus we see that the empirical rules for minimum reinforcement are in fact explicable by means of fracture mechanics. An interesting point, though, is that the precise value of the minimum reinforcement needed to prevent progressively wider opening of the cracks is not a constant but depends on the reinforcement outlay, the structural geometry, the distribution and history of pore humidity or temperature, etc.

The phenomenon just described may also be regarded as a kind of localization of the cracking strain into some preferred cracks.

### 9.3 Crack Spacing and Width in Beams

Although the current code provisions regulating the width of cracks are empirical, a deeper understanding can be gained through fracture mechanics. One must distinguish between: (1) crack initiation, which corresponds to the peak point of the stress-strain diagram and signals the start of development of microcracks, and (2) crack completion, which corresponds to a reduction of the tensile stress to zero and coalescence of microcracks into continuous cracks.

The crack initiation is governed by the strength criterion, while crack completion is governed by the fracture mechanics energy criterion. For approximate analysis, one need not write the energy balance condition for infinitely small crack length increments, but one can write it for the entire change from the uncracked to a fully cracked state:

$$\Delta U = \Delta W_f + \Delta W_b \quad (9.9)$$

in which  $\Delta U$  = total release of strain energy,  $\Delta W_f = G_f A_c$  = energy needed to produce fracture ( $A_c$  = area of all the cracks), and  $\Delta W_b$  = energy dissipated by bond slip which occurs simultaneously with cracking.

Consider now concrete that is restrained by steel bars which are sufficiently strong to prevent the previously discussed instabilities of crack systems in which some cracks close and the spacing of the open cracks multiplies. For the sake of simple illustration, consider a round concrete rod in tension, with a single steel bar in the middle (Fig. 9.2). This also approximately simulates the behavior of the concrete zone surrounding one of the bars in a beam, in which the cross section area is subdivided into non-overlapping zones of concrete, each interacting with one bar only. One may distinguish four simple, idealized cases (Bažant and Oh, 1983b, 1984).

**Case 1a. Strength Limit and No Bond Slip.** - In this case, the strain at which cracking begins is:

$$\epsilon_s \geq f'_t/E \quad (9.10)$$

**Case 1b. Strength Limit and Bond Slip.** - By force equivalence condition, the force across the crack plane,  $A_c f'_t$ , must be equal to the bond force  $U'_b L_b$  accumulated over the bond slip length  $L_b$  ( $U'_b$  = ultimate bond stress). Since  $s \geq L_b$  and  $A_c = \pi b^2/4$  ( $b$  = diameter of the concrete cross section, and the cross section of the bar is neglected), the cracks can begin to form in this manner if

$$s \geq (\pi f'_t/4U'_b) b^2 \quad (9.11)$$

**Case 2a. Energy Limit and No Bond Slip.** - As an approximation one can imagine that the full formation of a crack relieves the stress from the triangular areas cross-hatched in Fig. 9.2a. The volume of the region obtained by rotating this area about the bar axis is  $V_1 = \pi b^3/12k$ . Therefore,  $\Delta U = V_1 \sigma_1^2/2E$  ( $\sigma_1 = E\epsilon_s$ ). Also  $U'_b L_b = A_c f'_t$ . Neglecting  $\Delta W_b$ , we have  $\Delta U \geq \Delta W_f$ . So we find the condition for complete crack formation:

$$\epsilon_s \geq (6kG_f/E)^{1/2} b^{-1/2} \quad (9.12)$$

**Case 2b. Energy Limit and Bond Slip.** - In this case, instead of  $\sigma_1 = E\epsilon_s$  we have, from the condition of equilibrium with the bond stresses over length  $s$ ,  $\sigma_1 \pi b^2/4 = U'_b s$ , all the other equations being the same as in case 2a. It follows that complete cracks can form while there is bond slip if

$$s \geq (3\pi^2 k E G_f/8U'_b)^{1/2} b^{3/2} \quad (9.13)$$

The foregoing calculations (Bažant and Oh, 1983b, 1984) are based on the assumption that the stress release zones of adjacent cracks do not overlap, as shown in Fig. 9.2a. If they do, a slightly different calculation is required.

A somewhat more sophisticated calculation (Bažant and Oh, 1983b, 1984) yields continuous relations between spacing  $s$  and strain  $\epsilon_c$  representing a transition from microcrack initiation to complete crack formation. These calculations have been shown to agree with the test results of Clark (1956), Chi and Kirstein (1958), Mathey and Watstein (1960), Hognestad (1962), and Kaar and Mattock (1963).

As another illustration of the fracture approach to the formation of complete cracks, consider the cracking of the concrete cover associated with strain  $\epsilon_s$  in the concrete bar, shrinkage and temperature effects disregarded; Fig. 9.2b. For the sake of simplicity, consider two-dimensional action only. Formation of a complete crack relieves the initial strain energy density  $E\epsilon_s^2/2$  from volume  $V_1 = k h^2$  where  $V_1$  is the cross-hatched area shown in Fig. 9.2b, and  $k =$  some constant. Neglecting  $\Delta W_b$ , we must have  $\Delta U \geq \Delta W_f$  or  $G_f b h \leq (E\epsilon_s^2/2)V_1$ . Here we may substitute  $\epsilon_s = \delta_c/s$ . Furthermore, assuming the bar to be sufficiently strong, we know from the previous analysis of stability of a parallel crack system that the spacing of the open cracks will be  $s = k_1 h$  where  $k_1$  is some constant. Thus we obtain:

$$\delta_c \geq k_1 (2G_f b / k E)^{1/2} h^{1/2} \quad (9.14)$$

Eqs. 9.9 - 9.13 are interesting in that they rationalize the influence of the thickness  $b$  of concrete around the bar (or bar spacing) and the influence of the thickness of concrete cover. With regard to Eq. 9.13, one may recall the empirical formula established by extensive statistical analysis of test data by Gergely and Lutz (1968, see also Meier and Gergely, 1981), according to which the crack width  $\delta_c$  is roughly proportional to  $A_c^{1/3}$ . Since  $A_c$  is roughly proportional to  $h$ , this is only slightly different from Eq. 9.13. Under some more sophisticated assumptions, the proportionality of  $\delta_c$  to  $A_c^{1/3}$  can be obtained by fracture energy analysis (Bažant and Oh, 1983b, 1984).

The foregoing discussion makes it clear that various existing provisions regarding minimum reinforcement and crack width could be at least partially justified and probably also improved by the use of fracture mechanics.

#### 9.4 Interacting Microcracks

Modeling of the microcrack system in the fracture process zone helps in developing rational stress-displacement or stress-strain relations for the fracture process zone. In such models, it is important to take into account the interaction of individual microcracks. This interaction may lead to instabilities and localization of cracking.

Consider for example the idealized situation in Fig. 9.3. In the terminal phase of microcracking, two adjacent crack tips coalesce as the ligament between them is getting torn. This coalescence may be roughly modeled as the terminal propagation of a circumferential crack in a round bar (Fig. 9.3) while the radius of the circular ligament approaches zero. Based on the known solutions of the stress intensity factor for this problem, one can calculate the diagram of the applied remote stress vs. the displacement due to cracking; Fig. 9.3b. An interesting property of this diagram is that it possesses a maximum displacement after which there is a snapback instability.

It can be proven more generally that a maximum displacement with snapback instability must occur for every type of crack ligament tearing, provided the ligament transmits a force. On the other hand, if only a moment but no force is transmitted across the ligament, then no snapback occurs (Bažant, 1987b). Since the latter case is unlikely to prevail in the fracture process zone, it follows from this analysis that the stress-displacement (or stress-strain)

relations for the fracture process zone in nonlinear finite element analysis should exhibit a maximum displacement (or strain) at which the stress suddenly drops to zero. However, it is not certain whether this conclusion is also valid in the presence of friction and other inelastic phenomena.

A rather powerful approximate technique for considering interactions between randomly located cracks in a large body has recently been developed by Kachanov (1985, 1987); see also Benveniste, Dvorak, Zarzour and Wung (1988).

### CONCLUDING REMARKS

The present exposition of the state-of-the-art in concrete fracture concepts and determination of material properties reflects a tremendous surge in research activity in recent years and documents a large degree of progress which has been achieved over a relatively short span of time. While only about ten years ago the applicability of fracture mechanics to concrete structures was doubted, many experts now agree that fracture mechanics can have a considerable impact, improving the safety and economy of concrete structures and making new designs possible.

In three follow-up reports, ACI Committee 446 on Fracture Mechanics will attempt to review the state-of-the-art in applications of fracture mechanics to structural behavior, with a view toward potential code improvements, the state-of-the-art in finite element fracture analysis of concrete structures, and the state-of-the-art in modeling of the rate effects and dynamic fracture of concrete.

**Acknowledgment.** Thanks for help with compilation of the references and various revisions are due to J.-K. Kim, Y. Xi, M.R. Tabbara, and M.T. Kazemi (all graduate research assistants at Northwestern University).

## REFERENCES AND BIBLIOGRAPHY

1. ACI 226R-80: "Control of Cracking in Concrete Structures," reported by ACI Committee 226 (chaired by D. Darwin).
2. ACI 224.1R-84: "Causes, Evaluation and Repair of Cracks in Concrete Structures," Reported by ACI Committee 224 (chaired by D. Darwin).
3. Arrea, M., and Ingraffea, A. R., 1981, "Mixed-Mode Crack Propagation in Mortar and Concrete," Report 31-13, Cornell University, Ithaca.
4. ASTM, 1983, "Standard Test Method for Plane-Strain Fracture Toughness of Metallic Materials," Standard E399-83, Annual Book of ASTM Standards, V. 03.01, pp. 519-554.
5. Aveston, J., Cooper, G. A., and Kelly, A., 1971, "Single and Multiple Fracture," Proc. The Properties of Fiber Composites, National Physical Laboratory, Guildford, Surrey, U.K., IPC Science and Technology Press Ltd.
6. Barr, B., Hasso, A., and Khalifa, S., 1987, "A Study of Mode II Shear Fracture of Notched Beams, Cylinders and Cores," Proc., SEM-RILEM Int. Conf. on Fracture of Concrete and Rock, eds. Shah, S. P., and Swartz, S. E., Houston, pp. 370-382.
7. Barrenblatt, G. I., 1959, "The Formation of Equilibrium Cracks during Brittle Fracture, General Ideas and Hypothesis, Axially Symmetric Cracks," Prikl. Mat. Mekh., V. 23, No. 3, pp. 434-444.
8. Barrenblatt, G. I., 1962, "The Mathematical Theory of Equilibrium Cracks in Brittle Fracture," Advanced Appl. Mech., V. 7, pp. 55-129.
9. Batdorf, S. B., and Budianski, B., 1949, "A Mathematical Theory of Plasticity Based on the Concept of Slip," NACA Tech Note TN 1871.
10. Bažant, Z. P., 1976, "Instability, Ductility and Size Effect in Strain-Softening Concrete," J. of the Engng. Mech. Div., ASCE, V. 102, No. EM2, pp. 331-344.
11. Bažant, Z. P., 1982, "Crack Band Model for Fracture of Geomaterials," Proc., 4th Int. Conf. of Numer. Meth. in Geomech., ed. Eisenstein, Z., Edmonton, Alberta, V. 3, pp. 1137-1152.
12. Bažant, Z. P., 1983, "Comment on Orthotropic Models for Concrete and Geomaterials," J. Engng. Mech., ASCE, V. 109, No. 3, pp. 849-865.
13. Bažant, Z. P., 1984a, "Size Effect in Blunt Fracture: Concrete, Rock, Metal," J. Engng. Mech., ASCE, V. 110, No. 4, pp. 518-535.
14. Bažant, Z. P., 1984b, "Imbricate Continuum and Its Variational Derivation," J. Engng. Mech., ASCE, V. 110, No. 12, pp. 1693-1712.
15. Bažant, Z. P., 1985a, "Fracture Mechanics and Strain-Softening in Concrete," Preprints, U.S.-Japan Seminar on Finite Element Analysis of Reinforced Concrete Structures, Tokyo, V. 1, pp. 47-69.
16. Bažant, Z. P., 1985b, "Fracture in Concrete and Reinforced Concrete," in Mechanics of Geomaterials (Proc. of IUTAM Prager Symp. held at Northwestern Univ. in 1983), ed. Bažant, Z. P., John Wiley & Sons, Chichester and New York, pp. 259-303.
17. Bažant, Z. P., 1985c, "Mechanics of Fracture and Progressive Cracking in Concrete Structures," Chap 1 in Fracture Mechanics of Concrete: Structural Application and Numerical Calculation, ed. Sih, G.C., and Di Tommaso, A., Martinus-Nijhoff, Dordrecht-Boston, pp. 1-9.
18. Bažant, Z. P., 1986, "Mechanics of Distributed Cracking," Appl. Mech. Rev., ASME, V. 39, No. 5, pp. 675-705.
19. Bažant, Z. P., 1987a, "Fracture Energy of Heterogeneous Materials and Similitude," Proc. SEM-RILEM Int. Conf. on Fracture of Concrete and Rock, eds. Shah, S. P. and Swartz, S. E., Houston, pp. 390-402.
20. Bažant, Z. P., 1987b, "Snapback Instability at Crack Ligament Tearing and its Implication for Fracture Micromechanics," Cem. and Concr. Res., V. 17, No. 6, pp. 951-967.
21. Bažant, Z. P., 1988, "Stable States and Path of Structures with Plasticity or Damage," J. Eng. Mech., ASCE, V. 114, No. 12, pp. 2013-2034.
22. Bažant, Z. P., 1989a, "Identification of Strain-Softening Constitutive Equation from Specimens of Different Sizes," Cem. and Concr. Res., V. 19, pp. 973-977.
23. Bažant, Z. P., 1989b, "General Method for Determining Tangential Stiffness Matrix for Stability Analysis of Structures with Growing Interacting Cracks," Hillerborg's Anniversary Volume (Proc. of Conf. on Fracture of Concrete and Rock held in Lulea, Sweden, June 1989).
24. Bažant, Z. P., Belytschko, T. B., and Chang, T.-P., 1984, "Continuum Model for Strain-Softening," J. Engng. Mech., ASCE, V. 110, No. 12, pp. 1666-1692.
25. Bažant, Z. P., and Cao, Z., 1986a, "Size Effect in Brittle Failure of Unreinforced Pipes," ACI J., V. 83, pp. 365-373.
26. Bažant, Z. P., and Cao, Z., 1986b, "Size Effect in Shear Failure of Prestressed Concrete Beams," ACI J., V. 83, pp. 260-268.
27. Bažant, Z. P., and Cao, Z., 1987, "Size Effect in Punching Shear Failure of Slabs," ACI Struct. J., V. 84, pp. 44-53.
28. Bažant, Z. P., and Cedolin, L., 1979, "Blunt Crack Band Propagation in Finite Element Analysis," J. Engng. Mech. Div., ASCE, V. 105, No. EM2, Proc. Paper 14529, pp. 297-315.
29. Bažant, Z. P., and Cedolin, L., 1980, "Fracture Mechanics of Reinforced Concrete," J. Engng. Mech. Div., ASCE, V. 106, No. EM6, Proc. Paper 15917, pp. 1287-1306; with Discussion and Closure, V. 108, EM2, 1982, pp. 464-471.
30. Bažant, Z. P., and Cedolin, L., 1983, "Finite Element Modeling of Crack Band Propagation," J. Struct. Engng., ASCE, V. 109, No. ST2, pp. 69-92.

31. Bažant, Z. P., and Cedolin, L., 1984, "Approximate Linear Analysis of Concrete Fracture by R-curves," *J. Struct. Engng., ASCE*, V. 110, pp. 1336-1355.
32. Bažant, Z. P., and Cedolin, L., 1990, *Stability of Structures: Principles of Elastic, Inelastic and Damage Theories*, Oxford Univ. Press, New York, in press.
33. Bažant, Z. P., and Estenssoro, L. F., 1979, "Surface Singularity and Crack Propagation," *Int. J. of Solids and Struct.*, V. 15, pp. 405-426 (also V. 16, pp. 479-481.)
34. Bažant, Z. P., and Gambarova, P., 1980, "Rough Cracks in Reinforced Concrete," *J. of the Struct. Div., ASCE*, V. 106, No. ST4, pp. 819-842.
35. Bažant, Z. P., and Gambarova, R. G., 1984, "Crack Shear in Concrete: Crack Band Microplane Model," *J. of Engng. Mech., ASCE*, V. 110, pp. 2015-2035.
36. Bažant, Z. P., and Gettu, R., 1989, "Determination of Nonlinear Fracture Characteristics and Time-Dependence from Size-Effect," *Fracture of Concrete and Rock (Proc. of Int. Conf. on Recent Dev. in Fracture of Concrete held at Univ. of Wales, Cardiff, UK, Sept. 1989)*, eds. Shah, S. P., Swartz, S. E., and Barr, B., Elsevier, London pp. 549-565.
37. Bažant, Z. P.; Gettu, R.; and Kazemi, M. T., 1989, "Identification of Nonlinear Fracture Properties from Size Effect Tests and Structural Analysis Based on Geometry-Dependent R-curves," Report No. 89-3/498p, Center for Advanced Cement-Based Materials, Northwestern Univ., Evanston; submitted for publication, *Int. J. Rock Mech. Min. Sci.*, 1990.
38. Bažant, Z. P., and Kazemi, M.T., 1988, "Determination of Fracture Energy, Process Zone Length and Brittleness Number from Size Effect, with Application to Rock and Concrete," Report 88-7/498d Center for Concrete and Geomaterials, Northwestern Univ., Evanston; also *Int. J. of Fract.*, V. 44, 1990, pp. 111-131.
39. Bažant, Z. P., and Kazemi, M. T., 1989a, "Size Effect on Diagonal Shear Failure of Beams without Stirrups," Report No. 89-8/498S, Center for Advanced Cement-Based Materials, Northwestern Univ., Evanston.
40. Bažant, Z. P., and Kazemi, M. T., 1989b, "Size Dependence of Concrete Fracture Energy Determined by RILEM Work-of-Fracture Method," Report No. 89-12/B623s, Center for Advanced Cement-Based Materials, Northwestern Univ., Evanston; submitted to *Int. J. of Fract.*
41. Bažant, Z. P., Kazemi, M. T., Hasegawa, T., Mazars, J., 1991
42. Bažant, Z. P., and Kim, J. K., 1984, "Size Effect in Shear Failure of Longitudinally Reinforced Beams," *J. of ACI*, V. 81, No. 5, pp. 456-468; Discussion V. 82, No. 4, pp. 579-583.
43. Bažant, Z. P.; Kim, J. K.; and Pfeiffer, P. A., 1986, "Determination of Fracture Properties from Size Effect Tests," *J. of Struct. Engng., ASCE*, V. 112, No. 2, pp. 289-307.
44. Bažant, Z. P., Lee, S.-G., and Pfeiffer, P. A., 1987, "Size Effect Tests and Fracture Characteristics of Aluminum," *Engng. Fract. Mech.*, V. 26, No. 1, pp. 45-57.

45. Bažant, Z. P., and Lin, F.-B., 1988a, "Nonlocal Yield Limit Degradation," *Int. J. for Num. Meth. in Engng.*, V. 26, pp. 1805-1823.
46. Bažant, Z. P., and Lin, F.-B., 1988b, "Nonlocal Smeared Cracking Model for Concrete Fracture," *J. of Struct. Div., ASCE*, V. 114, No. 11, pp. 2493-2510.
47. Bažant, Z. P. and Oh, B.H., 1983a, "Crack Band Theory for Fracture of Concrete," *Mater. and Struct.*, V. 16, No. 93, pp. 155-177.
48. Bažant, Z. P., and Oh, B. H., 1983b, "Spacing of Cracks in Reinforced Concrete," *J. of Struct. Engng.*, V. 109, No. 9, pp. 2066-2085; see also "Crack Spacing in Reinforced Concrete: Approximate Solution," *J. of Struct. Engng.*, V. 109, No.9 pp. 2207-2212.
49. Bažant, Z. P., and Oh, B. H., 1984, "Deformations of Progressively Cracking Reinforced Concrete Beams," *ACI J.*, V. 81, No. 3, pp. 268-278.
50. Bažant, Z. P., and Oh, B. H., 1985, "Microplane Model for Progressive Fracture of Concrete and Rock," *J. of Engng. Mech., ASCE*, V. 111, pp. 559-582.
51. Bažant, Z. P., and Ohtsubo, H., 1977, "Stability Conditions for Propagation of a System of Cracks in a Brittle Solid," *Mechanics Research Communications*, V. 4, No. 5, pp. 353-366.
52. Bažant, Z. P., and Ohtsubo, R., 1978, "Geothermal Heat Extraction by Water Circulation Through a Large Crack in Dry Hot Rock Mass," *Int. J. for Num. and Anal. Meth. in Geomech.*, V. 2, pp. 317-327.
53. Bažant, Z. P., Ohtsubo, R., and Aoh, K., 1979, "Stability and Post-Critical Growth of a System of Cooling and Shrinkage Cracks," *Int. J. of Fract.*, V. 15, pp. 443-456.
54. Bažant, Z. P., and Ozbolt, J., 1989, "Nonlocal Microplane Model for Fracture, Damage and Size Effect in Structures," Report 89-10/498n, Center for Advanced Cement-Based Materials, Northwestern Univ., Evanston.
55. Bažant, Z. P., and Pfeiffer, P. A., 1985a, "Test of Shear Fracture and Strain-Softening in Concrete," 2nd Symposium on the Interaction of Non-Nuclear Munitions on Structures, Panama City Beach, FL, pp. 254-264.
56. Bažant, Z. P., and Pfeiffer, P.A., 1985b, "Comment on Ingraffea and Panthaki's Analysis of Shear Fracture Tests of Concrete," *Finite Element Analysis of Reinforced Concrete Structures*, Proc., US-Japan Seminar, ed. Meyer, C., and Okamura, M., held in Tokyo, ASCE, New York, pp. 174-183.
57. Bažant, Z. P., and Pfeiffer, P. A., 1986, "Shear Fracture Tests of Concrete," *Mater. and Struct.*, V. 19, No. 110, pp. 111-121.
58. Bažant, Z. P., and Pfeiffer, P. A., 1987, "Determination of Fracture Energy Properties from Size Effect and Brittleness Number," *ACI Mater. J.*, V. 84, No. 6, pp. 463-480.

59. Bažant, Z. P., and Pijaudier-Cabot, G., 1987, "Modeling of Distributed Damage by Nonlocal Continuum with Local Strain," Preprints, 4th Int. Conf. on Num. Meth. in Fract. Mech., eds. A. R. Luxmore, D. R. J. Owen, and M. F. Kanninen, held in San Antonio, Texas, pp. 441-432.
60. Bažant, Z. P., and Pijaudier-Cabot, G., 1988a, "Nonlocal Continuum Damage, Localization, Instability and Convergence," *J. of Appl. Mech.*, ASME, V. 55, pp. 287-293.
61. Bažant, Z. P., and Pijaudier-Cabot, G., 1988b, "Nonlocal Continuum Damage and Measurement of Characteristic Length," in *Mechanics of Composite Materials - 1988*, AMD 92, ed. G. J. Dvorak and N. Laws, Am. Soc. of Mech. Engrs., N.Y. (Joint ASME/SES Conf., Berkeley, CA), pp. 79-85.
62. Bažant, Z. P., and Pijaudier-Cabot, G., 1989, "Measurement of Characteristic Length of Nonlocal Continuum," *J. of Engng. Mech.*, ASCE, V. 115, No. 4, pp. 755-767.
63. Bažant, Z. P., and Prat, P. C., 1988a, "Measurement of Mode III Fracture Energy of Concrete," *Nuclear Engng. and Des.*, V. 106, pp. 1-8.
64. Bažant, Z. P., and Prat, P. C., 1988b, "Effect of Temperature and Humidity on Fracture Energy of Concrete," *ACI Mater. J.*, V. 84, pp. 262-271.
65. Bažant, Z. P., Prat, P. C., and Tabbara, M. R., 1988, "Antiplane Shear Fracture Tests (Mode III)," Report No. 88-6/498a, Center for Concrete and Geomaterials, Northwestern Univ., Evanston; also *ACI Mater. J.*, in press.
66. Bažant, Z. P., and Sener, S., 1988, "Size Effect in Pullout Tests," *ACI Mater. J.*, V. 85, pp. 347-351.
67. Bažant, Z. P.; Sener, S.; and Prat, P. C., 1988, "Size Effect Tests of Torsional Failure of Plain and Reinforced Concrete Beams," *Mater. and Struct.*, V. 21, pp. 425-430.
68. Bažant, Z. P., and Sun, H.-H., 1987, "Size Effect in Diagonal Shear Failure: Influence of Aggregate Size and Stirrups," *ACI Mater. J.*, V. 84, No. 4, pp. 259-272.
69. Bažant, Z. P., and Tabbara, M.R., 1989, "Bifurcation and Stability in Structures with Propagating Cracks," Parts I, II, Report, Dept. of Civil Engng., Northwestern Univ., Evanston.
70. Bažant, Z. P., Tabbara, M. R., Kazemi, M. T., and Pijaudier-Cabot, G., 1989, "Random Particle Model for Fracture of Aggregate or Fiber Composites, Report No. 89-7/498r, Center for Advanced Cement-Based Materials, Northwestern Univ., Evanston; also *J. of Engng. Mech.*, ASCE, V. 116, 1990, pp. 1686-1705.
71. Bažant, Z. P., and Wahab, A. B., 1978, "Instability and Spacing of Cooling or Shrinkage Cracks," *J. of the Engng. Mech. Div.*, ASCE, V. 105, pp. 873- 889.
72. Bažant, Z. P., and Wahab, A.B., 1980, "Stability of Parallel Cracks in Solids Reinforced by Bars," *Int. J. of Solids and Struct.*, V. 16, pp. 97- 105.
73. Bažant, Z.P., and Xu, K., 1989, "Size Effect in Fatigue Fracture of Concrete," Report No. 89-12/B627s, Center for Advanced Cement-Based Materials, Northwestern Univ., Evanston.

74. Belytschko, T., Fish, J., and Engelmann, B. E., 1988, "A Finite Element with Embedded Localization Zones," *Comp. Meth. in Appl. Mech. and Engng.*, V. 70, pp. 59-89, North-Holland.
75. Benveniste, Y., Dvorak, G. J., Zazour, J., and Wung, E. C. J., 1988, "On Interacting Cracks and Complex Crack Configurations in Linear Elastic Media," Report, Department of Civil Engineering, R.P.I., Troy, NY.
76. Bessendorff, M., and Chudnovsky, A., 1984, "The Crack Layer Approach to Toughness Characterization in Steel," *Proc., Int. Conf. on Fracture 6*, (held in New Delhi, India) eds. Valluri, S.R. et al., V. 6.
77. Brameshuber, W., 1988, "Fract. Mech. Properties of Young Concrete," (in German), Doctoral Dissertation, Universitat Karlsruhe, Germany.
78. Brameshuber, W., 1989, "Discussion of "Effect of Temperature and Humidity on Fracture Energy of Concrete," *ACI Mater. J.*, V. 86, pp. 330-331.
79. Bresler, B., and Wollack, E. (1952), "Shear Strength of Concrete," Report, Dept. of Civil Engng., University of California, Berkeley; presented at Annual Convention, Structural Engineers Association of California, held in Riverside, CA, Oct. 17, 1952.
80. Breyse, D., and Mazars, J., 1988, "Simplified Approach of Nonlinearity in R-C Beams," *J. of Struct. Engng.*, V. 114, No. 2, pp. 251-286.
81. Broek, D., 1982, "Elementary Engineering Fract. Mech.," 3rd ed., Martinus Nijhoff, Leyden, Netherlands, (also 4th ed., Martinus Nijhoff, Dordrecht, 1986.)
82. Bruhwiler, E., 1988, "Fract. Mech. of Dam Concrete Subjected to Quasi-Static and Seismic Loading Conditions," Laboratory for Building Materials (LMC), Swiss Federal Inst. of Tech., Lausanne, Thesis No. 739 (in German).
83. Bruhwiler, E., and Wittmann, F. H., 1989, "The Wedge Splitting Test, A Method of Performing Stable Fract. Mech. Test," Contribution to the Int. Conf. on Fracture and Damage of Concrete and Rock in Vienna 1988; *Engng. Fract. Mech.* (in press).
84. Burt, W. J., and Dougill, J. W., 1977, "Progressive Failure in a Model of Heterogeneous Medium," *J. of the Engng. Mech. Div.*, ASCE, V. 103, No. EM3, 365-376 pp.
85. Carpinteri, A., 1982, "Notch-Sensitivity and Fracture Testing of Aggregate Materials," *Engng. Fract. Mech.*, V. 16, No. 14, pp. 467-481.
86. Carpinteri, A., 1986, "Mechanical Damage and Crack Growth in Concrete," Martinus Nijhoff Publishers, Doordrecht.
87. Cedolin, L., Dei Poli, S., and Iori, I., 1987, "Tensile Behavior of Concrete," *J. of Engng. Mech. Div.*, ASCE, V. 113, No. 3, p. 431
88. Chana, P. S., 1981, "Some Aspects of Modeling the Behavior of Reinforced Concrete Under Shear Loading," Technical Report No. 543, Cement and Concrete Association, Wexham Springs, pp. 22.

89. Chi, M., and Kirstein, A. F., 1958, "Flexural Cracks in Reinforced Concrete Beams," *J. of the ACI, Proc.*, V. 54, No. 10, pp. 865-878.
90. Chudnovsky, A., 1986, "Crack Layer Theory", in 10th U.S. National Congress on Appl. Mech., Austin, Texas.
91. Clark, A. P., 1956, "Cracking in Reinforced Concrete Flexural Member," *J. of the ACI, Proc.*, V. 52, No. 8, pp. 851-862.
92. Clough, R. W., 1962, "Stress Distribution of Norfolk Dam," Department of Civil Engineering, Series 100, Issue 19, University of California, Berkeley.
93. Cope, R. J., 1984, "Material Modeling of Real, Reinforced Concrete Slabs," *Proc. of the Int. Conf. on Computer-Aided Analysis and Design of Concrete Structures*, held in Split, Yugoslavia, Part I, eds. Damjanić, F. et al., Pineridge Press, Swansea, U.K., 85-118 pp.
94. Crisfield, M. A. and Wills, J., 1989, "Analysis of R/C Panels using Different Concrete Models," *J. Engng. Mech., ASCE*, V. 115, No. 3, pp. 578-597.
95. Cundall, P. A., 1971, "A Computer Model for Simulating Progressive Large Scale Movements in Blocky Rock Systems," *Proc. of Int. Symp. on Rock Fracture, ISRM*, Nancy, France, pp. 2-8.
96. Cundall, P. A., and Strack, O. D. L., 1979, "A Discrete Numerical Model for Granular Subassemblies," *Geotechnique*, V. 29, pp. 47-65.
97. Darwin, D., 1985, "Concrete Crack Propagation - Study of Model Parameters," *Proc. Finite Element Analysis of Reinforced Concrete Structures*, eds. Meyer, C., and Okamura, H., ASCE, New York, pp. 184-203.
98. De Borst, R., 1984, "Application of Advanced Solution Techniques to Concrete Cracking and Non-Associated Plasticity," *Numerical Methods for Non-linear Problems*, eds. Taylor, C. et al., V. 2, Pineridge Press, Swansea, UK, pp. 314-325.
99. De Borst, R., 1987a, "Smearred cracking, Plasticity, Creep and Thermal Loading - A Unified Approach," *Comp. Meth. Appl. Mech. Engng.*, V. 62, pp. 89-110.
100. De Borst, R., 1987b, "Computation of Post-Bifurcation and Post-Failure Behavior of Strain-Softening Solids," *Comp. & Struct.*, V. 25, No. 2, pp. 211-224.
101. De Borst, R. and Nauta, P., 1985, "Non-Orthogonal Cracks in a Smearred Finite Element Model," *Engng. Computations*, V. 2, pp. 35-46.
102. Dharmarajan, N., and Vipulanandan, C., 1988, "Critical Stress Intensity Factor for Epoxy Mortar," *Polymer Engng. and Sci., Soc. of Plastic Engrs.*, V. 28, pp. 1182-1191.
103. Dougill, J. W., 1976, "On Stable Progressively Fracturing Solids," *J. Appl. Math. Phys. (ZAMP)*, V. 27, pp. 432-436.
104. Droz, P., 1987, "Modèle numérique du comportement non-linéaire d'ouvrages massifs en béton non armé", Doctoral Thesis, Ecole Polytechnique Fedarale de Lausanne, Switzerland.

105. Dugdale, D. S., 1960, "Yielding of Steel Sheets Containing Slits," *J. of Mech. and Phys. of Solids*, V. 8, pp. 100-108.
106. Dvorkin, E. N., Cuitino, A. M., and Gioia, G., 1989, "Finite Elements with Displacement Interpolated Embedded Localization Lines Insensitive to Mesh Size and Distortions," submitted to *Int. J. Num. Meth. in Engng.*
107. Elfgren, Z., 1989, ed., "Fract. Mech. of Concrete Structures," (Report of RILEM Techn. Committee TC 90-FMA), Chapman and Hall, London.
108. Eligehausen, and Ozbolt, J. (1990), 8th European Conference on Fracture, Torino - in press.
109. Eringen, A. C., and Edelen, D. G. B., 1972, "On Nonlocal Elasticity," *Int. J. Eng. Sci.*, V. 10, pp. 233-248.
110. Evans, A. G., 1974, "Slow Crack Growth in Brittle Materials under Dynamic Conditions," *Int. J. of Mech.*, V. 10, pp. 251-259.
111. Evans, R. H., and Marathe, M. S., 1968, "Microcracking and Stress-Strain Curves for Concrete in Tension," *Mater. and Struct.*, V. 1, pp. 61-64.
112. Gergely, P., and Lutz, L. A., 1968, "Maximum Crack Width in Reinforced Concrete Flexural Members", Causes, Mechanisms, and Control of Cracking in Concrete, SP-20, ACI, Detroit, pp. 87-117.
113. Gettu, R., Bazant, Z. P., and Karr, M.E., 1989, "Fracture Properties and Brittleness of High Strength Concrete," Report No. 89-10/B627f, Center for Advanced Cement-Based Materials, Northwestern Univ., Evanston; also *ACI Mater. J.*, in press, 1990.
114. Go, C. G., and Swartz, S. E., 1986, "Energy Methods for Fracture-Toughness Determination in Concrete," *Exp. Mech.*, V. 26, No. 3, pp. 292-296.
115. Go, C. G., Swartz, S. E., and Hu, K. K., 1984, "Stress Intensity Factors for Single Edge Notch Beam," Technical Note, *J. of Engng. Mech., ASCE*, V. 110, No. 4, pp. 629-632.
116. Gogotsi, G.A., Groushevsky, Y.L., and Strelov, K.K., 1978, "The Significance of Non-Elastic Deformation in the Fracture of Heterogeneous Ceramic Materials", *Ceramugia Int.*, U.K., V. 4, No. 3, pp. 113-118.
117. Gopalaratnam, V. S., and Shah, S. P., 1985, "Softening Response of Plain Concrete in Direct Tension," *J. of ACI*, V. 82.
118. Gopalaratnam, V. S., and Cheng, J., 1988, "On the Modeling of Inelastic Interfaces in Fibrous Composites," *Bonding in Cementitious Composites*, eds. Mindess, S., and Shah, S. P., *Mater. Res. Soc.*, Boston, V. 114, pp. 225-231.
119. Gopalaratnam, V. S., and Shah, S. P., 1987a, "Failure Mechanisms and Fracture of Fiber Reinforced Concrete," *Fiber Reinforced Concrete*, ACI SP - 105, eds. Shah, S. P., and Batson, G., pp. 1-25.

120. Gopalaratnam, V. S., and Shah, S. P., 1987b, "Tensile Failure of Steel Fiber-Reinforced Mortar," *J. of Engng. Mech., ASCE*, V. 113, No. 5, pp. 635- 652.
121. Griffith, A., 1921, "The Phenomenon of Rupture and Flow in Solids," *Phil. Trans. Royal Soc. of London, Series A*, V. 221, pp. 163-198.
122. Griffith, A., 1924, "Theory of Rupture," *Proc., 1st Int. Congress on Appl. Mech., Delft*, pp. 55-63.
123. Gupta, A. K., and Akbar, H., 1984, "Cracking in Reinforced Concrete Analysis," *J. of Struct. Engng., ASCE*, V. 110, No. 8, pp. 1735.
124. Gustafson, P. J., and Hillerborg, A., 1984, "Improvements in Concrete Design Achieved through the Application of Fract. Mech.," Preprints, NATO Advanced Research Workshop on Application of Fract. Mech. to Cementitious Composites, Northwestern Univ., Evanston, pp. 487-500.
125. Gustafson, P. J., and Hillerborg, A., 1988, "Sensitivity in Shear Strength of Longitudinally Reinforced Concrete Beams to Fracture Energy of Concrete," *ACI Struct. J.*, V. 85.
126. Hadamard, J., 1903, "Leçons sur la propagation des ondes," Chap VI, Hermann Paris.
127. Hasegawa, T., Shioya, T., and Okada, T., 1985, "Size Effect on Splitting Tensile Strength of Concrete," *Proc. Japan Concr. Inst. 7th Conf.*, pp. 309- 312.
128. Hassanzadeh, M., Hillerborg, A., and Ping, Z., 1987, "Tests of Material Properties in Mixed Mode I and II," *Proc., SEM-RILEM Int. Conf. on Fracture of Concrete and Rock*, eds. Shah, S. P., and Swartz, S. E., Houston, pp. 353- 358.
129. Hawkins, N.M., 1984, "The Role for Fracture Mechanics in Conventional Reinforced Concrete Design," NATO Advanced Research Workshop on Application of Fracture Mechanics to Cementitious Composites, September, Northwestern Univ. Evanston, IL.
130. Hellan, K., 1984, "Introduction to Fract. Mech.," McGraw Hill Co..
131. Hillemeier, B., and Hilsdorf, H. K., 1977, "Fract. Mech. Studies on Concrete Compounds," *Cem. and Concr. Res.*, V. 7, pp. 523-536.
132. Hillerborg, A., 1980, "Analysis of Fracture by Means of the Fictitious Crack Model, Particularly for Fiber Reinforced Concrete," *Int. J. of Cem. Compos- ites*, V. 2, No. 4, pp. 177-185.
133. Hillerborg, A., 1983, "Examples of Practical Results Achieved by Means of the Fictitious Crack Model," in Preprints, Prager Symp. on Mechanics of Geomaterials: Rocks, Concretes, Soils, ed. Bazant, Z. P., Northwestern Univ., Evanston, pp. 611-614.
134. Hillerborg, A., 1985a, "Numerical Methods to Simulate Softening and Fracture of Concrete," *Fract. Mech. of Concrete: Structural Application and Numerical Calculation*, eds. Sih, G. C., and DiTomasso, A., Martinus Nijhoff, Doordrecht-Boston, pp. 141-170.

135. Hillerborg, A., 1985b, "The Theoretical Basis of Method to Determine the Fracture Energy  $G_f$  of Concrete," *Mater. and Struct.* V. 18, No. 106, pp. 291-296
136. Hillerborg, A., 1985c, "Results of Three Comparative Test Series for Determining the Fracture Energy  $G_f$  of Concrete," *Mater. and Struct.*, V. 18, No. 107.
137. Hillerborg, A., Modeer, M., and Petersson, P. E., 1976, "Analysis of Crack Formation and Crack Growth in Concrete by Means of Fract. Mech. and Finite Elements," *Cem. and Concr. Res.*, V. 6, pp. 773-782.
138. Hognestad, E., 1962, "High Strength Bars as Concrete Reinforcement, Part 2. Control of Flexural Cracking," *J. of the PCA Research and Development Laboratories*, V. 4, No. 1, pp. 46-63.
139. Homeny, J., Darroudi, T., and Bradt, R.C., 1980, "J-Integral Measurements of the Fracture of 50% Alumina Refractories," *J. Am. Ceram. Soc.*, V. 63, No. 5- 6, pp. 326-331.
140. Horii, H., 1988, "Models of Fracture Process Zone and a System of Fract. Mech. for Concrete and Rock," *Proc., Int. Workshop on Fracture Toughness and Fracture Energy*, Sendai, Japan, pp. 325-337.
141. Horii, H., Hasegawa, A., and Nishino, F., 1989, "Fracture Process and Bridging Zone Model and Influencing Factors in Fracture of Concrete," in *Fracture of Concrete and Rock, SEM/RILEM Int. Conf.*, Houston, eds. Shah, S. P., and Swartz, S. E., Springer-Verlag, Berlin.
142. Horii, H., Shi, Z., and Gong, S.-X., 1988, "Models of Fracture Process Zone in Concrete, Rock, and Ceramics," in *Cracking and Damage, Proc. of France-US Workshop on Strain Localization and Size Effect*, Cachan, France, eds. Mazars, J., and Bazant, Z. P., Elsevier Applied Science, London, 1989.
143. Hughes, B. P., and Chapman, B. P., 1966, "The Complete Stress-Strain Curve for Concrete in Direct Tension," *RILEM (Paris) Bull.* No. 30, pp. 95-97.
144. Iguro, M., Shioya, T., Nojiri, Y., and Akiyama, H., 1985, "Experimental Studies on Shear Strength of Large Reinforced Concrete Beams under Uniformly Distributed Load," *Concrete Library Int.*, Japan Soc. of Civil Engrs., No. 5, pp. 137-154.
145. Inglis, C. E., 1913, "Stress in a Plate Due to the Presence of Cracks and Sharp Corners," *Tran. Inst. Naval Architects*, pp. 219-241.
146. Ingraffea, A.R., 1985, "Fracture Propagation in Rock," *Mechanics of Geomaterials: Rocks, Concretes, Soils*, ed. Bazant, Z. P., John Wiley and Sons, Inc., New York, N.Y., 219-258 pp.
147. Ingraffea, A. R., and Panthaki, M. J., 1985, "Shear Fracture Tests of Concrete Beams," *Finite Element Analysis of Reinforced Concrete Structures*, Tokyo, pp. 151-173.
148. Ingraffea, A. R., and Gerstle, W., 1985, "Nonlinear Fracture Models for Discrete Crack Propagation," *Application of Fract. Mech. to Cementitious Composites*, ed. Shah, S. P., Martinus Nijhoff, Publ., Doordrecht and Boston, pp. 171-209.

149. Ingraffea, A. R., and Saouma V., 1985, "Numerical Modeling of Discrete Crack Propagation in Reinforced and Plain Concrete," *Fract. Mech. of Concrete: Structural Application and Numerical Calculation*, eds. Sih, G. C., and DiTomasso, A., Martinus Nijhoff, Doordrecht-Boston, pp. 171-225.
150. Irwin, G.R., 1958, "Fracture," *Handbuch der Physik*, Vol. VI, ed. Flugge, Springer, pp. 551-590.
151. Jenq, Y. S., and Shah, S. P., 1985a, "A Fracture Toughness Criterion for Concrete," *Engng. Fract. Mech.*, V. 21, No. 5, pp. 1055-1069.
152. Jenq, Y. S., and Shah, S. P., 1985b, "Two Parameter Fracture Model for Concrete," *J. of Engng. Mech.*, ASCE, V. 111, No. 10, pp. 1227-1241.
153. Jenq, Y. S., and Shah, S. P., 1986, "Crack Propagation in Fiber Reinforced Concrete," *J. of Struc. Engng.*, ASCE, V. 112, No. 1, pp. 19-34.
154. Jenq, Y. S., and Shah, S. P., 1987a, "Fract. Mech. and Constitutive Modeling of Concrete," *Constitutive Laws for Engineering Materials: Theory and Applications*, ed. Desai, C. S. et al., Vol. II, Elsevier.
155. Jenq, Y. S., and Shah, S. P., 1987b, "Mixed Mode Fracture Parameters of Concrete," *Proc., SEM-RILEM Int. Conf. on Fracture of Concrete and Rock*, eds. Shah, S. P. and Swartz, S. E., Houston, pp. 359-369.
156. Jenq, Y. S., and Shah, S.P., 1988a, "Geometrical Effects on Mode I Fracture Parameters", Report to RILEM Committee 89-FMT.
157. Jenq, Y. S., and Shah, S. P., 1988b, "On the Concrete Fracture Testing Methods," *Preprints of the Proc., Int. Workshop on Fracture Toughness and Fracture Energy - Test Methods for Concrete and Rock*, Sendai, Japan.
158. John, R., and Shah, S. P., 1985, "Strain Rate Effects on Mode I Crack Propagation in Concrete," *Proc., Int. Conf. on Fract. Mech. of Concrete*, Lausanne.
159. John, R., and Shah, S. P., 1986, "Fracture of Concrete Subjected to Impact Loading," *Cem., Concr. and Aggregates*, ASTM.
160. John, R., and Shah, S. P., 1987, "Effect of High Strength and Rate of Loading on Fracture Parameters of Concrete," *Proc., SEM-RILEM Int. Conf. on Fracture of Concrete and Rock*, eds. Shah, S. P. and Swartz, S. E., Houston, pp. 35-52.
161. John, R., and Shah, S. P., 1989a, "Mixed Mode Fracture of Concrete Subjected to Impact Loading," *J. of Struct. Engng.*, ASCE, Mar. 1990, in press.
162. John, R., and Shah, S. P., 1989b, "Fract. Mech. Analysis of High Strength Concrete," *J. of Mater. in Civil Engng.*, ASCE, V. 1, No. 4, pp. 185-198.
163. John, R., Shah, S. P., and Jenq, Y. S., 1987, "A Fract. Mech. Model to Predict the Rate Sensitivity of Mode I Fracture of Concrete," *Cem. and Concr. Res.*

164. Karr, P. H., and Mattock, A. H., 1963, "High Strength Bars as Concrete Reinforcement, Part 4, Control of Cracking," *J. of the PCA Research and Development*, V. 5, No. 1, pp. 15-38.
165. Kachanov, M., 1985, "A Simple Technique of Stress Analysis in Elastic Solids with Many Cracks," *Int. J. of Fract.*, V. 28, R11-R19.
166. Kachanov, M., 1987, "Elastic Solids with Many Cracks: A Simple Method of Analysis," *Int. J. of Solids and Struct.*, V. 23, No. 1, pp. 23-43.
167. Kanninen, M. F., and Popelar, C. H., 1985, "Advanced Fract. Mech.," Oxford Univ. Press, Inc.
168. Kaplan, M. F., 1961, "Crack Propagation and the Fracture of Concrete," *ACI J.*, V. 58, No. 11.
169. Karihaloo, B. L., and Nallathambi, P., 1987, "Notched Beam Test: Mode I Fracture Toughness," draft report to RILEM Committee 89-FMT, *Fract. Mech. of Concrete: Test Method*, 1987.
170. Kawai, T., 1980, "Some Considerations on the Finite Element Method," *Int. J. Numer. Meth. Engng.*, V. 16, pp. 81-120.
171. Kesler, C. E.; Naus, D. J.; and Lott, J. L., 1971, "Fract. Mech.-Its Applicability to Concrete," *Proc., Int. Conf. on the Mechanical Behavior of Materials*, Kyoto, The Soc. of Mater. Sci., Vol. IV, 1972, pp. 113-124.
172. Kfoury, A. P., and Miller, K. J., 1974, "Stress Displacement, Line Integral and Closure Energy Determinations of Crack Tip Stress Intensity Factors," *Int. J. Pressure Vessel Piping*, V. 2, No. 3, pp. 179-191.
173. Knauss, W. C., 1974, "On the Steady Propagation of a Crack in a Viscoelastic Sheet; Experiments and Analysis," *The Deformation in Fracture High Polymers*, ed. H. H. Kausch, Plenum Press, pp. 501-541.
174. Knott, J. F., 1973, "Fundamentals of Fract. Mech.," Butterworths, London, UK.
175. Kraft, J. M., Sullivan, A. M., and Boyle, R. W., 1961, "Effect of Dimensions on Fast Fracture Instability of Notched Sheets, Crack Propagation Symp., Proc., U.K.
176. Krner, E., 1967, "Elasticity Theory of Materials with Long-Range Cohesive Forces," *Int. J. of Solids and Struct.*, No. 3, pp. 731-742.
177. Krumhansl, J. A., 1968, "Some Considerations of the Relation between Solid State Physics and Generalized Continuum Mechanics," *Mechanics of Generalized Continua*, ed. Krner, E., Springer, Berlin, pp. 330-340.
178. Kunin, I. A., 1968, "The Theory of Elastic Media with Microstructure and the Theory of Dislocations," *Mechanics of Generalized Continua*, ed. Krner, E., Springer, Berlin, pp. 330-340.

179. Labuz, J. F., Shah, S. P., and Dowding, C. H., 1985, "Experimental Analysis of Crack Propagation in Granite," *Int. J. of Rock Mech. and Min. Sci.*, V. 22, No. 2, pp. 85-98.
180. Lawrence, P., 1972, "Some Theoretical Considerations of Fibre Pull-Out from an Elastic Matrix," *J. of Mat. Sci.*, V. 7, pp. 1-6.
181. Laws, V., Lawrence, P., and Nurse, R. W., 1972, "Reinforcement of Brittle Matrices by Glass Fibers," *J. of Phys. D: Appl. Phys.*, V. 6, pp. 523-537.
182. Leibengood, L. D., Darwin, D., and Dodds, R. H., 1986, "Parameters Affecting FE Analysis of Concrete Structures," *J. Struct. Engng.*, V. 112, No. 2, pp. 326-341.
183. Leroy, Y. and Ortiz, M., 1989, "Finite Element Analysis of Strain Localization in Frictional Materials," *Int. J. Numer. Anal. Meth. Geomech.*, V. 13, pp. 53-74.
184. Lin, C. S., and Scordelis, A. C., 1975, "Nonlinear Analysis of RC Shells of General Forms," *J. Struct. Div., ASCE*, V. 101, pp. 523-538.
185. Linsbauer, H. N., and Tschegg, E. K., 1986, "Fracture Energy Determination of Concrete with Cube-Shaped Specimens," *Zement und Beton*, V. 32, pp. 38-40 (in German).
186. L'Hermite, R., 1959, "What do we Know About the Plastic Deformation and Creep of Concrete?," *RILEM Bull.*, No. 1, pp. 22-51.
187. Maji, A. K., and Shah, S. P., 1988, "Process Zone and Acoustic Emission Measurement in Concrete," *Exp. Mech.*, V. 28, pp. 27-33.
188. Marti, P., 1989, "Size Effect in Double-Punch Tests on Concrete Cylinders," *ACI Mater. J.*, V. 86, No. 6, pp. 597-601.
189. Mathey, R. G., and Watstein, D., 1960, "Effect of Tensile Properties of Reinforcement on the Flexural Characteristics of Beams," *J. of the ACI, Proc.*, V. 56, No. 12, pp. 1253-73.
190. Maturana, P., Planas, J., and Elices, M., 1988, "Evaluation of Fracture Behavior of Saturated Concrete in the Low Temperature Range," in *Fracture and Damage of Concrete and Rock*, ed. Rossmannith, P., *Int. Conf.*, Vienna.
191. Meier, S. W., and Gergely, P., 1981, "Flexural Crack Width in Prestressed Concrete Beams," *J. of the Struct. Div., ASCE*, V. 107, No. ST2, pp. 429-433.
192. Mihashi, H., and Zaitsev, J. W., 1981, "Statistical Nature of Crack Propagation," Section 4-2 in *Report to RILEM TC 50 - FMC*, ed. Wittmann, F. H.
193. Miller, R. A.; Shah, S. P.; and Bjelkhagen, H. I., 1988, "Crack Profiles in Mortar Measured by Holographic Interferometry," *Exp. Mech.*, V. 28, No. 4, pp. 338-394.
194. Mindess, S., 1983, "The Fracture of Fibre Reinforced and Polymer Impregnated Concretes: A Review," *Fract. Mech. of Concrete*, ed. Wittmann, F.H., Elsevier Science Publishers, Amsterdam, The Netherlands, pp. 481-501.

195. Mindess, S., 1984, "Rate of Loading Effects on the Fracture of Cementitious Materials," *Preprints, Applications of Fract. Mech. to Cementitious Composites*, NATO-ARW, ed. Shah, S. P., Northwestern Univ..
196. Mobasher, B., Ouyang, C., and Shah, S. P., 1989, "A R-Curve Approach to Predict Toughening of Cement-Based Matrices due to Fiber Reinforcement," submitted for publication; see also Mobasher, B., Ph.D. Thesis, Northwestern Univ., 1989.
197. Mobasher, B., and Shah, S. P., 1989, "Interaction Between Fibers and the Cement Matrix in Glass Fiber Reinforced Concrete," to be published, *ACI Special Volume*.
198. Mobasher, B., Stang, H., and Shah, S. P., 1989, "Microcracking in Fiber Reinforced Concrete," Accepted for publication, *Cem. and Concr. Res.*
199. Morrison, J. K., Shah, S. P., and Jenq, Y. S., 1988, "Analysis of the Debonding and Pull-Out Process in Fiber Composites," *J. of Engng. Mech., ASCE*, V. 114, No. 2, pp. 277-294.
200. Murakami, Y., 1987, editor-in-chief, "Stress Intensity Factors Handbook," Pergamon Press, Oxford.
201. Nakayama, J., 1965, "Direct Measurement of Fracture Energies of Brittle Heterogeneous Material," *J. of the Amer. Ceram. Soc.*, V. 48, No. 11.
202. Nallathambi, P., and Karihaloo, B. L., 1986a, "Determination of Specimen- Size Independent Fracture Toughness of Plain Concrete," *Mag. of Concr. Res.*, V. 38, No. 135, pp. 67-76.
203. Nallathambi, P., and Karihaloo, B. L., 1986b, "Stress Intensity Factor and Energy Release Rate for Three-Point Bend Specimen," *Engng. Fract. Mech.*, V. 25, No. 3, pp. 315-321.
204. Naus, D. J., and Lott, J. L., 1969, "Fracture Toughness of Portland Cement Concretes," *ACI J.*, V. 66, pp. 481-498.
205. Ngo, D., and Skordelis, A. C., 1967, "Finite Element Analysis of Reinforced Concrete Beams," *ACI Journal*, V. 64, No. 3, pp. 152-163.
206. Ortiz, M., 1988, "Extraction of Constitutive Data from Specimens Undergoing Localization," submitted to *J. of Engng. Mech., ASCE*.
207. Ortiz, M., Leroy, Y., and Needleman, A., 1987, "A Finite Element Method for Localized Failure Analysis," *Comp. Meth. Appl. Mech. Engr.*, V. 61, pp. 189-224.
208. Ottosen, N. S., and Dahlblom, O., 1986, "Smearred Crack Analysis Using a Nonlinear Fracture Model for Concrete," *Numerical Methods for Nonlinear Problems 3*, eds. Taylor, C. et al., Pineridge Press Ltd., Swansea, U.K., pp. 363-367.
209. Owen, D. R. J., and Fawkes, A. J., 1983, "Engineering Fract. Mech.: Numerical Methods and Application," Pineridge Press Ltd., Swansea, U.K.
210. Paris, P., and Erdogan, F., 1967, "A Critical Analysis of Crack Propagation Laws," *J. of Basic Engng.*, V. 87, pp. 528-534.

211. Perdikaris, P. C., and Calomino, A. M., 1987, "Kinetics of Crack Growth in Plain Concrete," Preprints, SEM/RILEM Int. Conf. on Fracture of Concrete and Rock, Houston, eds. Shah, S. P. and Swartz, S. E..
212. Petersson, P. E., 1980a, "Fracture Energy of Concrete: Method of Determination," *Cem. Concr. Res.*, V. 10, 1980, pp. 78-79; "Fracture Energy of Concrete, Practical Performance and Experimental Results," *Cem. Concr. Res.* V. 10, pp. 91-101.
213. Petersson, P.E., 1980b, "Fracture Mechanical Calculations and Tests for Fiber-Reinforced Concrete," Proc., *Advances in Cement Matrix Composites*, Mater. Res. Soc. Annual Meeting, Boston, pp. 95-106.
214. Petersson, P. E., 1981, "Crack Growth and Development of Fracture Zones in Plain Concrete and Similar Materials," Report TVBM-1006, Div. of Building Materials, Lund Inst. of Tech., Lund, Sweden.
215. Phillips, D. V., and Zienkiewicz, O. C., 1973, "Nonlinear Analyses of Structural Concrete by Finite Element Methods," Ph.D. Thesis, Univ. of Wales, Swansea, UK.
216. Phillips, D. V., and Zienkiewicz, O. C., 1976, "Finite Element Non-Linear Analysis of Concrete Structures," *Proc. Instn. Civ. Engrs.*, Part 1, V. 61, pp. 59-88.
217. Pietruszczak, S., and Mr'z, Z., 1981, "Finite Element Analysis of Deformation of Strain-Softening Materials," *Int. J. of Numer. Meth. of Engng.*, V. 17, pp. 327-334.
218. Pijaudier-Cabot, G., and Bažant, Z. P., 1987, "Nonlocal Damage Theory," *J. of Engng. Mech.*, ASCE, V. 113, No. 110, pp. 1512-1533.
219. Pijaudier-Cabot, G., and Bažant, Z. P., 1988, "Dynamic Stability Analysis with Nonlocal Damage," *Comp. & Struct.*, V. 29, No.3, pp. 503-507.
220. Pijaudier-Cabot, G., and Mazars, J., 1989, "Continuum Damage Theory Application to Concrete," *J. of Engng. Mech.*, ASCE, V. 115, No. 2, pp. 345- 368.
221. Pijaudier-Cabot, G., Mazars, J., and Polikowski, J., 1989, "Steel-Concrete Bond Analysis with Nonlocal Continuous Damage," Internal Report No. 96, Lab. of Mech. & Technology, Ecole Normal Supérieur, Cachan, France.
222. Planas, J., and Elices, M., 1988a, "Size-Effect in Concrete Structures: Mathematical Approximations and Experimental Validation," *Cracking and Damage, Strain Localization and Size Effect*, Proc. of France-U.S. Workshop, Cachan, France, eds. Mazars, J. and Bažant, Z. P., pp. 462-476.
223. Planas, J., and Elices, M., 1988b, "Conceptual and Experimental Problems in the Determination of the Fracture Energy of Concrete," Proc., Int. Workshop on "Fracture Toughness and Fracture Energy, Test Methods for Concrete and Rock," Tohoku Univ., Sendai, Japan, pp. 203-212.

224. Planas, J., Elices, M., and Toribio, J., 1989, "Approximation of Cohesive Crack Models by R-CTOD Curves," *Fracture of Concrete and Rock: Recent Developments*, eds. Shah, S. P., Swartz, S. E., and Barr, B., (Int. Conf. held at Cardiff, U.K.), Elsevier, London, pp. 203-212.
225. Plesha, M. E., and Aifantis, E. C., 1983, "On the Modeling of Rocks with Microstructure," Proc., 24th U.S. Symp. on Rock Mechanics, Texas A&M Univ., College Station, pp. 27-39.
226. Rashid, Y. R., 1968, "Analysis of Prestressed Concrete Pressure Vessels," *Nuclear Engng. and Des.*, V. 7, No. 4, pp. 334-355.
227. Read, H. E., and Hegemier, G. P., 1984, "Strain-Softening of Rock, Soil and Concrete - a Review Article," *Mech. and Mater.*, V. 3, pp. 271-294.
228. Refai, T. M. E., and Swartz, S. E., 1987, "Fracture Behavior of Concrete Beams in Three-Point Bending Considering the Influence of Size Effects," Report No. 190, Engineering Experiment Station, State Univ., Manhattan.
229. Refai, T. M. E., and Swartz, S. E., 1988, "Mode I Fracture Energy Measurements for Concrete," *Exp. Mech.*, V. 28.
230. Reinhardt, H. W. 1981a, "Size Effect in Shear Tests in the Light of Fract. Mech." (in German), *Beton-und Stahlbetonbau (West Berlin)* No. 1, pp. 19-21.
231. Reinhardt, H. W. 1981b, "Similitude of Brittle Fracture of Structural Concrete," *Advanced Mech. of Reinforced Concrete*, IABSE Colloquium, Delft, pp. 69-92.
232. Reinhardt, H. W., 1984, "Tensile Fracture of Concrete at High Rates of Loading," Preprints, *Application of Fract. Mech. to Cementitious Composites*, NATO-ARW, ed. Shah, S. P., Northwestern Univ., Evanston,.
233. Reinhardt, H. W., and Cornelissen, H. A. W., 1984, "Post-peak Cyclic Behavior of Concrete in Uniaxial Tensile and Alternating Tensile and Compressive Loading," *Cem. Concr. Res.*, V. 14, No. 2, pp. 263-270.
234. Reinhardt, H., Cornelissen, H., and Hordijk, D., 1987, "Mixed Mode Fracture Tests on Concrete," *Fracture of Concrete and Rock*, eds. Shah, S. P., and Swartz, S. E., (Int. Conf. held in Houston), Springer-Verlag, N.Y., 1989, pp. 117-130.
235. RILEM, 1985-TC 50-FMC, *Fract. Mech. of Concrete*, "Determination of the Fracture Energy of Mortar and Concrete by Means of Three-Point Bend Tests on Notched Beams," RILEM Recommendation, *Mater. and Struct.*, V. 18, No. 106.
236. Roelfstra, P.E., Sadouki, H., and Wittmann, F.H., 1985, "Le Beton Numerique," *Mater. and Struct.*, V. 107.
237. Roelfstra, P.E., 1987, "Numerical Analysis and Simulation of Crack Formation in Composite Materials such as Concrete," in *Fracture of Non-Metallic Materials*, eds. Herman, K. P, and Larsson, L. H., ECSC, EEC, EAEC, Brussels and Luxembourg, pp. 358-384.

238. Romualdi, J. P., and Batson, G. B., 1963, "Mechanics of Crack Arrest in Concrete," *J. of Engng. Mech.*, ASCE, V. 89, No. EM3, pp. 147-168.
239. Romualdi, J. P. and Mandel, J. A., 1964, "Tensile Strength of Concrete Affected by Uniformly Distributed Closely Spaced Short Lengths of Wire Reinforcement," *ACI J.*, V. 61, No. 6, pp. 657-670.
240. Rots, J. G., 1988, "Stress Rotation and Stress Locking in Smeared Analysis of Separation," *Proc., Int. Workshop on "Fracture Toughness and Fracture Energy, Test Methods for Concrete and Rock,"* Tohoku Univ., Sendai, Japan.
241. Rots, J. G., and Blaauwendraad, J., 1989, "Crack Models for Concrete: Discrete or Smeared? Fixed, Multi-Directional or Rotating," *HERON*, V. 34, No. 1.
242. Rots, J. G., and de Borst, R., 1987, "Analysis of Mixed-Mode Fracture in Concrete," *J. of Engng. Mech.*, ASCE, V. 113, No. 11, pp. 1739-1758.
243. Rots, J. G., Nauta, P., Kusters, G. M. A., and Blaauwendraad, J., 1985, "Smeared Crack Approach and Fracture Localization in Concrete," *HERON*, V. 30, No. 1.
244. Rusch, H., and Hilsdorf, H., 1963, "Deformation Characteristics of Concrete under Axial Tension," *Voruntersuchungen*, Munich, Bericht 44.
245. Sahudin, A.H., 1987, "Nonlinear Finite Element Study of Axisymmetric Fiber Pull-Out," M.S. Thesis, Univ. of Missouri-Columbia, pp. 110.
246. Saouma, V. E., Ingraffea, A. R., and Catalano, D. M., 1982, "Fracture Toughness of Concrete: K Revisited," *J. of Engng. Mech. Div.*, V. 108, No. EM6, pp. 1152-1166.
247. Sandler, I. S., 1986, "Strain-Softening for Static and Dynamic Problems," in *Proc. of Symp. on Constitutive Equations: Micro, Macro and Computational Aspects*, ASME Winter Annual Meet., New Orleans, ed. William, K., ASME, N.Y., pp. 217-231.
248. Saouridis, C., 1989, *Doctoral Thesis on Damage Analysis in Concrete*, Lab of Mechanics and Technology, Ecole Normal Sup rieur, Cachan, France.
249. Saouma, V. E., Broz, J. J., Brühwiler, E., and Boggs, H., 1989, "Fracture Properties of Dam Concrete. Part I: Laboratory Experiments," submitted to *J. of Mater. in Civil Engng.*, ASCE.
250. Scanlon, A., 1971, "Time Dependent Deflections of Reinforced Concrete Slabs," *Doctoral Thesis*, Univ. of Alberta, Edmonton, Canada.
251. Schreyer, H. L., and Chen, Z., 1986, "One Dimensional Softening with Localization," *J. of Appl. Mech.*, V. 53, pp. 791-797.
252. Serrano, A.A., and Rodriguez-Ortiz, J.M., 1973, "A Contribution to the Mechanics of Heterogeneous Granular Media," *Proc., Symp. on Plasticity and Soil Mech.*, Cambridge, U.K.
253. Shah, S. P., 1988, "Fracture Toughness of Cement Based Materials," *Mater. and Struct.*, V. 21, pp. 145-150.

254. Shah, S. P., and McGarry, F. J., 1971, "Griffith Fracture Criterion and Concrete," *J. of the Engng. Mech. Div.*, ASCE, Vo9l. 97, No. EM6, pp. 1663- 1676.
255. Shah, S. P., and Sankar, R., 1987, "Internal Cracking and Strain-Softening Response of Concrete under Uniaxial Compression," *ACI Mater. J.*, V. 84, pp.200-212.
256. Stang, H., Mobasher, B., and Shah, S. P., 1989, "Quantitative Damage Characterization in Polypropylene Fiber Reinforced Concrete," Accepted for publication, *Cem. and Concr. Res.*
257. Stang, H., and Shah, S. P., 1986, "Failure of Fiber Reinforced Composites by Pull-Out Fracture," *J. of Mat. Sci.*, V. 21, No. 3, pp. 935-957.
258. Stang, H., and Shah, S. P., 1989, "Damage Evolution in FRC Materials Modelling and Experimental Observation," *Fiber Reinforced Cements and Concretes, Recent Developments*, eds. Swamy, R. N., and Barr, B., Elsevier Applied Science, pp. 378-387.
259. Suidan, M., and Schnobrich, W. C., 1973, "Finite Element Analysis of Reinforced Concrete," *J. of Struct. Engng.*, ASCE V. 99, No. 10, pp. 2109- 2122.
260. Sulem, J., and Vardoulakis, I., 1989, "Bifurcation Analysis of the Triaxial Test on Rock Specimens," *Cracking and Damage, Proc., France-US Workshop on Strain Localization and Size Effect due to Cracking and Damage*, (held at Cachan, France, Sep., 1988), eds. Mazars, J., and Bažant, Z.P., Elsevier Applied Science, London, pp. 308-322.
261. Swartz, S. E. and Go, C. G., 1984, "Validity of Compliance Calibration to Cracked Concrete Beams in Bending," *Exp. Mech.*, V. 24, No. 2, pp. 129-134.
262. Swartz, S. E., Hu, K. K., and Jones, G. L., 1978, "Compliance Monitoring of Crack Growth in Concrete," *J. of the Engng. Mech. Div.*, ASCE, V. 104, No. EM4, pp. 789-800.
263. Swartz, S. E., Hu, K. K., Fartash, M., and Huang, C. M. J., 1982, "Stress Intensity Factors for Plain Concrete in Bending - Prenotched Versus Precracked Beams," *Exp. Mech.*, V. 22, No. 11, pp. 412-417.
264. Swartz, S. E., Huang, J., and Hu, K. K., 1982, "Crack Growth and Fracture in Plain Concrete - Static vs. Fatigue Loading," in *Fatigue of Concrete Structures*, ed. Shah, S. P., ACI SP-75, pp. 7-20.
265. Swartz, S. E., Lu, L. W., and Tang, L. D., 1988, "Mixed-Mode Fracture Toughness Testing of Concrete Beams in Three-Point Bending," *Mater. and Struct.*, V. 21, pp. 33-40.
266. Swartz, S. E., Lu, L. W., Tang, L. D., and Refai, T. M. E., 1988, "Mode II Fracture Parameter Estimates for Concrete from Beam Specimens," *Exp. Mech.*, V. 28, No. 2, pp. 146-153.
267. Swartz, S. E., and Refai, T. M. E., 1989, "Influence of Size Effects on Opening Mode Fracture Parameters for Precracked Concrete Beams in Bending," *Fracture of Concrete and Rock*, eds. Shah, S. P., and Swartz, S. E., SEM- RILEM Int. Conf., Houston, 1987, Springer-Verlag, pp. 242-254.
268. Swartz, S. E., and Taha, N. M., 1987, "Preliminary Investigation of the Suitability of the Iosipescu Test Specimen for Determining Mixed Mode Fracture Properties of Concrete," Report No. 191, Engineering Experiment Station, Kansas State Univ., Manhattan.

269. Swartz, S. E., and Yap, S. T., 1988, "The Influence of Dead Load on Fracture Energy Measurements Using the RILEM Method," *Mater. and Struct.*, V. 21, pp. 410-415.
270. Swenson, D. V., 1986, "Modeling Mixed-Mode Dynamic Crack Propagation Using Finite Elements," Department of Struct. Engng., Report No. 85-10, Cornell Univ., Ithaca.
271. Tada, H., Paris, P. C., and Irwin, 1985, "The Stress Analysis of Cracks Handbook 2nd ed., Paris Productions, St. Louis.
272. Tattersall, H. G., and Tappin, G., 1966, "The Work of Fracture and its Measurement in Metals, Ceramics and Other Materials," *J. of Mater. Sci.*, V. 1, No. 3, pp. 296-301.
273. Taylor, G. I., 1938, "Plastic Strain in Metals," *J. of the Inst. of Metals*, London, UK, V. 62, pp. 307-324.
274. Taylor, H. P. J., 1972, "The Shear Strength of Large Beams," *J. of Struct. Engng.*, ASCE, pp. 2473-2490.
275. Thomas, T. Y., 1961, "Plastic Flow and Fracture in Solids," Academic, New York.
276. van Mier, J. G. M., 1984, "Strain-Softening of Concrete under Multiaxial Loading Conditions," Doctoral Thesis, Delft Univ. of Technology, The Netherlands.
277. van Mier, J. G. M., 1986, "Multiaxial Strain-Softening of Concrete; Part I: Fracture, Part II: Load Histories," *Mater. and Struct.*, V. 111, No. 19, pp. 179-200.
278. Vipulanandan, C., and Dharmarajan, N., 1987, "Fracture Properties of Epoxy Polymer Concrete," eds. Shah, S. P., and Swartz, S. E., SEM-RILEM Int. Conf. on Fracture of Concrete and Rock, Houston, pp. 668-678.
279. Vipulanandan, C., and Dharmarajan, N., 1988, "Effect of Temperature on the Fracture Properties of Epoxy Polymer Concrete," *Cem. and Conc. Res.*, V. 18, No. 2, pp. 265-276.
280. Vipulanandan, C., and Dharmarajan, N., 1989a, "Critical Crack Tip Opening Displacement for Polymer Composites," *Engng. Fract. Mech.*, V. 33, No. 3, pp. 409-420.
281. Vipulanandan, C., and Dharmarajan, N., 1989b, "Analysis of Fracture Parameters of Epoxy Polymer Concrete," *ACI Material J.*, V. 86, No. 4, pp. 409-420.
282. Vipulanandan, C., and Dharmarajan, N., 1989c, "Influence of Aggregate on the Fracture Properties of Polyester Polymer Concrete," *ACI Special Publication (SP-116)*.
283. Visalvanich, K., and Naaman, A. E., 1982, "Fracture Model for Fiber Reinforced Concrete," *ACI J.*, V. 80, No. 2, pp. 128-138.
284. Walsh, P. F., 1972, "Fracture of Plain Concrete," *Indian Concr. J.*, V. 46, No. 11.
285. Walsh, P. F., 1976, "Crack Initiation in Plain Concrete," *Mag. of Concr. Res.* V. 28, pp. 37-41.
286. Wecharatana, M., and Shah, S. P., 1980, "Double Torsion Tests for Studying Slow Crack Growth of Portland Cement Mortar," *Cem. and Conc. Res.*, V. 10, pp. 833-844.

287. Wecharatana, M., and Shah, S. P., 1982, "Slow Crack Growth in Cement Composites," *J. of the Struct. Div.*, ASCE, V. 108, No. 6, pp. 1400-1413.
288. Wecharatana, M. and Shah, S. P., 1983a, "Predictions of Nonlinear Fracture Process Zone in Concrete," *J. Engng. Mech.*, V. 109, No. 5, pp. 1231-1246.
289. Wecharatana, M., and Shah, S. P., 1983b, "A Model for Predicting Fracture Resistance of Fiber Reinforced Concrete," *Cem. and Conc. Res.*, V. 13, No. 6, pp. 819-829.
290. Weibull, W., 1939, "Phenomenon of Rupture in Solids," *Ingenioersvetenskap- sakad Handl.*, V. 153, pp. 1-55.
291. Willam, K. J., Bicanic, N., and Sture, S., 1985, "Experimental, Constitutive and Computational Aspects of Concrete Failure," U.S.-Japan Seminar on Finite Element Analysis of Reinforced Concrete, pp. 149-172.
292. Willam, K. J., Bicanic, N., Pramono, E., and Sture, S., 1986, "Composite Fracture Model for Strain-Softening Computations of Concrete," in "Fracture Toughness and Fracture Energy of Concrete," ed. Wittmann, F. H., Elsevier, New York, pp. 149-162.
293. Willam K., Pramono, E., and Sture, S., 1987, "Fundamental Issues of Smeared Crack Models," *Proc. SEM-RILEM Int. Conf. on Fracture of Concrete and Rock*, eds. Shah, S. P., and Swartz, S. E., SEM, Bethel, pp. 192-207.
294. Wittmann, F. H., ed., 1983, "Fract. Mech. of Concrete," Elsevier, Amsterdam.
295. Wittmann, F.H., Roelfstra, P.E., and Sadouki, H., 1984, "Simulation and Analysis of Composite Structures," *Mater. Sci. and Engng.*, V. 68, pp. 239-248.
296. Wittmann, F.H., Roelfstra, P.E., Mihashi, H., Huang, Y.-Y., Zhang, X.-H., and Nomura, N., 1987, "Influence of Age of Loading, Water-Cement Ratio and Rate of Loading on Fracture Energy of Concrete," *Mater. and Struct.*, V. 20, pp. 103-110.
297. Wnuk, M. P., 1974, "Quasi-Static Extension of a Tensile Crack Contained in Viscoelastic Plastic Solid," *J. of Appl. Mech.*, ASME, V. 41, No. 1, pp. 234-248.
298. Wu, F. H., and Freund, L. B., 1984, "Deformation Trapping due to Thermoplastic Instability in One-Dimensional Wave Propagation," *J. of Mech. and Phys. of Solids*, V. 32, No. 2, pp. 119-132.
299. Xu, D., and Reinhardt, H. W., 1989, "Softening of Concrete Under Torsional Loading," *Fracture of Concrete and Rock: Recent Developments*, eds. Shah, S. P., Swartz, S. E., and Barr, B., Int. Conf. held at Cardiff, U.K., Elsevier Applied Science, London, U.K., pp. 39-50.
300. Yuzugullu, O., and Schnobrich, W. C., 1973, "A Numerical Procedure for the Determination of the Behavior of a Shear Wall Frame System," *ACI J.*, V. 70, No. 7, pp. 474-479.
301. Zaitsev, J. W., and Wittmann, F. H., 1974, "A Statistical Approach to the Study of the Mechanical Behavior of Porous Materials under Multiaxial State of Stress," *Proc. of the 1973 Symp. on Mechanical Behavior on Materials*, Kyoto, Japan, 705 p.
302. Zubelewicz, A., and Bazant, Z. P., 1987, "Interface Element Modeling of Fracture in Aggregate Composites," *J. of Engng. Mech. Div.*, ASCE, V. 113, No. 11, pp. 1619-1630.

## Appendix I.- Derivations of Some Formulas

Derivation of Eq. 1.4: The size effect law in Eq. 4.1 can be derived most generally by dimensional analysis and similitude arguments (Bažant, 1984a) on the basis of the following hypotheses: (I.) The energy release of the structure is a function of both: (a) the length of fracture,  $a$ , and (b) the characteristic fracture process zone,  $c_f$ . (II.) The length  $a$ , at maximum load is not negligible and is proportional to structure size  $d$ , while  $c_f$  is a structural property independent of  $d$ .

The total amount of energy released from the structure into the fracture must be expressible in the form

$$W = \frac{1}{2E'} \sigma_N^2 b d^2 F(\theta_1, \theta_2), \quad \theta_1 = \frac{a}{d}, \theta_2 = \frac{c_f}{d} \quad (\text{A.1})$$

where  $\sigma_N = P/bd$ ;  $\theta_1, \theta_2$  are independent nondimensional parameters (their number follows from Buckingham's theorem of dimensional analysis), and  $F$  is a certain function which may be expected to be smooth. From the crack propagation condition  $\partial W/\partial a = G_f b$ , one gets

$$\sigma_N^2 = \frac{2E'G_f}{d} \left[ \frac{\partial F(\theta_1, \theta_2)}{\partial \theta_1} \right]^{-1} \quad (\text{A.2})$$

We now choose the state  $\theta_2 = 0$  (which corresponds to  $d \rightarrow \infty$ ) as the reference state, and expand  $\partial F/\partial \theta_1$  into Taylor series about this state i.e.,  $\partial F/\partial \theta_1 = F_1 + F_2\theta_2 + F_3\theta_2^2 + F_4\theta_2^3 + \dots$  where  $F_1, F_2, \dots$  are constants if geometrically similar shapes (same  $\theta_1$ ) are considered. Substitution into Eq. (A.2) and truncation of the series after the linear term yields:

$$\sigma_N = \left( \frac{2E'G_f}{F_2c_f + F_1d} \right)^{1/2} \quad (\text{A.3})$$

This yields Eq. 4.1 if one denotes  $B = \sqrt{(2E'G_f)/(F_2c_f)}$  and  $d_0 = F_2c_f/F_1$ , and notes that  $B$  and  $d_0$  are constants.

From the size effect law (Eq. 1.4), we have  $P^2 = (\sigma_N b d / c_n)^2 = (B f_u b d / c_n)^2 d_0 / (d + d_0)$ . Substituting for  $P^2$  in Eq. 5.2 and noting Eq. 6.24 for  $G_f$  we get

$$G(\alpha) = G_f \frac{g(a)}{g(\alpha_0)} \frac{d}{d + d_0} \quad (\text{A.4})$$

The critical state occurs if fracture propagation is possible also for the next adjacent state, i.e. if  $\partial(G - R)/\partial d = 0$ . Because  $\partial R(c)/\partial d = 0$ , we must have  $\partial G/\partial d = 0$ . Since  $\alpha = a/d = (a_0 + c)/d$ , we find  $\partial \alpha / \partial d = -c/d^2 = (\alpha_0 - \alpha)/d$ , and so substitution of Eq. A.4 into  $\partial G/\partial d = [\partial G(\alpha)/\partial \alpha] \partial \alpha / \partial d + \partial G/\partial d = 0$  provides

$$d + d_0 = d_0 g(\alpha) / [g'(\alpha)(\alpha - \alpha_0)] \quad (\text{A.5})$$

Substituting this for  $(d + d_0)$  in Eq. A.4, we further obtain  $G(\alpha) = G_f [g'(\alpha)/g(\alpha_0)] c / d_0$ . Finally, noting that  $d_0 = c_f g(\alpha_0) / g'(\alpha_0)$  (from Eq. 5.6), we obtain Eq. 4.1 (Bažant and Kazemi, 1988). Furthermore, substituting Eq. 4.1 into Eq. A.4 in which  $(R = G)$  and eliminating  $d$  with the help of Eq. A.5, Eq. 4.2 ensues.

## Part II Conference Papers